Spring 2010

Analysis of Helicopter Downwash/Frigate Airwake Interaction Using Statistically Designed Experiments

Yavuz Nacakli
Old Dominion University

ANALYSIS OF HELICOPTER DOWNWASH/FRIGATE AIRWAKE INTERACTION USING STATISTICALLY DESIGNED EXPERIMENTS

by

YAVUZ NACAKLI
B.S. August 1997, Air Force Academy, Turkey
M.S. June 2003, Middle East Technical University, Turkey

A Dissertation Submitted to the Faculty of
Old Dominion University in Partial Fulfillment of the
Requirement for the Degree of

DOCTOR OF PHILOSOPHY

AEROSPACE ENGINEERING

OLD DOMINION UNIVERSITY
May 2010

Approved by:

Drew Landman (Director)

Oktay Baysal (Member)

Colin P. Britcher (Member)

M. Fevzi Unal (Member)

ANALYSIS OF HELICOPTER DOWNWASH/FRIGATE AIRWAKE INTERACTION USING STATISTICALLY DESIGNED EXPERIMENTS

Yavuz Nacakli
Old Dominion University, 2010
Director: Dr. Drew Landman

A research program to investigate helicopter downwash/frigate airwake interaction has been initiated using a statistically robust experimental program featuring Design of Experiments. Engineering analysis of the helicopter/frigate interface is complicated by the fact that two flowfields become inherently coupled as separation distance decreases. The final objective of this work is to develop experimental methods to determine when computer simulations need to include the effects of a coupled flowfield versus using a simplified representation by superposing the velocity fields of the individual flowfields. The work presented was performed in the Old Dominion University Low Speed Wind Tunnel using a simplified 1/50 scale frigate waterline model and traverse mounted powered rotor with thrust measurement. Particle Image Velocimetry (PIV) velocity surveys were used with rotor thrust coefficient measurements at locations of identified interaction to help understand the underlying flow physics. Initially, PIV surveys of the frigate model landing deck in isolation and the rotor in isolation were performed to provide a baseline flow understanding. Next a designed experiment was devised yielding a response model for thrust coefficient as a function of vertical and longitudinal distance from the hangar door (base of the step), both with and without the rotor. This first experiment showed that thrust coefficient could be measured with enough precision to identify changes due to location using an advance ratio of 0.075 (V_∞ = 5.14 m/s and ω =

5000 rpm). A second designed experiment determined the practical spatial resolution for mapping the thrust coefficient response along the frigate's longitudinal center plane. Finally, a third designed experiment directly compared rotor thrust measurements between airwake and no-airwake cases and successfully identified regions that differed with statistical significance. Lastly, a qualitative comparison study was performed to investigate the limit to direct superposition of rotor downwash and frigate velocity fields using PIV results.

ACKNOWLEDGMENTS

It is a hard task to name and thank all the people who contributed to this achievement. I would like to thank first and foremost my advisor Dr. Drew Landman for his endless help, guidance and encouragement during the course of this project; without him this work would not be possible.

A sincere and special thank you is owed to my committee members Dr. Oktay Baysal and Dr. Colin P. Britcher for their valuable guidance and support. Dr. Baysal has guided and supported me throughout my stay in both the US and Turkey. Dr. Britcher was someone upon whose knowledge and help I would always depend.

I would like to thank to Dr. M. Fevzi Unal for his valuable guidance with this study. I am also very grateful to Dr. Ilteris Koc for his contribution to this work, especially in the wind tunnel. I would also like to thank to my friends Bedri Yagiz, Murat Barisik, Can Sabuncu, Dr. Bayram Celik, Murat Gecgel and Huseyin Kudak for their friendship and technical support. I would also like to acknowledge Tom Galloway and Kevin Colvin from Batten Model Shop for helping me build the experimental set-up and manual traverse mechanism.

Finally, I would like to thank my family, whose love and attention made the time and distance between us appear much less than it really was. I could never have come to this point without their support and love.

TABLE OF CONTENTS

Page

NOMENCLATURE..... ix

LIST OF FIGURES.....xi

LIST OF TABLES.....xvii

1. INTRODUCTION.....1

1.1 Background..... 1
1.2 Objectives..... 2
1.3 Operational Problems of Airwakes..... 3
1.3.1 Ship Airwakes..... 3
1.3.2 Effect on Pilot Workload and Performance..... 5
1.3.3 Ship Helicopter Operating Limits (SHOL)..... 5
1.4 Simulation in Support of Deck Landing Training..... 7
1.5 The Role of Modeling and Simulation..... 8
1.6 Role of Wind Tunnel Testing..... 9
1.7 Guiding Computational Fluid Mechanics (CFD) Solutions..... 10
1.8 Statement of the Problem and Motivation..... 12

2. LITERATURE SURVEY..... 14

2.1 Background..... 14
2.2 Experimental Aerodynamic Measurements of Rotorcraft Operating from Ships 15
2.3 Numerical Work to Simulate the Flowfield of Rotorcraft Operating from Ships 20

3. EXPERIMENTAL SETUP..... 23

3.1 Introduction..... 23
3.2 Test Facility..... 23
3.2.1 The ODU Low-Speed Wind Tunnel..... 23
3.3 Models..... 25
3.4 Data Acquisition and Measurement System Software..... 32
3.5 Partical Image Velocimetry (PIV) System..... 33
3.5.1 Introduction to the PIV System..... 33
3.5.2 PIV System Hardware Overwiew..... 33
3.5.3 PIV Settings for the Experiments Performed..... 36

4. DESIGN AND ANALYSIS OF GENERAL FACTOR EXPERIMENTS..... 38

4.1 Background..... 38
4.2 Definition and Principles 39
4.3 Foundations of Experimental Design..... 41
4.4 Statistical Analysis of the Single Factor Experiment 43
4.4.1 Analysis of Variance..... 43
4.4.1.1 Models for the Data 44
4.4.1.2 Partitioning Variance 46
4.4.1.3 Hypothesis Testing..... 48
4.4.2 Statistical Analysis of the Single Factor Experiment 54
4.4.2.1 Model Adequacy Checking..... 60
4.4.2.2 The Normality Assumption..... 61
4.4.2.3 Plot of Residuals in Time Sequence 63
4.4.2.4 Plot of Residuals versus Fitted Values..... 65
4.4.2.5 Regression Model 66
4.5 Statistical Analysis of the General Factorial Experiment..... 68
4.5.1 A Full Factorial DOE 69
4.5.1.1 The Normality Assumption..... 76
4.5.1.2 Plot of Residuals in Time Squence 77

5. EXPERIMENTS PERFORMED 79
5.1 Baseline Partical Image Velocimetry (PIV) Flowfield Surveys 79
5.1.1 Frigate Airwake Character..... 81
5.2 Investigation of the Measurement Techniques 83
5.2.1 Thrust Change as a Function of Presence of Frigate, Lateral and Longitudinal Distance.....83
5.2.2 Vertical Seperation Sensitivity Study-Single Factor Experiment 84
5.2.3 Identification of Regions of Airwake Influence 84
5.2.3.1 The Normality Assumption..... 88
5.2.3.2 Plot of Residuals in Time Sequence 89
5.2.3.3 Plot of Residuals versus Fitted Values..... 91
5.2.3.4 Regression Model and Uncertainty Estimates 92
5.2.3.5 Determining Airwake Influence 95
5.2.4 Detailed PIV Surveys 97
5.2.5 Initial Coupling Experiments..... 98
5.2.5.1 Investigation of the Feasibility of Identifying Coupled Regions..... 98
5.2.5.2 Isolated Ship and Rotor PIV Surveys 99
5.2.5.3 Comparision of Ship Airwake/Rotor Downwash Combined Measurements with the Rotor Velocity Field Superposed on Ship Airwake 101

6. RESULTS..... 102
6.1 Introduction..... 102
6.2 Ship in Isolation Case 104

6.3 Rotor in Isolation Case 106
6.4 Rotor Downwash with Ship Airwake in the Longitudinal Plane 109
6.5 Rotor Downwash with Ship Airwake in the Lateral Plane 130
6.6 Example of Coupled Flow 142

7. DISCUSSION, CONCLUSIONS AND FUTURE WORK 144
7.1 Discussion of Results 144
7.2 Conclusions and Future Work 148

REFERENCES 150

VITA 154

APPENDIX-A TECHNICAL DRAWINGS 155

NOMENCLATURE

Variables

C_T	Thrust Coefficient
D	Rotor Diameter
T	Thrust
U	Flow velocity
V_∞	Flow freestream velocity
V_{Tip}	Speed of the Rotor tip

Greek Symbols

α	Significance level
β	Type II error
μ_i	Mean of the i_{th} factor level
σ	Population standard deviation
δ	Difference in means
ε_{ij}	Random error component
ω	Rotor rotational speed
ρ	Air density

Acronyms

ANOVA	Analysis of Variance
CFD	Computational Fluid Mechanics

DOE	Design of Experiments
PIV	Particle Image Velocimetry
RPM	Revolution per minute

LIST OF FIGURES

Figure

Page

1.1 MH-60 Seahawk hovering above a frigate landing deck 3

1.2 SH-2F Helicopter crash on board USS Trippe[5] 4

1.3 Difficulties of handling a helicopter on a frigate[9] 6

1.4 A Typical SHOL[8]..... 7

1.5 Case for coupled flow 11

1.6 Case for uncoupled flow..... 12

3.1 ODU Low-Speed Wind Tunnel 24

3.2 Hewlett Packard 3497A Data Acquisition and Control Unit 25

3.3 Simple Frigate Model 26

3.4 Raised Ground Board with the Simple Frigate Model 26

3.5 Astro Flight Cobalt 40 DC Motor 27

3.6 Sorensen DCS 55-55E 3kW DC Power Supply 28

3.7 Tachometer with slotted disc and photo interrupter 28

3.8 Omega LCAE Single-point Load Cell 29

3.9 DC Motor, Load Cell and Tachometer Combination 30

3.10 Manual Traverse Mechanism 31

3.11 Coordinate System 31

3.12 LabView based Data Acquisition Screen 32

3.13 Hardware arrangements of PIV System 34

3.14 Dual Nd:YAG Laser 35

3.15 TSI PIVCAM 13-8 Model 630047 35

3.16 2-D and Stereo PIV Setup 35

3.17 Smoke Generator 36

3.18 Overall Experimental Setup 36

4.1 General Model of Process or System 38

4.2 Thrust Measurement Single Factor Experiment Case 55

4.3 Design Expert ANOVA Report for Single Factor Experiment 58

4.4 Normal Probability Plot of Residuals for Single Factor Experiment 62

4.5 Plot of Residuals versus Run Order Time for Single Factorial Experiment 64

4.6 Plot of Residuals versus Fitted Values for Single Factor Experiment 65

4.7 Cubic Regression Model for Single Factor Experiment 67

4.8 Design Points for 1st Experiments 71

4.9 Design Expert ANOVA Report for 1st Experiment for case V_∞=2.57 m/s 73

4.10 Design Expert ANOVA Report for 1st Experiment for case V_∞=5.14 m/s 74

4.11 The R-Squared Values for case V_∞=2.57 m/s 75

4.12 The R-Squared Values for case V_∞=5.14 m/s 75

4.13 Normal Probability Plot of Residuals for case V_∞=2.57 m/s 76

4.14 Normal Probability Plot of Residuals for case V_∞=5.14 m/s 77

4.15 Plot of Residuals versus Run Order Time for case V_∞=2.57 m/s 78

4.16 Plot of Residuals versus Run Order Time for case V_∞=5.14 m/s 78

5.1 Frigate and the Rotor Used in Initial PIV Flowfield Surveys 80

5.2 PIV Velocity Survey over Frigate Landing Deck 85

5.3 Full Factorial Designs for the 3rd Experiments (Airwake Case left) 85

5.4 Design Expert ANOVA Report for V_∞=0 m/s Case 86

5.5 Design Expert ANOVA Report for V_∞=5.14 m/s Case 87

5.6 Normal Probability Plot of Residuals for V_∞=5.14 m/s Case 88

5.7 Normal Probability Plot of Residuals for V_∞=0 m/s Case 89

5.8 Plot of Residuals versus Run Order Time for V_∞=5.14 m/s Case 90

5.9 Plot of Residuals versus Run Order Time for V_∞=0 m/s Case 90

5.10 Plot of Residuals versus Fitted Values for V_∞=5.14 m/s Case 91

5.11 Plot of Residuals versus Fitted Values for V_∞=0 m/s Case 92

5.12 Thrust Coefficient Contour Plot for V_∞=5.14 m/s Case 93

5.13 Thrust Coefficient Contour Plot for V_∞=0 m/s Case 93

5.14 Response Surface Plot for V_∞=5.14 m/s Case 94

5.15 Response Surface Plot for V_∞=0 m/s Case 94

5.16 Thrust Coefficient-Difference Significance 96

5.17 PIV Survey for Longitudinal Plane (x/D=0.5; z/D=0.55) 97

5.18 PIV Survey for Lateral Plane (x/D=0.5; z/D=0.55) 98

5.19 PIV Survey in Interaction Region (x/D=0.5; z/D=0.55) 99

5.20 PIV Survey for Ship in Isolation Case 100

5.21 PIV Survey for Rotor in Isolation Case 100

5.22 Superposition of Rotor Downwash/Ship Airwake 101

6.1 Velocity Vector (m/s) over Frigate Landing Deck in the x-z plane 105

6.2 Contour Plot over Frigate Landing Deck in the x-z plane 105

6.3 Velocity Vector (m/s) for Rotor in Isolation Case (C_T=0.01087) 106

6.4 Contour Plot for Rotor in Isolation Case 107

6.5 Rotor in Isolation with V_∞=5.14 m/s Case (C_T=0.01145) 108

6.6 Rotor in Isolation with V_∞= 5.14 m/s Case (Contour Plot) 108

6.7 Rotor with ship airwake V_∞= 5.14 m/s (x/D=0.5; z/D=0.25) (C_T=0.01638) .. 109

6.8 Rotor with ship airwake V_∞= 5.14 m/s (x/D=0.5; z/D=0.25) (Contour Plot) . 110

6.9 Rotor with ship airwake V_∞= 5.14 m/s (x/D=0.5; z/D=0.55) (C_T=0.0174) 111

6.10 Rotor with ship airwake V_∞= 5.14 m/s (x/D=0.5; z/D=0.55) (Contour Plot) 112

6.11 Rotor with ship airwake V_∞= 5.14 m/s (x/D=0.5; z/D=0.75) (C_T=0.0177) .. 113

6.12 Rotor with ship airwake V_∞= 5.14 m/s (x/D=0.5; z/D=0.75) (Contour Plot) 113

6.13 Rotor with ship airwake V_∞=5.14 m/s (x/D=0.8; z/D=0.45) (CT=0.0174)... 114

6.14 Rotor with ship airwake V_∞= 5.14 m/s (x/D=0.8; z/D=0.45) (Contour Plot) 115

6.15 Rotor with ship airwake V_∞= 5.14 m/s (x/D=0.8; z/D=0.65) (C_T=0.0176) .. 115

6.16 Rotor with ship airwake V_∞= 5.14 m/s (x/D=0.8; z/D=0.65) (Contour Plot) 116

6.17 Rotor with ship airwake V_∞= 5.14 m/s (x/D=0.8; z/D=0.85) (C_T=0.0175) .. 116

6.18 Rotor with ship airwake V_∞= 5.14 m/s (x/D=0.8; z/D=0.85) (Contour Plot) 117

6.19 Rotor with ship airwake V_∞=5.14 m/s (x/D=1.1; z/D=0.35) (C_T=0.0174) ... 118

6.20 Rotor with ship airwake V_∞=5.14 m/s (x/D=1.1; z/D=0.35) (Contour Plot) 118

6.21 Rotor with ship airwake V_∞=5.14 m/s (x/D=1.1; z/D=0.55) (C_T=0.0176) ... 119

6.22 Rotor with ship airwake V_∞=5.14 m/s (x/D=1.1; z/D=0.55) (Contour Plot) 119

6.23 Rotor with ship airwake V_∞=5.14 m/s (x/D=1.1; z/D=0.75) (C_T=0.0175) ... 120

6.24 Rotor with ship airwake V_∞=5.14 m/s (x/D=1.1; z/D=0.75) (Contour Plot) 120

6.25 Rotor with ship airwake V_∞=5.14 m/s (x/D=1.4; z/D=0.45) (C_T=0.0176) ... 121

6.26 Rotor with ship airwake V_∞=5.14 m/s (x/D=1.4; z/D=0.45) (Contour Plot) 121

6.27 Rotor with ship airwake V_∞=5.14 m/s (x/D=1.4; z/D=0.65) (C_T=0.0176) ... 122

6.28 Rotor with ship airwake V_∞=5.14 m/s (x/D=1.4; z/D=0.65) (Contour Plot) 122

6.29 Rotor with ship airwake V_∞=5.14 m/s (x/D=1.4; z/D=0.85) (C_T=0.0173) ... 123

6.30 Rotor with ship airwake V_∞=5.14 m/s (x/D=1.4; z/D=0.85) (Contour Plot) 123

6.31 Rotor with ship airwake V_∞=5.14 m/s (x/D=1.7; z/D=0.35) (C_T=0.0173) ... 124

6.32 Rotor with ship airwake V_∞=5.14 m/s (x/D=1.7; z/D=0.35) (Contour Plot) 125

6.33 Rotor with ship airwake V_∞=5.14 m/s (x/D=1.7; z/D=0.55) (C_T=0.0175) ... 125

6.34 Rotor with ship airwake V_∞=5.14 m/s (x/D=1.7; z/D=0.55) (Contour Plot) 126

6.35 Rotor with ship airwake V_∞=5.14 m/s (x/D=1.7; z/D=0.75) (C_T=0.0175) ... 126

6.36 Rotor with ship airwake V_∞=5.14 m/s (x/D=1.7; z/D=0.75) (Contour Plot) 127

6.37 Rotor with ship airwake V_∞=5.14 m/s (x/D=2; z/D=0.45) (C_T=0.0172) 127

6.38 Rotor with ship airwake V_∞=5.14 m/s (x/D=2; z/D=0.45) (Contour Plot) ... 128

6.39 Rotor with ship airwake V_∞=5.14 m/s (x/D=2; z/D=0.65) (C_T=0.0174) 128

6.40 Rotor with ship airwake V_∞=5.14 m/s (x/D=2; z/D=0.65) (Contour Plot) ... 129

6.41 Rotor with ship airwake V_∞=5.14 m/s (x/D=2; z/D=0.85) (C_T=0.0175) 129

6.42 Rotor with ship airwake V_∞=5.14 m/s (x/D=2; z/D=0.85) (Contour Plot) ... 130

6.43 Rotor with ship airwake V_∞=5.14 m/s (x/D=0.5; z/D=0.35) (C_T=0.0166) ... 131

6.44 Rotor with ship airwake V_∞=5.14 m/s (x/D=0.5; z/D=0.35) (Contour Plot) 131

6.45 Rotor with ship airwake V_∞=5.14 m/s (x/D=0.5; z/D=0.55) (C_T=0.0174) ... 132

6.46 Rotor with ship airwake V_∞=5.14 m/s (x/D=0.5; z/D=0.55) (Contour Plot) 133

6.47 Rotor with ship airwake V_∞=5.14 m/s (x/D=0.5; z/D=0.75) (C_T=0.0177) ... 133

6.48 Rotor with ship airwake V_∞=5.14 m/s (x/D=0.5; z/D=0.75) (Contour Plot) 134

6.49 Rotor with ship airwake V_∞=5.14 m/s (x/D=1; z/D=0.35) (C_T=0.0174) 135

6.50 Rotor with ship airwake V_∞=5.14 m/s (x/D=1; z/D=0.35) (Contour Plot) ... 135

6.51 Rotor with ship airwake V_∞=5.14 m/s (x/D=1; z/D=0.55) (C_T=0.0176) 136

6.52 Rotor with ship airwake V_∞=5.14 m/s (x/D=1; z/D=0.55) (Contour Plot) ... 137

6.53 Rotor with ship airwake V_∞=5.14 m/s (x/D=1; z/D=0.75) (C_T=0.0175) 137

6.54 Rotor with ship airwake V_∞=5.14 m/s (x/D=1; z/D=0.75) (Contour Plot) ... 138

6.55 Rotor with ship airwake V_∞=5.14 m/s (x/D=1.5; z/D=0.35) (C_T=0.0174) ... 139

6.56 Rotor with ship airwake V_∞=5.14 m/s (x/D=1.5; z/D=0.35) (Contour Plot) 139

6.57 Rotor with ship airwake V_∞=5.14 m/s (x/D=1.5; z/D=0.55) (C_T=0.0176) ... 140

6.58 Rotor with ship airwake V_∞=5.14 m/s (x/D=1.5; z/D=0.55) (Contour Plot) 140

6.59 Rotor with ship airwake V_∞=5.14 m/s (x/D=1.5; z/D=0.75) (C_T=0.0175) ... 141

6.60 Rotor with ship airwake V_∞=5.14 m/s (x/D=1.5; z/D=0.75) (Contour Plot) 142

6.61 Ship Airwake + Rotor Downwash (Superposed) 143

6.62 Ship airwake/Rotor Downwash (Measured) 143

7.1 Flowfield over the Frigate Landing Deck 145

7.2 Flowfield with Rotor near Hangar Door and Deck 146

7.3 Flowfield with Rotor position aft of Mid Deck..... 147

7.4 Flowfield with Rotor position at the Stern 148

LIST OF TABLES

Table

Page

3.1 Resolution Values for Camera Setup 37

4.1 Typical Data for a Single Factor Experiment 46

4.2 Various Types of H_0 and H_1 for Means Testing 50

4.3 Formal Statistic Hypothesis for Means Testing 51

4.4 Types of Error 52

4.5 The ANOVA Table for Single Factor, Fixed Effects Model 53

4.6 Grid of Measurement Locations 56

4.7 Statistical Significance According to P-Values 59

4.8 Grid of Thrust Measurement Points for 1st Experiment 71

4.9 Randomized Run Order Test Matrix for 1st Experiment 72

6.1 Experimental Cases 102

1. INTRODUCTION

1.1 Background

The operation of helicopters from ships began just before World War II. Naval combatant ships are designed to allow helicopter operations for different purposes like tactical missions, replenishment of stores and ammunition, transport of personnel, search and rescue, medical evacuation, delivery of the mail, etc. Helicopter flight onto and from the decks of frigate type non-aviation ships can be considerably more difficult than the execution of the same maneuver on land. A typical helicopter landing on a frigate landing deck is presented in Figure 1.1. Shipboard operation of the helicopter remains a topic of significant interest not only for military but also civilian operators, particularly, in the launch and recovery regimes where the helicopter is in close proximity to the ship and its airwake. The ship dynamics, the ship induced airwake, and the aircraft/ship interaction strongly affect the shipboard helicopter's take off and landing processes[1]. Helicopter shipboard operations impose more flight envelope restrictions on the rotorcraft due to a harsher environment that includes ship airwake due to the ship's motion and superstructure, and a respectively smaller landing area.

The handling of the helicopter is made more difficult as the helicopter enters the ship`s airwake, which is the region of separated flow on the lee side of the superstructure and hangar door. Such a region of flow contains significant gradients in mean wind speed and direction as well as a high level of turbulence due to the shedding of vorticies and movement of one or more unsteady shear layers separating from the superstructure[2].

The format of this dissertation is based on *AIAA Journal.*

The time-averaged and unsteady flow phenomena both can influence the rotor generated loads and lead to increased pilot workload in a hazardous situation. The mean flow gradients and unsteady shear layers both will alter the rotor performance, possibly increasing pilot workload, due to the fact that a typical frigate superstructure is of the same geometric size as a helicopter rotor diameter. The scale of turbulence shed from a superstructure, responsible for eddies that can also be expected to affect the rotor loads, will vary in size with characteristic dimensions less than or equal to the superstructure[3]. Engineering analysis of the helicopter/ship interface is complicated by the fact that the problem is inherently coupled. That is, the ship airwake affects the rotor output and vice versa[2].

1.2 Objectives

There are problems specific to the helicopter/ship dynamic interface that limit helicopter operations and cause difficulty associated with landing on a moving platform. The ship airwake is considered a crucial factor in limiting these operations due to associated large velocity gradients and areas of turbulence. For this reason, knowledge of the air flow around the ship and through the helicopter`s rotors is necessary to understand the problems that the helicopter encounters as it lands and takes off.

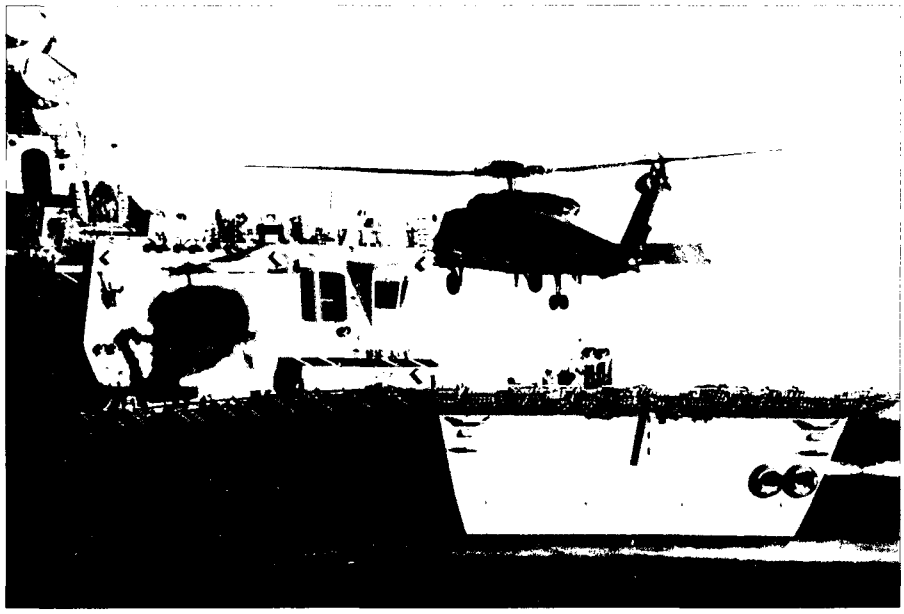

Figure 1.1 MH-60 Seahawk hovering above a frigate landing deck

1.3 Operational Problems of Airwakes

1.3.1 Ship Airwakes

Among all piloting tasks, landing a helicopter on the flight deck of a moving ship is one of the most demanding ones. The difficulties are frequently compounded by low visibility obscuring the horizon and high sea states resulting in severe ship motion. At night the visual cues available to the pilot are degraded or lost altogether and lighting is often limited due to tactical considerations. Whatever the conditions, the pilot is still expected to land on the deck within a tightly defined area without overstressing the undercarriage. The unsteady airwake generated by the ship as the wind flows over the superstructure aggravates the problem still further and can impact the operational availability of the helicopter severely. The pilot is forced to compensate for disturbances after the helicopter enters the ship airwake, initially to the aircraft flight path, and finally

to the position over the landing spot. An unexpected gust may force the aircraft dangerously close to the flight deck and superstructure or may move the helicopter away from the ship into a position where the pilot loses vital visual references. While the pilot is trying to maintain an accurate position, he has less spare capacity to consider his next move and the situation becomes unpredictable. In extreme wind conditions, the pilot may reach the limits of control authority with the result that there is insufficient maneuver power to compensate for the airwake disturbance. These kinds of difficulties for pilots can sometimes cause unexpected helicopter/ship accidents, which can be seen in Figure 1.2.

Photo # USN 1172866 SH-2F helicopter crashed on board USS Trippe, February 1978

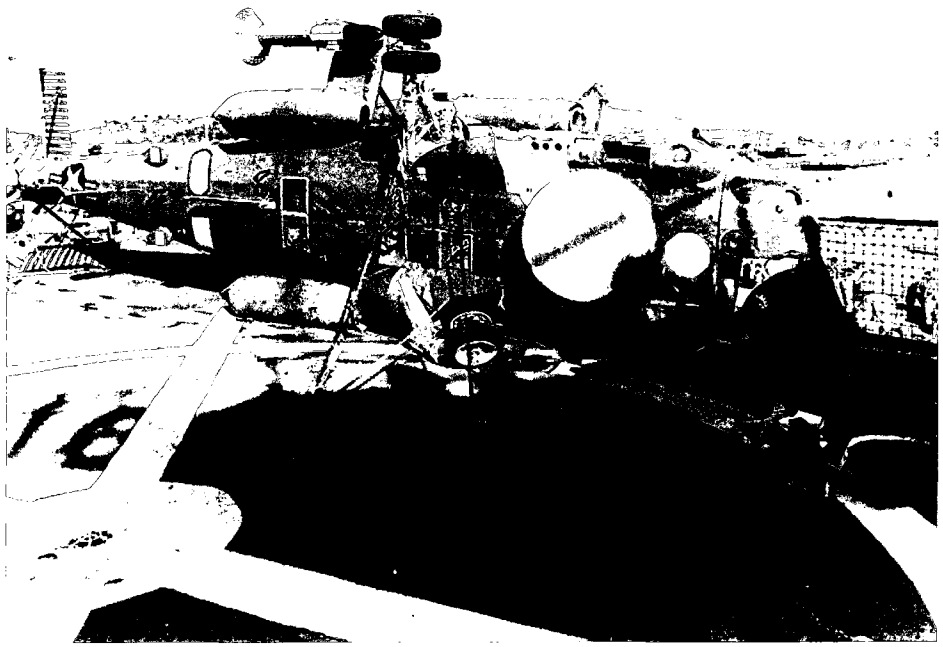

Figure 1.2 SH-2F Helicopter crash on board USS Trippe[4]

1.3.2 Effect on Pilot Workload and Performance

When departing or returning to the ship, helicopter pilots need to consider the conditions that enable them to safely land on a moving deck. Although the size of the deck area varies considerably for different classes of ship, for ships such as destroyers and frigates the area is frequently not much larger than the helicopter. Pilots must position the helicopter with sufficient accuracy to engage an aircraft-mounted probe in a ship-mounted capture mechanism, which may be as small as 2 square meters[5]. Significant factors affecting such operations include visibility day, night, or degraded through poor weather conditions or spray, ship motion, and aerodynamic interactions of the helicopter with the turbulent airflow near the ship. These all contribute to pilot workload, which may not allow the pilot to safely take-off or land. Difficulties of handling a helicopter on a frigate are represented in Figure 1.3. Other factors including exceeding torque and control limits also affect launch and recovery operations of a helicopter on the ship landing deck. The pilot may have insufficient control authority in certain wind conditions, in particular tail rotor authority in a crosswind, to maintain positive relative to the ship[5].

1.3.3 Ship Helicopter Operating Limits (SHOL)

In order to assist pilots, maritime helicopter operators develop SHOLs to define safe operating parameters. These are usually represented in diagrammatic form, an example of which is shown in Figure 1.4. The wind speed (increasing on the radius) and relative direction (shown in 15 degree increments with 0 on the nose) must be within the safe operating envelope shown on the diagram (gray area) for the helicopter to land or take-off

safely. If they are not, the ship may be forced to change course and/or speed to achieve a safe wind condition. SHOLs may also include structural limits of both ship and aircraft, as well as on deck limits to prevent toppling and sliding, with and without securing devices such as lashings or a ship-mounted capture system[5]. However, these limits are not considered in this dissertation.

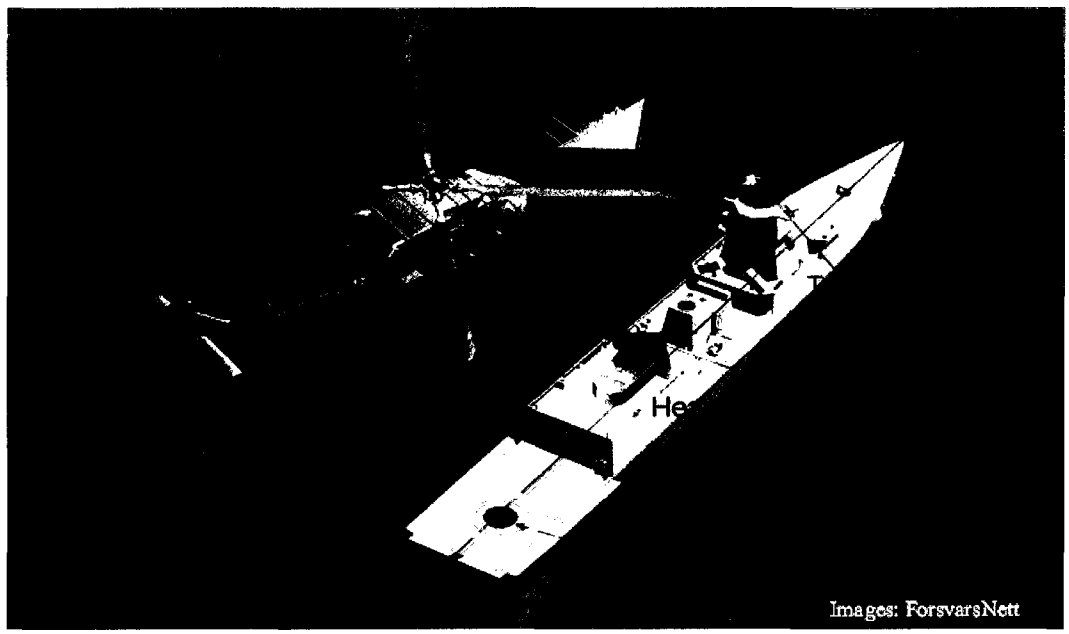

Figure 1.3 Difficulties of handling a helicopter on a frigate[6]

The proliferation of ship and helicopter type variations means that each individual country generally operates its own unique combinations of ships and helicopters. There are no agreed upon international standards for SHOLs, and each country usually determines their own. The development of these SHOLs is an expensive and exacting task currently determined through intensive and costly First of Class Flying Trials (FOCFTs), which limit the final operational envelopes to environmental conditions

similar to those encountered during the trials[5]. The use of modeling and simulation to support SHOL development offers substantial benefits in terms of reduced costs, improved safety and potentially larger operating envelopes. The most important component of such a simulation is probably a high fidelity air wake model that generates representative levels of workload in piloted simulations which allows aircraft control limits to be accurately predicted.

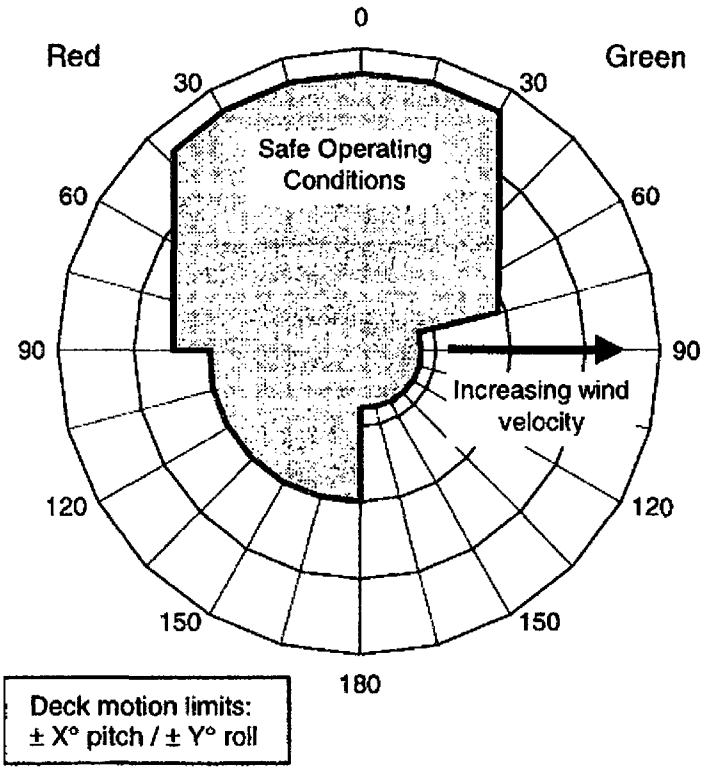

Figure 1.4 A Typical SHOL[5]

1.4 Simulation in Support of Deck Landing Training

Until recently, deck landing training for helicopter pilots has not been possible in a simulator due to insufficient visual and environmental fidelity in the vicinity of the flight

deck. The trainee pilot`s first introduction to the hostile environment of the dynamic interface is when he first flies to the ship, and while his initial deck landings will be conducted under the control of an instructor, he is unlikely to experience the most severe conditions until he is flying operationally. Simulation technologies have reached an advanced stage, coupled with an improved understanding of the dynamic characteristics of helicopters in this environment. With this progress, comprehensive aircrew training in helicopter/ship operations is now believed to be possible. This opens opportunities for the trainee pilot to encounter the full range of operating conditions before he ever joins a ship, with obvious advantages in terms of safety and cost[5].

In flight training, it is important that the student replicates the same control strategy in the simulator as in flight. Failure to do so will negate the advantages of simulator training and may prove dangerous. The airwake has an important part to play in deck landing training as it has a considerable impact on both pilot workload and performance, which will influence the control strategy adopted by the pilot. If the simulated airwake is more benign than reality, a student may gain a false sense of security in the simulator. If the airwake is too severe, there is a danger that the pilot will lose confidence before he has even started. An airwake model of appropriate fidelity is, therefore, an essential element of a training simulation.

1.5 The Role of Modeling and Simulation

The operators of maritime helicopters would aim for maximum aircraft availability and the ability to operate in the most severe environmental conditions. This is particularly

true for the military, but an all-weather capability is also of prime importance to civilian operators, for example, those serving off-shore oil installations[5]. Modeling and simulation offers substantial opportunities to increase the operational availability of maritime helicopters through improved training, as well as the development of procedures, new technologies and qualification techniques. With simulation, control of the environment can be maintained such as the airwake, sea state, light level and visibility without worrying about the flight safety issues associated with live flying. Piloted flight simulation enables aircrew training to be conducted safely. It also significantly reduces the requirement to dedicate costly ships or aircraft to this non-operational role. Off-line simulation can be used to test new ship designs for aircraft compatibility before the ship is built.

Modeling the ship airwake and its effect on helicopter behavior is one of the most significant technical challenges for the dynamic interface (DI) simulation community. A highly complex and dynamic flowfield dominated by separations, vortical flows and recirculation produced due to the irregular nature of a typical ship superstructure, the effect of ship motion and the influence of helicopter rotor. Validation of an airwake prediction is complicated by the difficulties associated with gathering quantitative measurements of the flowfield around a ship at full-scale or in a wind tunnel.

1.6 The Role of Wind Tunnel Testing

There are many difficulties in making accurate full-scale shipboard-operations measurements. Variability of the wind both in magnitude and direction and the difficulty

of measuring the wind velocity free from any influence of the ship itself are major concerns. Waiting for quiescent atmospheric conditions and then sailing at a known speed can eliminate this difficulty. Unfortunately, this approach is economically unfeasible. In addition to the variability of the mean velocity of the wind, full-scale testing must cope with the presence of an atmospheric boundary layer of variable thickness, plus gusts or turbulence[13]. Sea trials must also cope with motion of the flight deck caused by wave motion (surge, sway and heave; roll, pitch and yaw). The wind tunnel is the ideal environment for such studies because the wind tunnel provides accurate control over test conditions.

1.7 Guiding Computational Fluid Mechanics (CFD) Solutions

Piloted simulation has a potentially major role to play in training, test and evaluation and research in support of the helicopter/ship dynamic interface. The combination of visual/motion cueing and vehicle/environment modeling problems makes the helicopter/ship dynamic interface one of the most challenging in the simulation of aerospace vehicles[8]. The operation of helicopters from particularly small ships, such as frigates, presents a demanding task for both the aircraft and the pilot. Simulation of rotorcraft is also exacting. It follows that high fidelity piloted simulation of helicopters at the ship interface is a major challenge. It is not only necessary to simulate the aircraft, but also the ship and the environmental conditions that affect both. Consequently, although piloted simulation has been used extensively in many fixed wing and rotary wing applications, it has not seen widely used for the helicopter/ship interface environment.

CFD is a method for solving complex fluid flow problems using computer simulations. The region of interest is divided into millions of computational cells-a process called 'meshing'. The governing equations of mass and momentum conservation are then solved on each of these cells in turn, giving a complete picture of velocity and pressure distribution. The effects of turbulence are usually accounted for through the use of turbulence models, which vary in complexity and performance. It is also possible to run CFD in unsteady mode to calculate how flow variables change over time[15].

A goal of this project is to help understand ship airwake/helicopter downwash interaction and how it might affect CFD modeling. The Naval Air Systems Command (NAVAIR) CFD modelers define coupling as the region of the dynamic interface where the downwash of the rotor has an impact on the inflow to the rotor due to the presence of a nearby surface. A full time-accurate solution is required for flight simulations in the regions with coupling. Figure 1.5 shows the case for the coupled flow.

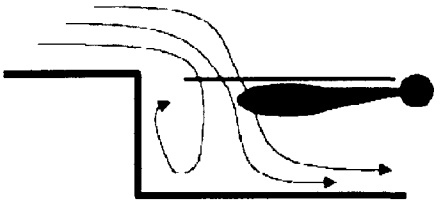

Figure 1.5 Case for coupled flow

A superposition of an isolated rotor velocity field with an isolated ship airwake velocity field will suffice for flight simulations in regions without coupling. The case for the uncoupled flow is presented in Figure 1.6.

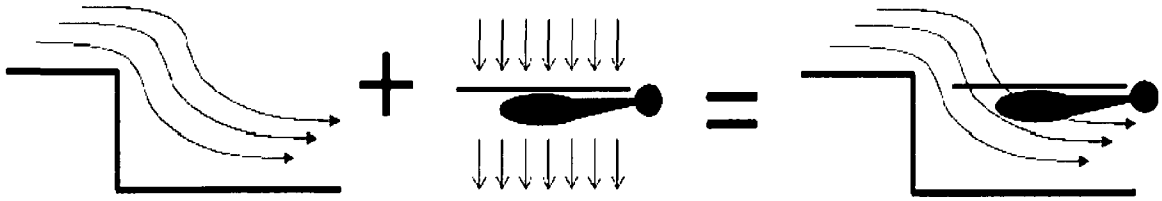

Figure 1.6 Case for uncoupled flow

1.8 Statement of the Problem and Motivation

As stated in previous sections, helicopter flight onto and from the decks of non-aviation ships such as frigates can be considerably more difficult than the execution of the same maneuver on land. The helicopter is immersed in the unsteady airwake in the lee of the ship superstructure. The airwake contains significant gradients in mean wind speed and direction as well as increased turbulence intensities compared to those of the natural wind. The mean flow gradients are associated with shear layers that arise due to flow separations from the superstructure.

Analysis of the helicopter/ship dynamic interface is further complicated by the coupling of the rotor downwash and the ship airwake. Several works address the analysis of ship airwake and/or rotorcraft downwash as well as thrust measurement, but little is found on the interaction of the rotor downwash and the ship airwake.

The author is not aware of any such work carried out elsewhere that directly addresses the ship airwake/rotor downwash interaction for a frigate type geometry, or backward facing step, that correlates the velocity field and the thrust measurements. This research concentrates on investigation of the ship airwake/rotor downwash interaction

using a statistically robust experimental program featuring Design of Experiments (DOE).

The following road map is established for this study:

1. Representative scaled flow conditions are chosen with a simplified ship model and driven rotor.
2. Rotor thrust coefficient is used as a response to identify the locations where interaction is encountered.
3. Variables of rotor height above deck and downstream displacement are chosen on the longitudinal centerplane over the landing deck.
4. Particle Image Velocimetry (PIV) is used for velocity surveys in locations where rotor wake and airwake interact to help understand the underlying flow structures.

2. LITERATURE SURVEY

2.1 Background

Sharp-edged box-like ship superstructures create numerous aerodynamic and fluid dynamic problems. Unsteady separated flow from sharp edges make landing helicopters on ships a very hazardous operation. In addition, the strong unsteady flows can cause severe rotor blade deformations. There have been numerous incidents where the helicopter blades have actually impacted the helicopter fuselage. This is called a 'tunnel strike'[10,11]. In order to avoid this and other engage/disengage problems, determining safe operating envelopes has become very costly and time consuming. Few numerical simulation attempts of this flowfield have been successful due to the inherently unsteady nature of the flow and the low-speed character of the flow (which may cause numerical stiffness)[12].

Research on ship airwakes has been conducted using several different approaches including wind tunnel studies, computer simulations, and shipboard measurements[13]. One of the sources of relevant research is building (architectural) aerodynamics, which shows the general features of flow about blunt bodies of different aspect ratios. The simplest model of a ship is a sharp edged blunt body. The superstructure of most modern ships is very complicated, including towers, antenna, radar dishes, exhaust stacks, etc. The flow around these obstacles is very difficult to predict.

2.2 Experimental Aerodynamic Measurements of Rotorcraft Operating From Ships

Geometrically precise studies are needed and have been done in wind tunnels[14,15,16]. There have also been full scale tests performed by the US Navy[17], which gives some important information on real ship airwakes. Of course it is difficult to perform very controlled experiments on real ships. It is also difficult to measure the flowfield accurately in the harsh ocean environment and not possible to gather data for all locations simultaneously. Further, it is also not possible to control the weather, making airwake development from at-sea data unrealistic. It is also seen from the previous studies that much at-sea airwake data is contaminated by the high levels of electro-magnetic interference (EMI) that inherently exist around naval vessels.

Wind tunnel testing to determine ship airwake characteristics started at least 25 years ago when a U.S. destroyer was tested in a large Boeing wind tunnel[18]. In the intervening years, many other subscale wind tunnel tests have been undertaken, with varied degrees of success. Most wind tunnel tests include measurements made in the wake of a model ship exposed to a uniform velocity profile and almost zero turbulence level. A more realistic test was conducted at NASA Ames in the 'Shipboard Simulator' with a neutrally buoyant atmospheric boundary layer[14].

Another reference for simulations is the National Research Center in Canada (NRC-CNRC) [2]. A wind tunnel investigation of the characteristics of the airwake behind a model of a generic frigate was conducted. The wind tunnel simulation incorporated a correctly-scaled atmospheric boundary layer. Measurements of streamwise and vertical

components of airwake velocity were performed. Time average, standard deviations, spectral densities and time correlations are presented for velocity components in various positions in the airwake.

The wind tunnel tests have to suitably scale the environment and structure to model size, make the appropriate measurements in the wake of the model and then rescale the results back to full size. All these experimental tests are important for validating numerical models. Wind tunnel tests can be quite costly, but in comparison flow measurements on real naval ships are very difficult and costly to obtain.

Experiments conducted in wind tunnels about frigates are mainly interested in studying the hangar deck area (aft portion of the ship), and the separated flow that effects this region. The forward portion of the deck is primarily influenced by the separated flow off the deck edge. Very strong vortex sheets emanate from these edges.

To support current simulation requirements, quantitative time-varying airwake data are required. This is usually obtained with thermal anemometry, Laser-Doppler anemometry, and more recently with Particle Image Velocimetry. The latter two techniques can provide data from within the recirculating flows that are commonly found behind frigates and destroyers[19]. Thermal anemometry can also work in this area, provided the probe is 'flying'[20]. Quite dense spatial resolution for flow mapping is required to effectively capture vertical flow structures and shear layers, because the airwake can vary significantly over a distance equivalent to a rotor diameter. Knowledge of spatial and temporal correlations in the flow is important, as the aircraft response to turbulence is governed by the frequency content and structure of the airwake. Turbulence

in the near wake of a frigate is rapidly distorted over the flight deck, so that if the length scale concept is used when discussing turbulence, it does not strictly apply in this case, although time-correlation measurements can be made from which auto-correlations can be derived[2]. Results from reference [2] show that the flow remains significantly correlated over a distance of 10 m, roughly a rotor radius for many maritime helicopters. This illustrates the importance of modeling the spatial and temporal correlation of the flow. Multiple multi-component hot-films and wires can be used to gather correlated airwake data in a wind tunnel experiment. These are usually physically small enough and have adequate frequency response. In practice, it is not feasible to measure and characterize spatial and temporal correlations for three dimensions simultaneously using theis method[19]. Spatial and temporal correlations of the streamwise and vertical velocities were measured in a wind tunnel in a horizontal plane over the flight deck of a generic frigate model[3]. The data gathered from this wind tunnel experiment were used to recreate a numerical airwake with the correct spectral and temporal correlations through which a validated blade-element rotor model was 'flown'. Time histories of rotor outputs were generated and analyzed as spectra. It was found that the fluctuating vertical component of the airwake generated the most significant unsteady rotor response. The work also examined the sensitivity of the rotor response to the number of blade elements.

Taghizad et al.[21] describe a series of wind tunnel tests to generate airwake data for simulation purposes. A small frigate model was used in this case. A single X-wire probe was employed, so no spatial correlations were obtainable, however, the spectral representations of the airwake were reliable due to time histories of significant length that

were carefully acquired. It is stated in the experiment that the majority of the airwake turbulence is present at frequencies below 6 rad/s. Measurements were conducted for a range of wind speeds, headings and roll angles. Techniques for interpolation to other wind angles are also discussed. Challenges in, and compromises associated with, producing a representative airwake for real-time simulation are described. It was noted in the discussion that cross-correlation information of the airwake data in simulation was not measured, and therefore, could not be modeled.

Fang et al.[22] describe the application of wind tunnels in support of first-of-class flight trials conducted by the National Aerospace Laboratory in the Netherlands (NLR). Measurements are made of the ship-exhaust plume dispersion, in addition to airwake measurements made over the landing spot. Exhaust gases that travel over the flight deck and are ingested by the helicopter engine cause a decrease in power. The increase in temperature also reduces the aerodynamic performance of the rotor system. This aerodynamic performance decrease requires an increase in collective, torque, and power to maintain hover. Density changes to the flow over the flight deck are reported to be reliably predicted, allowing accurate predictions to be made of changes in helicopter performance in this study. It is also stated that measurements of airwakes for multi-spot ships permit some 'read-across'. This read-across allows the envelope established at one spot to serve as a basis from which an envelope can be extracted for another spot. The NLR states that it has "100 percent confidence in the wind tunnel data" in terms of correlation with full-scale measurements of airwakes. The NRC experience concurs with this statement.

Lee and Zan[23] provide unsteady aerodynamic coefficients over representative frequencies for a helicopter fuselage without a rotor in a ship airwake. These were obtained from a wind tunnel test by measuring the unsteady loading on a fuselage model with an integral high-frequency response loads balance. The measurements inherently include the imperfect loading correlations. With a rotor in place, the unsteady aerodynamic loads acting on the fuselage were shown to increase[24], but the general spectral character remains unchanged.

Adverse airwake effects occur with so-called 'flattop' ships as well as with frigates[19]. The deck-edge vortices generated at the leading edge of a frigate can propagate along the entire deck length with the core aligned closely with the axis of the ship for a headwind. For fixed wing operations, such a vortex could be expected to induce rolling of aircraft. However, when the aircraft is on deck the encounter will generally occur after touchdown. The axis of a deck-edge vortex is not absolutely fixed in position with respect to the ship, but rather will move in a random fashion about a mean position. This movement generates unsteady forcing that may worsen an encounter for fixed or rotary wing operations, although, the frequency content of the forcing is unknown. The vortex may rise to a higher elevation above water such that it crosses the glide path, depending on atmospheric conditions including stability.

Maslov et al.[25] describe research efforts within Russia and the former Soviet Union aimed at reducing the adverse effects of aircraft carrier airwakes for air operations. Analysis of the airwake effects on flight operations is mentioned but not in sufficient

enough detail to understand clearly what role simulation played. The authors present the effects of static ship roll and pitch angles on airwake development.

2.3 Numerical Work to Simulate the Flowfield of Rotorcraft Operating From Ships

One approach to acquiring airwake data for input to high-fidelity simulation is to use CFD. CFD has the advantage that it can provide detailed information on flow over the entire flight path for launch and recovery. It has been shown that time-accurate codes are required in order to obtain airwake information with the correct spectra and correlations[26].

Recently, Polsky and Ghee[27] conducted an experimental and computational study that examines the requirements for geometric fidelity in support of airwake modeling. A generic ship configuration was used to study airwakes and provide validation data for CFD as part of an international collaboration under the auspices of The Technical Cooperation Program (http://www.dtic.mil//ttcp1). The effects of the masts, antenna, weapons systems, etc. were found to affect the airwake sufficiently so as to impact the launch and recovery envelope for high-fidelity simulation.

Landsberg et al.[28], from Naval Research Laboratory for computational physics and fluid mechanics, developed an unsteady flow solver, FAST3D, that is capable of determining the unsteady airwake over the ship superstructure. A helicopter downwash model was implemented in FAST3D to examine the nonlinear coupled interaction of an airwake with the downwash from a helicopter. Landberg used a CFD approach to

estimate the interaction of main rotor downwash and a destroyer airwake. In this case, the airwake was computed initially and a uniform downwash was superimposed onto the ship airwake. The focus was not on the helicopter operation but on the ingestion and recirculation of hot exhaust gases for health and safety concerns. Little has been published in this area of research, but it is an important aspect of the dynamic interface.

Tattersall et al.[29] describe the integration of a rotor model into a CFD code, in order to capture the coupling to some degree, in an iterative fashion. In the rotor code, the pressure jump across the disc varied in the radial and azimuthal directions. These jumps were input to the CFD code from which a steady flowfield was calculated. The flowfield at the rotor boundary was used as input to modify the rotor control angles in the rotor code, which in turn modify the variations in loading across the disk. These new loadings are fed back into the CFD solver, and the process is repeated until the two programs converge on a solution. The results should be representative of the study flowfield around the ship. Results also provide some indication of control inputs required to respond to the time-invariant airwake. It is stated that it was not possible at the time to execute a time-accurate code, but it is possible that the steady-state solution is not the same as the average of the time-accurate results. In the latter case, the rotor would never converge to a single control position, and the user would have to decide when sufficient iterations were completed such that meaningful results could be extracted.

Syms[30] performed computations on a generic frigate model using a commercial code which has a Lattice-Boltzmann approach as a basis. The code has the potential to capture well the inherent unsteadiness of a ship airwake because it is an inherently-stable

explicit time-marching algorithm. The volume elements used within the code can be easily fit to any complex geometry, such as ship superstructure - a significant advantage of a Lattice-Boltzmann approach. Syms shows good agreement with the experimental on-deck time-averaged topology and pressure coefficients presented in the study of Zan[31]. The agreement begins to lessen as the wind direction moves from bow to beam winds. Others have reported this phenomenon as well. It is noted that grids are often arranged with a bias along the ship axis. That is, the grid will be several ship lengths long and it will be several ship beams wide. It is stated that this geometrical arrangement may suffice for bow winds, but a completely different grid would be preferable for beam winds. In this case, the grid should extend several ship lengths in the wind direction and at least one and one-half ship lengths along the ship axis. Experimentalists are also cautioned that the analogous situation holds true in the wind tunnel. This requires prudence for beam-wind studies.

3. EXPERIMENTAL SETUP

3.1 Introduction

In this chapter the ODU low-speed wind tunnel, the instrumentation used for data acquisition, the frigate model, rotor, manual traverse mechanism, and the Particle Image Velocimetry (PIV) system are introduced. A manual traverse mechanism was designed, built and installed in order to place the rotor over the frigate landing deck at a desired position.

3.2 Test Facility

3.2.1 The ODU Low-Speed Wind Tunnel

The Old Dominion University Low-Speed Wind Tunnel is an atmospheric pressure, closed return, fan-driven type that has two tandem closed test sections at 7x8x7 ft and 3x4x8 ft (HxWxL) respectively (Figure 3.1). The drive power of the tunnel is provided by a 125 hp AC induction motor. The motor drives a 14 bladed fan by means of a belt system. The speed of the tunnel is adjusted by a variable frequency controller[32].

As can be seen from Figure 3.1, tests can be performed in either of the two tandem test sections. In the first entry PIV measurements were performed in the downstream 'high-speed' test section that has a cross-section of 3x4 feet at the entrance. The floor and ceiling of the tunnel are steel and do not diverge along the test section, although the sidewalls diverge at an included angle of approximately 0.6°. This divergence prevents the wall boundary layer growth from producing a longitudinal static pressure gradient.

The tunnel test section dynamic pressure value is in the range of 1 to 30 psf (48 to 1436 Pa), which equates to an indicated-velocity range of 30 to 165 fps (10 to 55 m/s). The lower bound is set by the stability of the fan RPM while the upper is set by the maximum drive power. The tunnel has two 20 mesh/inch, 0.017 inch wire screens with 0.564 solidity (0.436 open area ratio) that provide flow conditioning and suppression of the lateral variations of the longitudinal velocities. There is also one honeycomb with 0.512 inch (13 mm) diameter cells to break up large-scale turbulence and suppress swirl. In the empty test section, the free stream turbulence is around 0.2%, slightly decreasing at higher velocities[33]. Although there is no thermal control for the test section, a steady-state condition is reached below about 70% of the maximum speed. Tunnel reference dynamic pressure was measured directly by a PPT0100AWN2VA model number Honeywell Precision Pressure Transducer (±0.05% FS, 12-bit on internal A/D). Test section temperatures were acquired from a type J thermocouple read through a Hewlett Packard 3497A Data Acquisition and Control Unit with 6.5 digit accuracy (Figure 3.2).

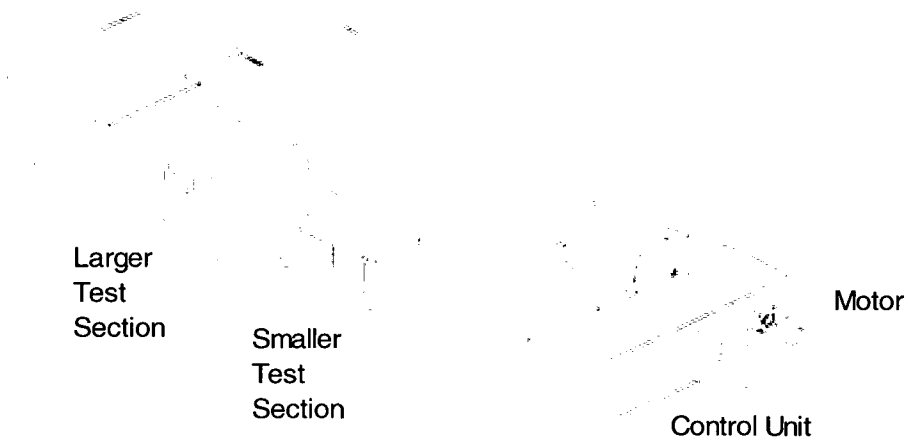

Figure 3.1 ODU Low-Speed Wind Tunnel

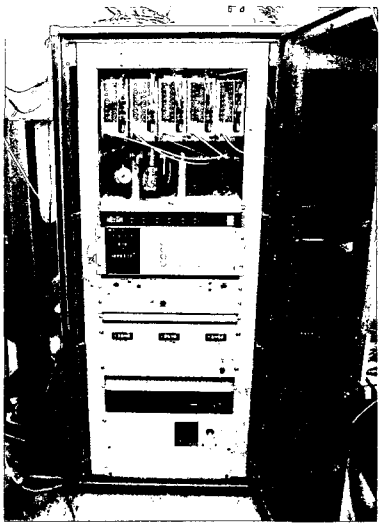

Figure 3.2 Hewlett Packard 3497A Data Acquisition and Control Unit

3.3 Models

A simple frigate model was used in this experimental study. The model, constructed of wood at a geometric scale of 1:50, was fabricated and supplied by NAVAIR. The ship superstructure does not reproduce the details of a typical frigate superstructure; however, from an aerodynamic point of view the airwake should still be representative of that for an actual frigate since the investigation is concerned with the macro flow properties in the deck hangar wake[2]. A three dimensional view of the frigate is presented in Figure 3.3 where the coordinate system is presented in Figure 3.4. A 30 x 74 inch raised ground board was designed and fabricated in order to place the frigate model in the 7 x 8 x 7 ft. low speed test section as can be seen in Figure 3.4. Detailed drawings for the NAVAIR supplied frigate model are found in Appendix A.

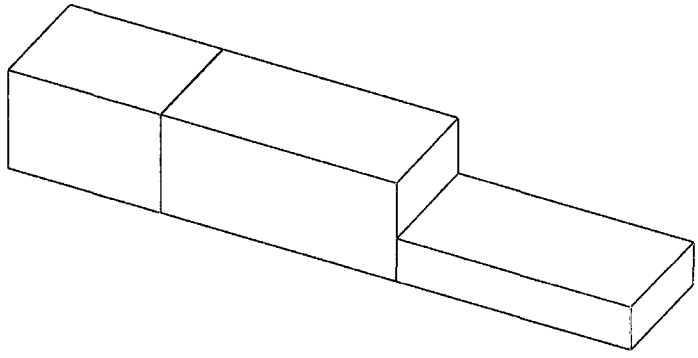

Figure 3.3 Simple Frigate Model

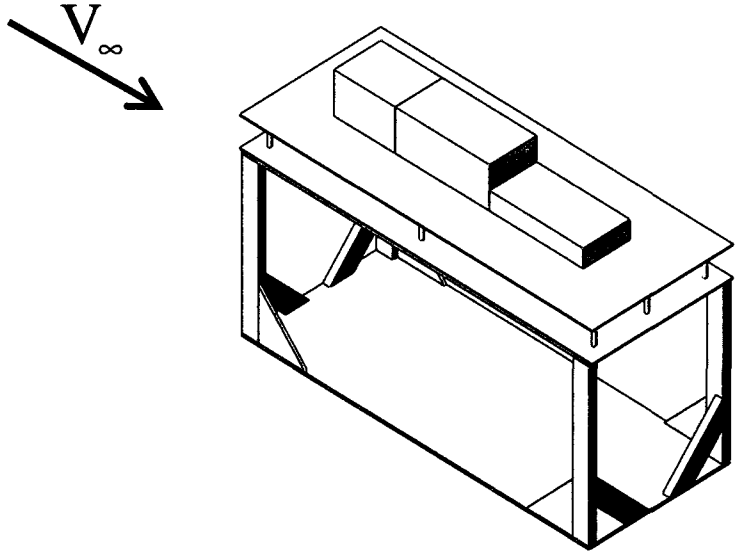

Figure 3.4 Raised Ground Board with the Simple Frigate Model

A four-bladed, 10 inch diameter (10x6), long-fiber composite propeller supplied by NAVAIR was used to represent the rotor during wind tunnel tests. The manufacturer states that the airfoil may have arbitrary shape varying along the blade radius that is defined by splined cubic fits between analytical functions typically used for NACA airfoils. The dominant basis for the primary airfoil shapes used in this propeller are the NACA 4412 and Clark-Y airfoils.[34]

An Astro Flight Cobalt 40 DC brushed motor with Sorensen DCS 55-55E model 3kW DC power supply was used to power the four-bladed rotor (NAVAIR) and are shown in Figure 3.5 and Figure 3.6, respectively

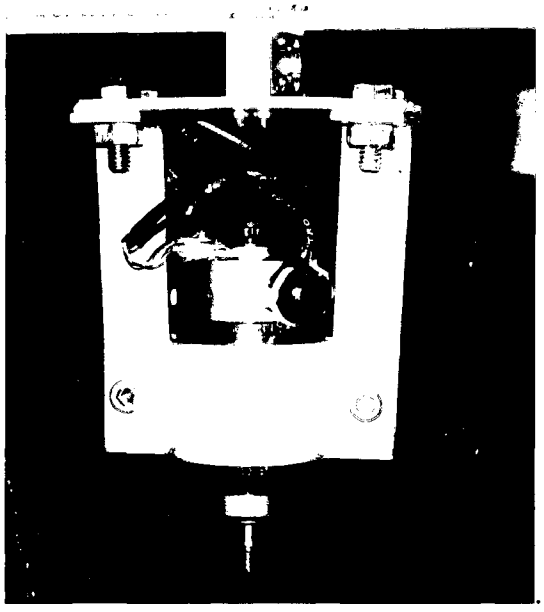

Figure 3.5 Astro Flight Cobalt 40 DC Motor

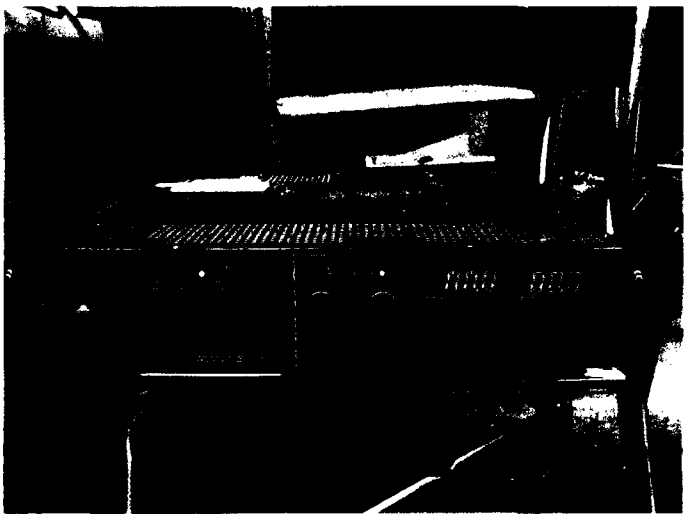

Figure 3.6 Sorensen DCS 55-55E 3kW DC Power Supply

A custom optical tachometer and signal conditioner were built to monitor rotor velocity. The tachometer uses a motor-mounted optical interrupter and slotted disk for accurate direct RPM measurements through counters as can be seen in Figure 3.7.

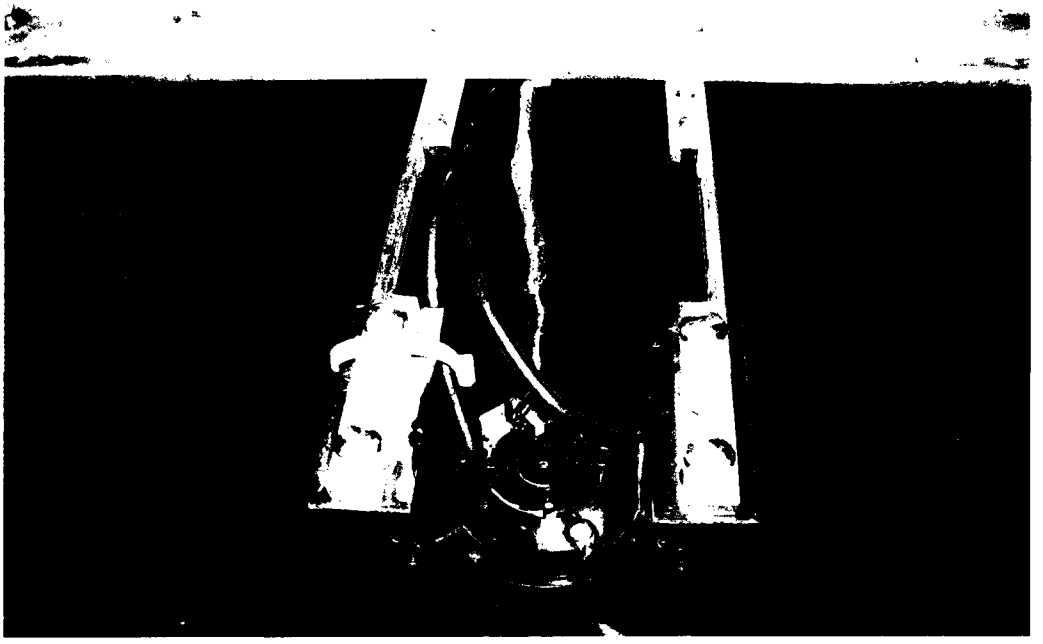

Figure 3.7 Tachometer with slotted disc and photo interrupter

A 3 kg capacity, temperature compensated, single-point, Omega LCDA strain gage load cell was positioned between the traverse support and the motor for direct measurement of rotor thrust. A custom signal conditioner and amplifier provided an analog output to the PC based data acquisition system. The load cell was calibrated before use and tested over the rotor speed range to verify that any inherent vibrations in either the load cell or traverse mounting did not reach resonance. The overall dimensions of the load cell are presented in Figure 3.8. The assembly of the DC motor, load cell, tachometer, and manual traverse mechanism, are presented in Figure 3.9.

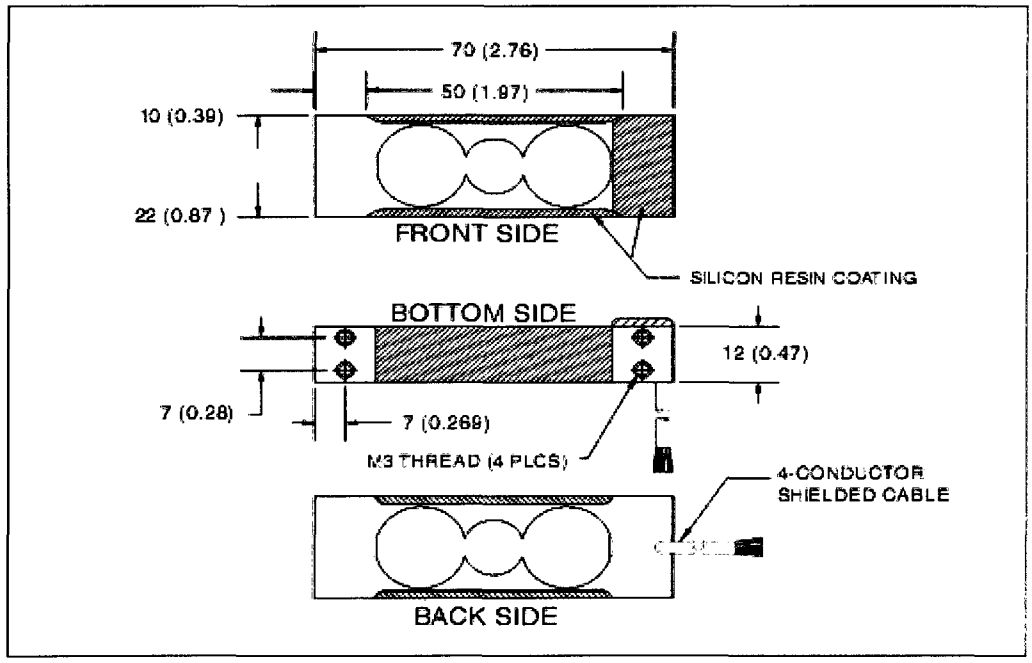

Figure 3.8 Omega LCAE Single-point Load Cell

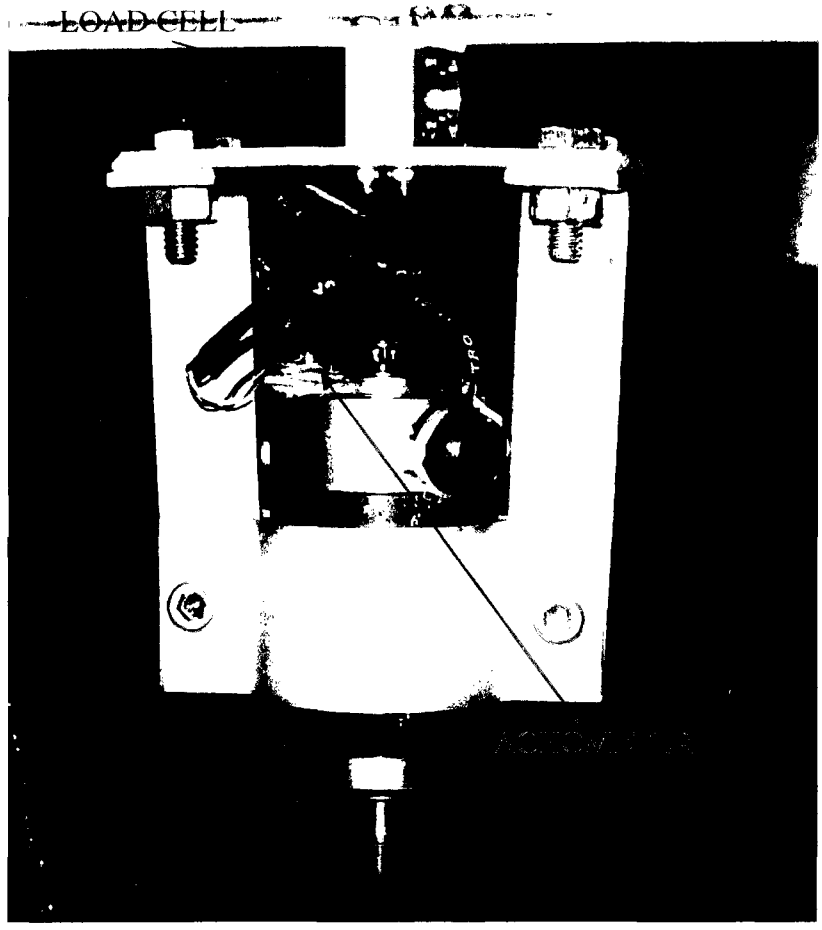

Figure 3.9 DC Motor, Load Cell and Tachometer Combination

A small two degree-of-freedom traverse was designed, built, and leveled to position the rotor over the longitudinal center plane of the frigate deck and allow movement in the longitudinal and vertical direction (x and z). The manual traverse mechanism is presented in Figure 3.10 and the coordinate system used for all data reported is shown in figure 3.11.

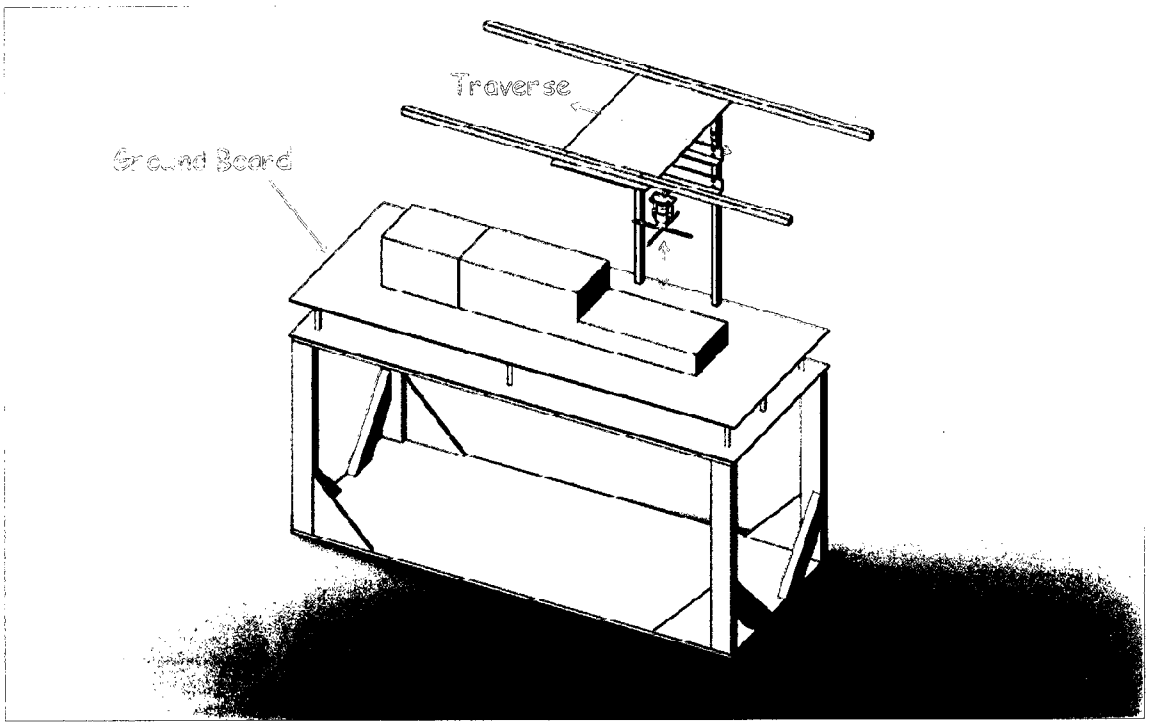

Figure 3.10 Manual Traverse Mechanism

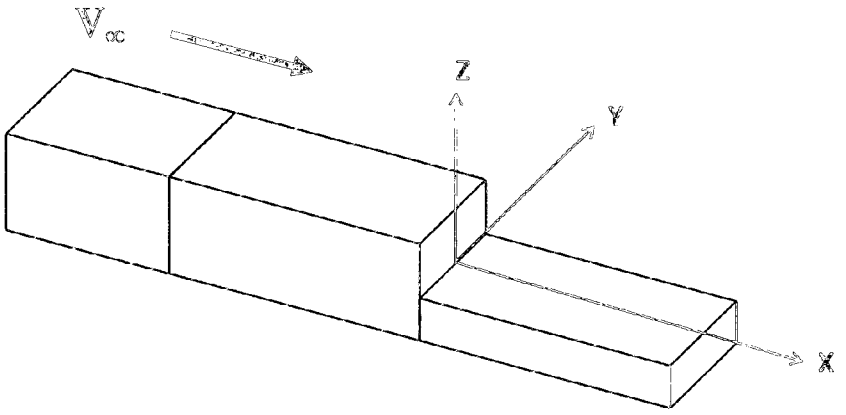

Figure 3.11 Coordinate System

3.4 Data Acquisition and Measurement System Software

A 16-bit National Instruments NI PCI-6221 data acquisition board and PC were used to digitize the rotor load cell output voltage and provide the counting function for computing RPM. A LabView® program integrated the acquisition of wind tunnel speed, temperature, dynamic pressure, rotor RPM and thrust measurement readings for the experiments. The measurement program control provided adjustable sampling rates as well as real-time monitoring of all parameters. The LabView program screen prepared for this study can be seen in Figure 3.12.

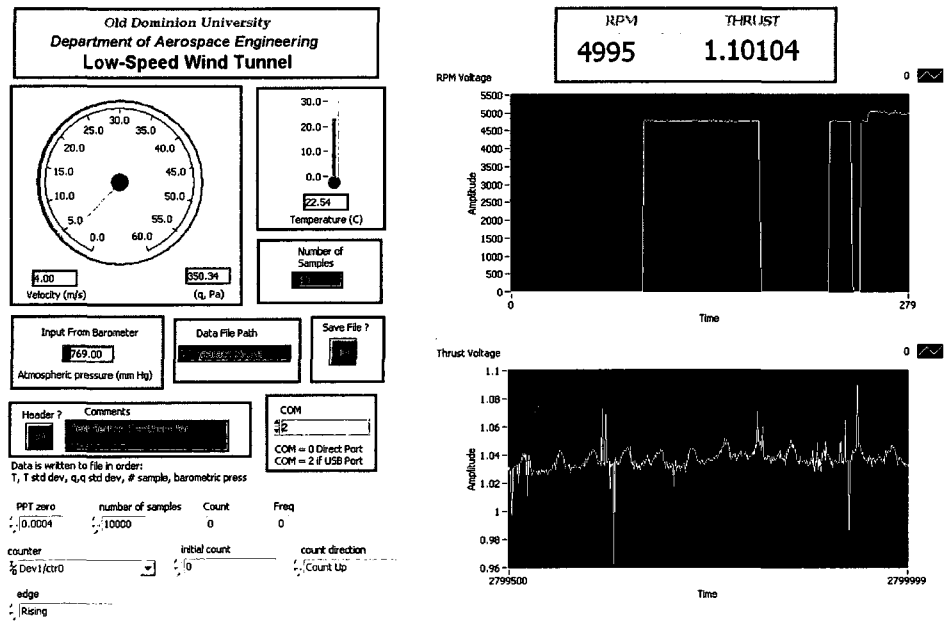

Figure 3.12 LabView based Data Acquisition Screen

3.5 Particle Image Velocimetry (PIV) System

3.5.1 Introduction to the PIV System

The ODU PIV system has the ability to measure a global velocity vector field over a planar slice of flowfield limited to approximately 8.5 x 11 inches. It can be configured either to obtain all three components of a velocity vector, or it can be limited to the two components in the survey plane. Valuable information for understanding flowfield structures and temporal statistics can be developed from multiple sequential measurements using the PIV system.

For observation of the flowfield, illumination with two consecutive bright light flashes is required and pulsed lasers are currently the best light sources for this purpose. Velocity vectors are resolved from the displacements of seeding particles introduced into the flow by vaporizing mineral oil. CCD cameras are used to capture two images of the laser illuminated flowfield. PC based image processing is then used to track particle displacements from one frame to the second and by knowing the time delay between frames, velocity is calculated.

3.5.2 PIV System Hardware Overview

Synchronizers for timing laser pulses, cameras and the laser light source make up the hardware essential to PIV measurements (Figure 3.13). The ODU PIV system is manufactured by TSI and composed of a dual pulse New Wave Solo PIV Nd-YAG laser capable of 50 mJ/pulse (Figure 3.14), a PIVCam 13-8 cross correlation camera with 1280x1024 pixel resolution, and a 12-bit intensity dynamic range PC frame grabber card

(Figure 3.15). The system is controlled by TSI Insight software with a maximum frame rate of 3.75 fps for 2-D and 1.875 fps for stereo measurements. The 2-D and stereo camera setup can be seen in Figure 3.16[35]. The air flow is seeded with mineral oil 'smoke' to make it visible to the CCD camera using a smoke generator (Figure 3.17). A Magnum 550 theatrical 'fog' generator provided the required smoke for all PIV measurements in this experiment.

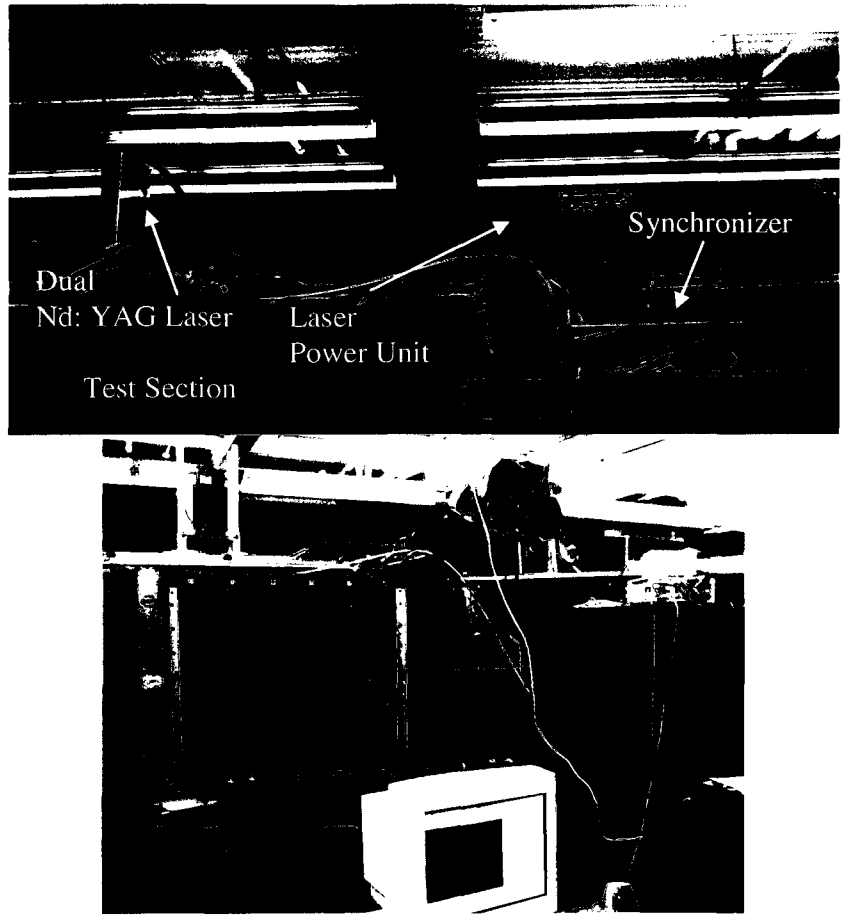

Figure 3.13 Hardware arrangements of PIV System

Figure 3.14 Dual Nd:YAG Laser

Figure 3.15 TSI PIVCAM 13-8 Model 630047

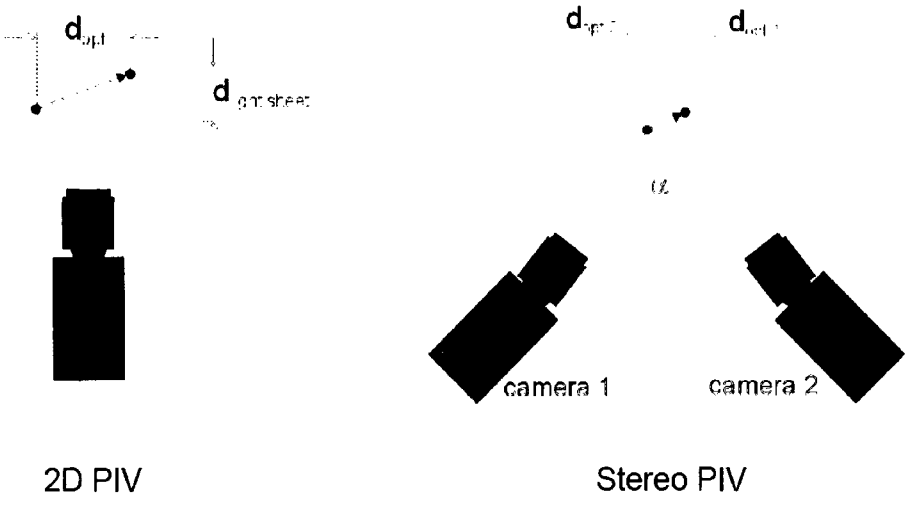

Figure 3.16 2-D and Stereo PIV Camera Setup

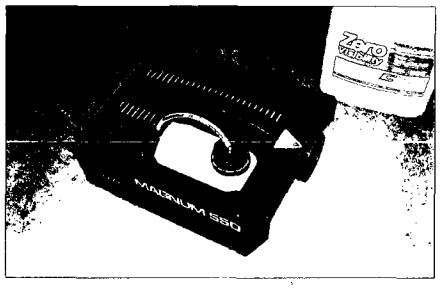

Figure 3.17 Smoke Generator

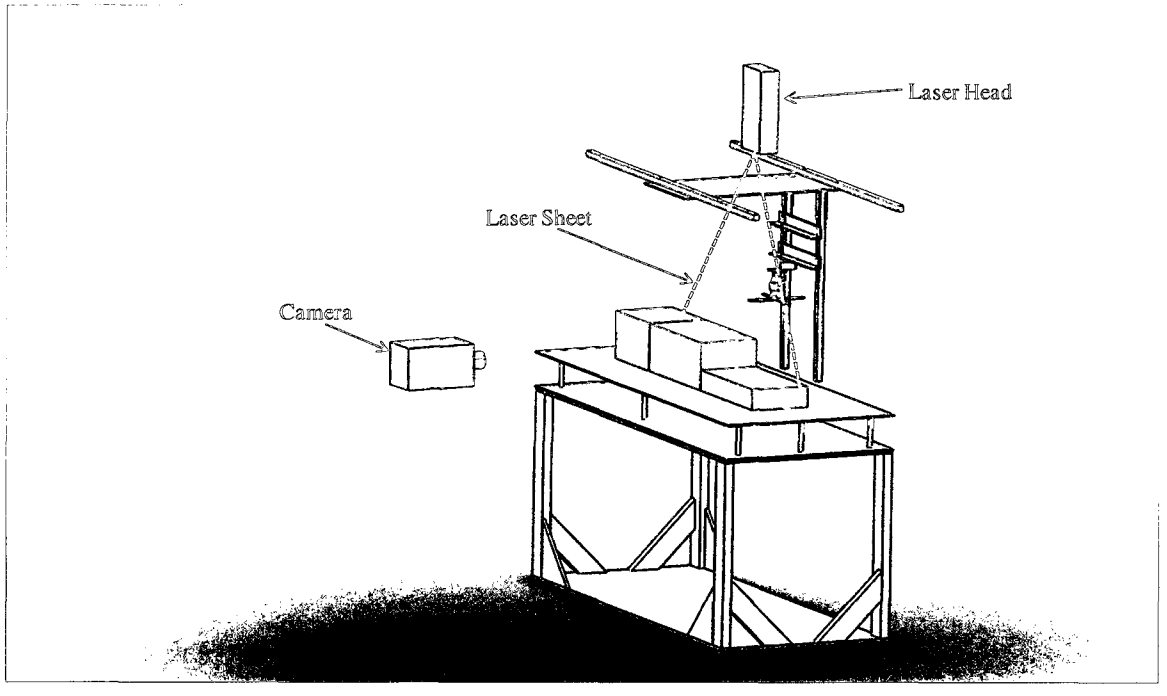

Figure 3.18 Overall Experimental Setup

3.5.3 PIV Settings for the Experiments Performed

The ODU PIV system is composed of a dual pulse Nd-YAG laser capable of 50 mJ/pulse, a PIVCam 13-8 cross correlation camera with 1280x1024 pixel resolution, and a 12-bit intensity dynamic range PC frame grabber card. The system is controlled by TSI Insight software with a frame rate of 3.75 fps for 2D measurements.

PIV settings for the low speed test section are presented below:

- Lens: 50mm, f 2.8
- Timing, dT (μs): 50
- Laser Pulse Rep Rate (Hz): 3.75
- Shutter Open Time (μs): 255
- Timeout (μs): 5000
- Model: New Wave Solo Mini Yag
- Resolution:

	X	Y
Pixels	1280	1024
Spacing (μm)	6.7	6.7

Table 3.1 Resolution Values for Camera Setup

4. DESIGN AND ANALYSIS OF GENERAL FACTORIAL EXPERIMENTS

4.1 Background

Design of Experiments (DOE) is a systematic approach to investigation of a system or process[36]. Experimental methods are widely used in research as well as in industrial settings. An experiment can be defined as a test. Furthermore, an experiment can be defined as a test or a series of tests in which purposeful changes are made to input variables of a process or system so that we may observe and identify the reasons for changes that may be observed in the output response[37]. In general, experiments are used to study the performance of processes and systems. The process or system can be represented by the model shown in Figure 4.1. The process can be visualized as a combination of operations, machines, methods, people, and other resources that transform some input into an output that has one or more observable response variables.

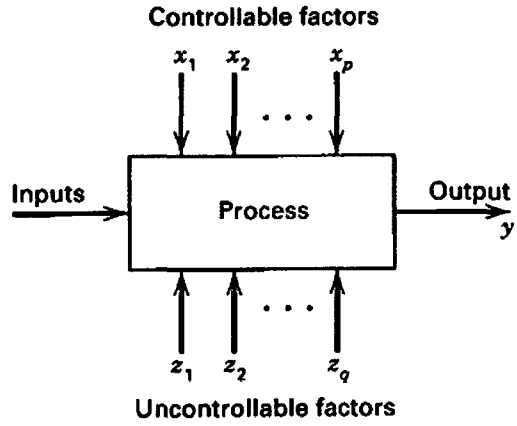

Figure 4.1 General Model of Process or System[39]

Experiments are widely used throughout the engineering world for process characterization and optimization, evaluation of material properties, product design and development, as well as component and system tolerance determination.

DOE is important as a way of maximizing information gained for resources required. It has more to offer than 'one factor at a time' experimental methods, because it allows a judgment of the significance of the output due to input variables acting alone, as well as input variables acting in combination with one another. 'One Factor At a Time' (OFAT) testing always carries the risk that the experimenter may find one input variable to have a significant effect on the response (output) while failing to discover that changing another variable may alter the effect of the first (i.e. a dependency or interaction). This is because the temptation is to stop the test when this first significant effect has been found. In order to reveal an interaction or dependency, 'one change at a time' testing relies on the experimenter carrying out the tests in the appropriate direction. However, DOE plans for all possible dependencies in the first place and then prescribes exactly what data are needed to assess them, i.e. whether input variables change the response on their own, when combined, or not at all. In terms of resources, the exact length and size of the experiment are set by the design before testing begins[37].

4.2 Definitions and Principles

DOE begins with determining the objectives of an experiment and selecting the process factors for the study or test. An experimental design is the laying out of a detailed experimental plan in advance of doing the experiment. The amount of information that

can be obtained for a given amount of experimental effort can be maximized by well chosen experimental designs.

In an experiment, factors are the design variables and the values of design variables are called levels. Factors (also called treatments) are process inputs an investigator manipulates to cause a change in the output. A factor is an independent treatment variable whose settings (values) are controlled and varied by the experimenter. Some factors cannot be controlled by the experimenter but may affect the responses. Noise factors are variables over which we have no control. Control factors are the variables which we can control. Outputs are known as responses (or observations) in an experiment.

Experimental data are used to derive an empirical (approximation) model linking the outputs and inputs. The most common empirical models fit to the experimental data take either a first order form or quadratic form. A first order model with two factors, X_1 and X_2, can be written as

$$Y = \beta_0 + \beta_1 \chi_1 + \beta_2 \chi_2 + \beta_{12} \chi_1 \chi_2 + \textit{experimental error} \qquad (4.1)$$

Here, Y is the response for given levels of the main effects X_1 and X_2. The X_1X_2 term is included to account for a possible interaction effect between the factors X_1 and X_2. The constant β_0 is the response of Y when both main effects are 0. For a more complicated example, a first order model with three factors, X_1, X_2, X_3, and one response, Y, can be written as follows;

$$Y = \beta_0 + \beta_1 \chi_1 + \beta_2 \chi_2 + \beta_3 \chi_3 + \beta_{12} \chi_1 \chi_2 + \beta_{13} \chi_3 + \beta_{23} \chi_2 \chi_3 + \beta_{123} \chi_1 \chi_2 \chi_3 + \textit{experimental error}$$

The three terms with single X's are the main effects terms. There are k*(k-1)/2 = 3*2/2 = 3 two-way interaction terms and 1 three-way interaction term. When the experimental data are analyzed, the entire unknown β parameters are estimated, and the coefficients of the X terms are tested to see which ones are significantly different from 0.

A pure second-order (quadratic) model does not include the three-way interaction term, but adds three more terms to the linear model, namely

$$Y = \beta_{11}\chi_1^2 + \beta_{22}\chi_2^2 + \beta_{33}\chi_3^2$$

4.3 Foundations of Experimental Design

A methodology for designing experiments was proposed by Ronald A. Fisher in his innovative book *The Design of Experiments*. As an example, he described how to test the hypothesis that a certain lady could distinguish by flavor alone whether the milk or the tea was first placed in the cup. While this sounds like a frivolous application, it allowed him to illustrate the most important ideas of experimental design. Fisher systematically introduced statistical thinking and principles into designing experimental investigations, including the factorial design concept and analysis of variance.

Steps to a successful designed experiment can be defined as:

1. Recognition of and statement of problem;
2. Choice of factors, levels, and ranges;
3. Selection of the response variable(s);
4. Choice of design (such as factorial);

5. Conducting the experiment;

6. Statistical analysis and model building;

7. Discovery, Interpretation, Optimization.

Statistical design of experiments refers to the process of planning the experiment so that the appropriate data that can be analyzed by statistical methods will be collected resulting in valid and objective conclusions. The statistical approach to experimental design is necessary to draw meaningful conclusions from the data. When the problem involves data that are subject to experimental errors, statistical methods are the only objective approach to analysis[37]. Thus, there are two aspects to any experimental problem. These are the design of the experiment and the statistical analysis of the data. These two subjects are closely related because the method of analysis depends directly on the design employed.

The three basic principles of experimental design are randomization, replication and blocking. Randomization is a schedule for allocating treatment material and for conducting treatment combinations in a DOE such that the conditions in one run neither depend on the conditions of the previous run nor predict the conditions in the subsequent runs. By randomization we mean that both the allocation of the experimental material and the order in which the individual runs or trials of the experiment are to be performed are randomly determined. Randomization refers to the order in which the trials of an experiment are performed. A randomized sequence helps eliminate effects of unknown or uncontrolled variables.

Replication is an independent repeat of a factor combination. It can also be defined as performing the same treatment combination more than once. Replication has two important properties. First, it allows the experimenter to obtain an estimate of the experimental error. This estimate of error becomes a basic unit of measurement for determining whether observed differences in the data are really statistically different. Second, if the sample mean is used to estimate the true mean response for one of the factor levels in the experiment, replication permits the experimenter to obtain a more precise estimate of this parameter.

Blocking is a design technique used to improve the precision of comparisons among the factors of interest. It is a schedule for conducting treatment combinations in an experimental study such that any effects on the experimental results due to a known change in raw materials, operators, machines, etc., become concentrated in the levels of the blocking variable[37,38]. The reason for blocking is to isolate a systematic effect and prevent it from obscuring the main effects. Blocking is achieved by restricting randomization. Often blocking is used to reduce or eliminate the variability transmitted from nuisance factors. That is, factors that may influence the experimental response but in which experimenter is not interested.

4.4 Statistical Analysis of the Single Factor Experiment

4.4.1 Analysis of Variance

Analysis of Variance (ANOVA) can be described as a mathematical process for separating the variability of a group of observations into assignable causes and setting up

various significance tests[37,39]. This name is derived from the fact that in order to test for statistical significance between means, variances are actually compared (i.e., analyzed). The procedure known as ANOVA is used to test hypotheses concerning means when there are several populations. ANOVA is a general technique that can be used to test the hypothesis that the means among two or more groups are equal, under the assumption that the sampled populations are normally distributed[40].

At the heart of ANOVA is the fact that variances can be partitioned- that is, divided into component contributions. The name analysis of variance stems from a partitioning of the total variability in the response variable into components that are consistent with a model for the experiment. The variance is computed as the sum of squared deviations from the overall mean, divided by the available degrees of freedom, n-1 (sample size minus one – due to estimating the mean)

$$S^2 = \frac{1}{n-1}\sum_{i=1}^{n}(y_i - \bar{y})^2 \quad (4.2)$$

Thus, given a certain n, the sample variance is a function of the sums of (deviation) squares[37].

4.4.1.1 Models for the Data

It is useful to describe the observations from an experiment with a model. One way to write this model is

$$y_{ij} = \mu_i + \varepsilon_{ij} \begin{cases} i=1, 2, 3, \ldots, a \\ j=1, 2, 3, \ldots, n \end{cases} \quad (4.3)$$

where y_{ij} is the *ij*th observation, μ_{ij} is the mean of the *i*th factor level or treatment, and ε_{ij} is a random error component that incorporates all other sources of variability in the experiment. These sources include variability arising from uncontrolled factors, differences between the experimental units to which the treatments are applied, and the general background noise in the process (such as variability over time, effects of environmental variables)[37]. It is convenient to think of the errors as having mean zero, so that $E(y_{ij}) = \mu_i$.

Equation 4.3 is called the means model. An alternative way to write a model for the data is to define

$$\mu_i = \mu + \tau_i, \qquad i = 1, 2, 3, \ldots, a$$

so that Equation 4.3 becomes

$$y_{ij} = \mu + \tau_i + \varepsilon_{ij} \quad \begin{cases} i=1, 2, 3, \ldots, a \\ j=1, 2, 3, \ldots, n \end{cases} \tag{4.4}$$

In this form of the model, known as the effects model, μ is a parameter common to all treatments called the overall mean, and τ_i is a parameter unique to the *ith* treatment called the *ith* treatment effect. Here the effects are seen to vary from the overall mean μ by the treatment effect τ. Both the means model and the effects model are linear statistical models. That is, the response variable y_{ij} is a linear function of the model parameters. The effects model is more widely encountered in the experimental design literature, although both forms of the model are useful. It has some intuitive appeal in that

μ is a constant and the treatment effects τ_i represent deviation from this constant when the specific treatments are applied.

Equation 4.4 (or Equation 4.3) is also called the one-way or single-factor analysis of variance (ANOVA) model because only one factor is investigated.

4.4.1.2 Partitioning Variance

A typical dataset for a single factor experiment is presented in Table 4.1. A dot indicates summation on the index it replaces and each individual observation will be shown as y_{ij} where the i subscript indicates the treatment level and j the replicate at this treatment level.

Treatment(level)	Observations	Totals	Averages
1	y_{11} y_{12} ... y_{1n}	$y_{1.}$	$\bar{y}_{1.}$
2	y_{21} y_{22} ... y_{2n}	$y_{2.}$	$\bar{y}_{2.}$
.	. . ... .	.	.
A	y_{a1} y_{a2} ... y_{an}	$y_{a.}$	$\bar{y}_{a.}$

Table 4.1 Typical Data for a Single Factor Experiment

The name ANOVA is derived from a partitioning of total variability into its component parts. The total corrected sum of squares

$$SS_T = \sum_{i=1}^{a}\sum_{j=1}^{n}\left(y_{ij} - \bar{y}_{..}\right)^2$$

is used as a measure of overall variability in the data. This is reasonable due to division of SS_T by the appropriate number of degrees of freedom; the resultant will be the sample variance of the y's. The sample variance is a standard measure of variability.

The total corrected sum of squares SS_T may be written as

$$\sum_{i=1}^{a}\sum_{j=1}^{n}\left(y_{ij} - \bar{y}_{..}\right)^2 = \sum_{i=1}^{a}\sum_{j=1}^{n}\left[\left(\bar{y}_{i.} - \bar{y}_{..}\right) + \left(y_{ij} - \bar{y}_{i.}\right)\right]^2 \qquad (4.5)$$

or

$$\sum_{i=1}^{a}\sum_{j=1}^{n}\left(y_{ij} - \bar{y}_{..}\right)^2 = n\sum_{i=1}^{a}\left(\bar{y}_{i.} - \bar{y}_{..}\right)^2 + \sum_{i=1}^{a}\sum_{j=1}^{n}\left(y_{ij} - \bar{y}_{i.}\right)^2 + 2\sum_{i=1}^{a}\sum_{j=1}^{n}\left(\bar{y}_{i.} - \bar{y}_{..}\right)\left(y_{ij} - \bar{y}_{i.}\right)$$

However, the cross-product term in this last equation is zero because

$$\sum_{j=1}^{n}\left(y_{ij} - \bar{y}_{i.}\right) = y_{i.} - n\bar{y}_{i.} = y_{i.} - n\left(y_{i.}/n\right) = 0$$

Therefore, the resultant is

$$SS_T = \sum_{i=1}^{a}\sum_{j=1}^{n}\left(y_{ij} - \bar{y}_{..}\right)^2 = n\sum_{i=1}^{a}\left(\bar{y}_{i.} - \bar{y}_{..}\right)^2 + \sum_{i=1}^{a}\sum_{j=1}^{n}\left(y_{ij} - \bar{y}_{i.}\right)^2 \qquad (4.6)$$

Equation 4.6 is the fundamental ANOVA identity[37,38,40]. It states that the total variability in the data, as measured by the total corrected some of squares, can be partitioned into a sum of squares of the differences between the treatment means and the

grand mean, plus a sum of squares of the differences of observations within treatments from the treatment mean. The difference between the observed treatment means and the grand mean is a measure of the differences between treatment means. The differences of observations within a treatment from the treatment average can be due only to random error. Thus, Equation 4.5 can be written symbolically as

$$SS_T = SS_{\text{Treatments}} + SS_E$$

where $SS_{\text{Treatments}}$ is called the sum of squares due to treatments (i.e. between treatments), and SS_E is called the sum of squares due to error (i.e. within treatments). There are $an=N$ total observations, thus SS_T has N-1 degrees of freedom. There are a levels of the factor (and a treatment means), so $SS_{\text{Treatments}}$ has a-1 degrees of freedom. There are n replicates providing n-1 degrees of freedom with which to estimate the experimental error, within any treatment. Because there are a treatments, there are $a(n\text{-}1) = an\text{-}a=N\text{-}a$ degrees of freedom for error.

4.4.1.3 Hypothesis Testing

There are two types of statistical inferences. These are estimation of population parameters and hypothesis testing. Hypothesis testing is one of the most important tools when applying statistics to real life problems[36]. Fundamentally, a hypothesis is a statement. The decision making procedure to prove or disprove the statement is called a hypothesis test. A statistical hypothesis is a statement about the parameters of one or more populations. Most often, decisions are required to be made concerning populations on the basis of sample information. Statistical tests are used in arriving at these decisions.

A hypothesis test relies on information from random samples from a population of interest. If the information is consistent with the hypothesis then it is concluded that it is true. If the information is inconsistent then it is concluded that it is false.

A test statistic is a quantity calculated from the sample of data that is studied. Its value is used to decide whether or not the null hypothesis should be rejected in the hypothesis test. The choice of a test statistic will depend on the assumed probability model and the hypotheses under question.

There are five ingredients to any statistical test:

1. Null Hypothesis;
2. Alternate Hypothesis;
3. Test Statistics;
4. Rejection/Critical Region;
5. Conclusion.

In attempting to reach a decision, it is useful to make an educated guess or assumption about the population involved, such as the type of distribution.

Statistical hypotheses are often defined as assertions about the parameter or parameters of a population, for example the mean or the variance of a normal population[40]. They may also concern the type, nature or probability distribution of the population. Statistical hypotheses are based on the concept of proof by contradiction. This proof of contradiction is done by formulating a null hypothesis.

A null hypothesis is a hypothesis that states that there is no difference between procedures and is denoted by H_0. The null hypothesis is always tested, i.e., the null hypothesis shall be either accepted or rejected. The alternative hypothesis is a hypothesis that states that there is a difference between the procedures and is denoted by H_1.

Special consideration is given to the null hypothesis, because the null hypothesis relates to the statement being tested, whereas the alternative hypothesis relates to the statement to be accepted if / when the null is rejected. Statisticians will always state the final conclusion once the test has been carried out in terms of the null hypothesis. The conclusion is either 'Reject H_0' or 'Do not reject H_0; it is never concluded that 'Reject H_1', or even 'Accept H_1'. If the conclusion is 'Do not reject H_0', this does not necessarily mean that the null hypothesis is true. It only suggests that there is not sufficient evidence against H_0 in favour of H_1. Rejecting the null hypothesis, then, suggests that the alternative hypothesis may be true. Various types of the null and the alternative hypothesis are represented in Table 4.2.

Case	Null Hypothesis H_0	Alternate Hypothesis H_1
1	$\mu_1=\mu_2$	$\mu_1\neq\mu_2$
2	$\mu_1\leq\mu_2$	$\mu_1>\mu_2$
3	$\mu_1\geq\mu_2$	$\mu_1<\mu_2$

Table 4.2 Various Types of H_0 and H_1 for Means Testing

The formal statistical hypothesis can be seen in Table 4.3.

Means Model	Effects Model
$H_0=\mu_1=\mu_2=.....=\mu_a$	$H_1=\tau_1=\tau_2=.....=\tau_a$
H_1: At least one mean different	H_1: At least one $\tau_i \neq 0$

Table 4.3 Formal Statistic Hypothesis for Means Testing

The sums of squares cannot be directly compared to test the hypothesis of equal means but mean squares can be compared. A mean square is a sum of squares divided by its degrees of freedom.

$$df_{Total} = df_{Treatments} + df_{Mean}$$

$$an-1=a-1+a(n-1)$$

$$MS_{Treatments} = \frac{SS_{Treatments}}{a-1}\ ;\ MS_{Error} = \frac{SS_{Error}}{a(n-1)}$$

In the case of performing multiple comparisons by one way ANOVA, the F-statistic is normally used. It is defined as the ratio of the mean square due to the variability between groups to the mean square due to the variability within groups. It is most often used when comparing statistical models that have been fit to a data set, in order to identify the model that best fits the population from which the data were sampled[37,40]. The F statistic is used to test for equal variances of random variables from normally distributed populations.

$$F_0 = \frac{MS_{Treatmnts}}{MS_E} \qquad (4.7)$$

The implicit assumption is that the residuals will be independent, normally distributed and have relatively constant variance. The critical value of F is obtained from tables of the F-distribution (or software) knowing the type I error and the degrees of freedom between and within the groups. In a hypothesis test, a type I error occurs when the null hypothesis is rejected when it is in fact true. That is, H_0 is wrongly rejected. Type I error occurs with probability α, called the significance level. The significance level of a statistical hypothesis test is a fixed probability of wrongly rejecting the null hypothesis H_0, if it is in fact true. It is the probability of a type I error and is set by the investigator in relation to the consequences of such an error before testing begins. It is desired to choose a significance level as small as possible in order to protect the null hypothesis and to prevent, as far as possible, the investigator from inadvertently making false claims.

In a hypothesis test, a type II error (with probability of β) occurs when the null hypothesis H_0, is not rejected when it is in fact false. Table 4.4 gives a summary of possible types of error and their associated probabilities.

Type of Decision	**H_0 True in Reality**	**H_0 False in Reality**
Reject H_0	Type I error (α)	Correct decision ($1-\beta$)
Accept H_0	Correct decision ($1-\alpha$)	Type II error (β)

Table 4.4 Types of Error

A related concept is power, which is the probability of rejecting the null hypothesis when it is actually false. Power is simply 1 minus the type II error rate, and is expressed as 1-β. When choosing the probability level of a test, it is possible to control the risk of committing a type I error by choosing an appropriate α. The type II error will depend on α, the number of samples, n, the population standard deviation (σ) and the difference in means you are trying to detect (δ). The reference distribution for F_0 is the $F_{\alpha,a-1,a(n-1)}$ distribution. If $F_0 > F_{\alpha,a-1,a(n-1)}$ then there is evidence that at least one of the treatment means is different than the grand mean. Null hypothesis is rejected if $F_0 > F_{\alpha,a-1,a(n-1)}$.

The ANOVA table for the single factor, fixed effects model is presented in Table 4.5.

Table 3-3 The Analysis of Variance Table for the Single-Factor, Fixed Effects Model

Source of Variation	Sum of Squares	Degrees of Freedom	Mean Square	F_0
Between treatments	$SS_{\text{Treatments}} = n\sum_{i=1}^{a}(\bar{y}_{i.} - \bar{y}_{..})^2$	$a - 1$	$MS_{\text{Treatments}}$	$F_0 = \frac{MS_{\text{Treatments}}}{MS_E}$
Error (within treatments)	$SS_E = SS_T - SS_{\text{Treatments}}$	$N - a$	MS_E	
Total	$SS_T = \sum_{i=1}^{a}\sum_{j=1}^{n}(y_{ij} - \bar{y}_{..})^2$	$N - 1$		

Table 4.5 The ANOVA Table for Single Factor, Fixed Effects Model[37]

Steps in hypothesis testing can be given as below:

1. Identify the null hypothesis H_0 and the alternate hypothesis H_1.
2. Choose α. The value should be small, usually less than 10%. It is important to consider the consequences of both types of errors.

3. Select the test statistic and determine its value from the sample data. This value is called the observed value of the test statistic.
4. Compare the observed value of the statistic to the critical value obtained for the chosen α.
5. Make a decision.
6. If the test statistic falls in the critical region, Reject H_0 in favour of H_1.
7. If the test statistic does not fall in the critical region: Conclude that there is not enough evidence to reject H_0.

ANOVA test is based on the variability between the sample means. This variability is measured in relation to the variability of the data values within the samples. These two variances are compared through means of the *F* ratio test. If there is a large variability between the sample means, this suggests that not all the population means are equal. When the variability between the sample means is large compared to the variability within the samples, it can be concluded that not all the population means are equal.

4.4.2 Statistical Analysis of the Single Factor Experiment

A small scale simple frigate model and powered rotor are being used to investigate the wake interaction between rotor downwash and the ship airwake in this study. A characterization experiment was performed with one factor which is vertical distance (z). We are interested in the effect of changing the vertical distance of the rotor from the ships landing deck on thrust coefficient change (C_T), which is a single factor characterization experiment that will serve as an example here.

The experimental case for a single factor experiment is presented schematically in Figure 4.3. A grid of thrust measurement locations for this single factor experiment can be seen in Table 4.6.

Six levels of vertical distance (A,B,C,D,E,F) are chosen for this single factor experiment. The experiment is replicated 2 times and runs made in random order. This test used a rotor rotational speed of 5,000 rpm and a tunnel freestream velocity of 5.14 m/s in order to give an advance ratio of approximately 0.075 which replicates a full-scale frigate velocity of 32 knots.

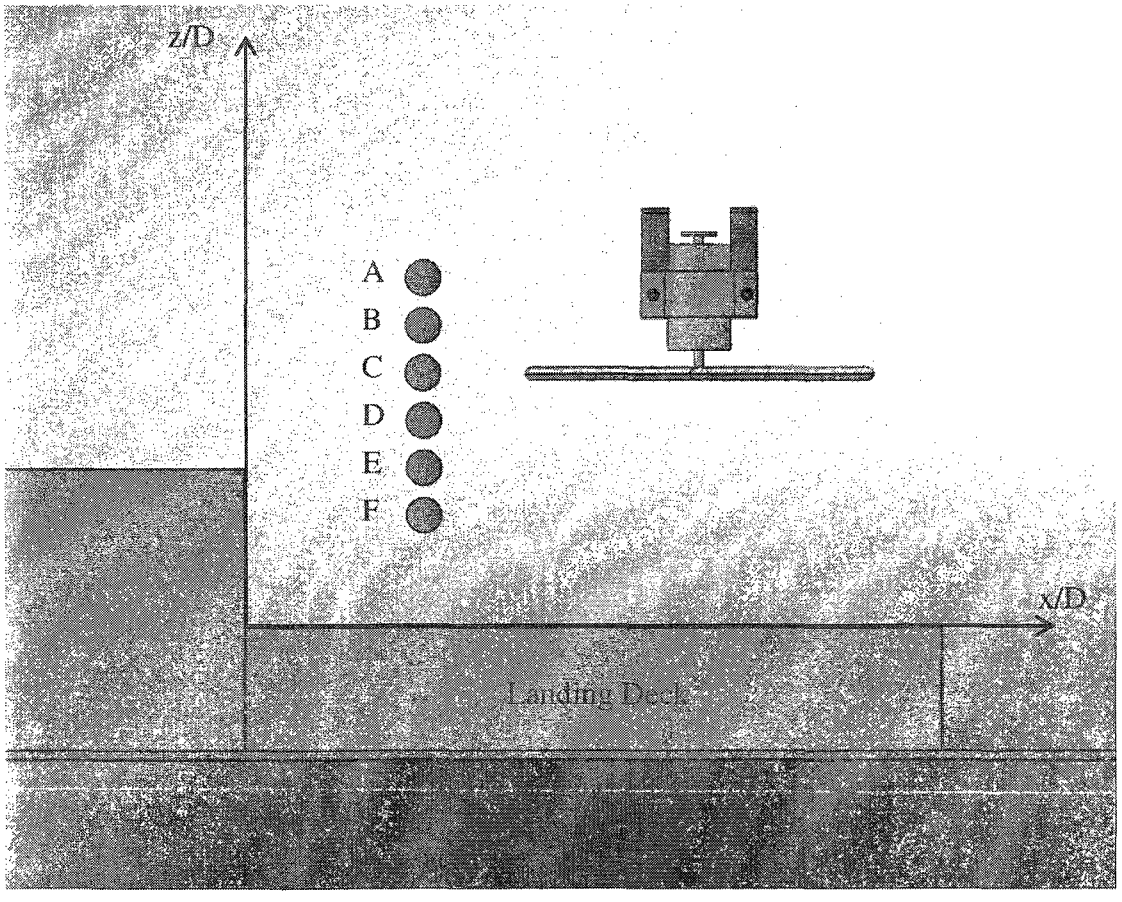

Figure 4.2 Thrust Measurement Single Factor Experiment Case

Points	(x/D; z/D)
A	(0.5125 ;0.85)
B	(0.5125 ;0.75)
C	(0.5125 ;0.65)
D	(0.5125 ;0.55)
E	(0.5125 ;0.45)
F	(0.5125 ;0.35)
Height of hangar	(0 ;0.45)

Table 4.6 Grid of Measurement Locations

The 1st single factorial experiment was performed to investigate the feasibility of measuring significant changes in thrust coefficient (C_T) due to the (factor) vertical distance (z) above landing deck. A regression model with thrust coefficient as the response {C_T = f [z]} and the significance of the regression model coefficients tested using ANOVA. Stat-Ease® version 7.1 of Design Expert software for design of experiments (DOE) was used to analyze the single factor experiment. Design Expert ANOVA output for C_T change is presented in Figure 4.4 for the single factorial experiment performed. From the ANOVA report of the software, it can be clearly seen that the model is statistically significant. This is based on the default confidence level of 95% (5% level of significance). The annotated ANOVA report also includes an

indication as to whether or not the lack of fit test for the selected model is statistically significant or not. Lack of fit is the variation of the data around the fitted model. If the model does not fit the data well, this will be significant. Measures of goodness of fit typically summarize the discrepancy between observed values and the values expected under the model in question. Here the lack of fit test requires calculation of a mean square composed of a sum of squares of residuals from fitted versus measured response, adjusted for the degrees of freedom. This mean square due to lack of fit serves as the numerator for an F-test with the mean square for pure error as the denominator. The mean square for pure error is a model-independent measure obtained from pure replicates. The test is evaluating the variance estimates from model residuals versus the variance estimates from random error. In the single factor example case shown here, the lack of fit test for the model is statistically insignificant.

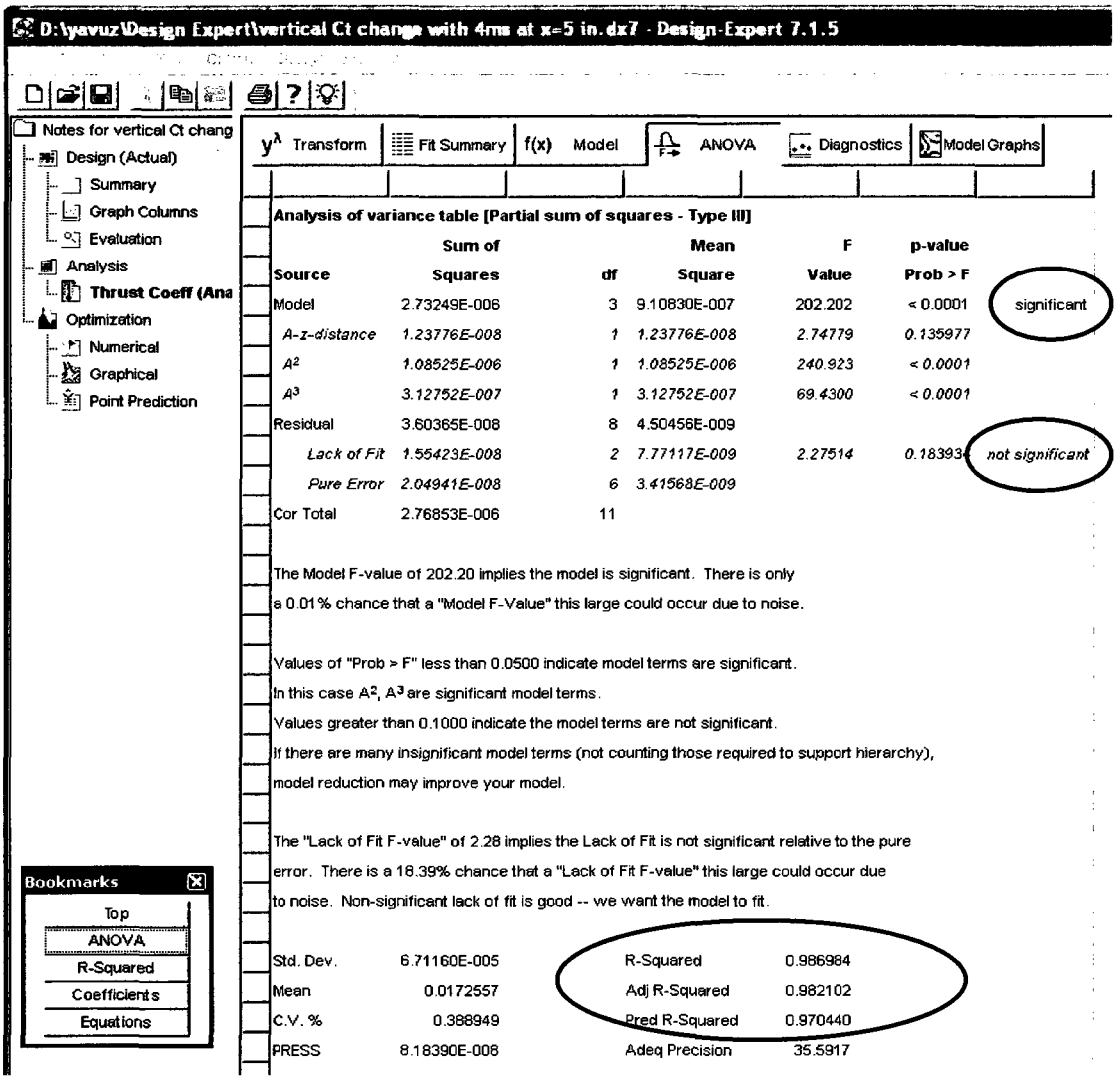

Figure 4.3 Design Expert ANOVA Report for Single Factor Experiment

In statistics, a result is called statistically significant if it is unlikely to have occurred by chance, a statistically significant difference means there is statistical evidence that there is a difference. It does not mean the difference is necessarily large, important, or significant in the common meaning of the word[39]. The significance level is a traditional statistical hypothesis testing concept. In simple cases, it is defined as the probability of making a decision to reject the null hypothesis when the null hypothesis is

actually true. The decision is often made using the p-value. If the p-value is less than the significance level, the null hypothesis is rejected. The p-value is a measure of how much evidence we have against the null hypothesis and is expressed as a probability. It is the smallest level of significance that would lead to rejection of the null hypothesis. Table 4.7 presents the relative statistical significance in cases according to p-value for a 5% level of significance (0.05 probability).

P-Value	Interpretation
Less than 0.01	Highly statistically significant: Very strong evidence against the null hypothesis
0.01 to 0.05	Statistically significant: Adequate evidence against the null hypothesis
Greater than 0.05	Insufficient evidence against the null hypothesis

Table 4.7 Statistical Significance According to P-Values

The coefficient of determination, called R-Squared is a measure of the amount of variation around the mean explained by the model. It provides a measure of the proportion of variability in the data explained by the ANOVA model.

$$R^2 = \frac{SS_{Model}}{SS_{Total}} \quad \text{where } 0 \leq R^2 \leq 1$$

Adjusted R-Squared is a measure of the amount of variation around the mean explained by the model, adjusted for the number of terms in the model. The adjusted R-squared decreases as the number of terms in the model increases if those additional terms do not add value to the model. It takes into account the number of factors. Predicted R-Squared is a measure of the amount of variation in new data explained by the model. It provides a measure of how the model will predict the new responses. As a rule of thumb the predicted R-squared and the adjusted R-squared should be within 0.20 of each other. Otherwise, there may be a problem with either the data or the model. For the 1st experiments performed, it can be seen from the ANOVA table (Figure 4.4) that both the predicted R-squared and the adjusted R-squared values are within 0.20.

4.4.2.1 Model Adequacy Checking

The decomposition of the variability in the observations through an analysis of variance identity (Equation 4.6) is a purely algebraic relationship[37]. The use of the partitioning to test formally for no differences in treatment means requires that certain assumptions be satisfied. Specifically, these assumptions are that the observations are adequately described by the model

$$y_{ij} = \mu + \tau_i + \varepsilon_{ij}$$

and that the errors are normally and independently distributed with mean zero and constant but unknown variance σ^2. If these assumptions are valid, the analysis of variance procedure is an exact test of the hypothesis of no difference in treatment means.

In practice, these assumptions will usually not hold exactly[37]. It is usually unwise to rely on the analysis of variance until the validity of these assumptions has been checked. Violations of the basic assumptions and model adequacy can be easily investigated by the examination of residuals. The residual for observation *j* in treatment *i* can be defined as

$$e_{ij} = y_{ij} - \hat{y}_{ij} \qquad (4.8)$$

where $\hat{y}_{ij}$ is an estimate of the corresponding observation y_{ij} obtained as follows

$$\hat{y}_{ij} = \hat{\mu} + \hat{\tau}_i = \bar{y}_{..} + (\bar{y}_{i.} - \bar{y}_{..}) = \bar{y}_{i.} \qquad (4.9)$$

Equation (4.9) shows that the best estimate for the response at the ith treatment level is just the corresponding treatment average. Examination of the residuals should be an automatic part of any analysis of variance. If the model is adequate, the residuals should contain no obvious patterns. Many types of model inadequacies and violations of the underlying assumptions can be discovered through analysis of residuals.

4.4.2.2 The Normality Assumption

A check of the normality assumption could be made by plotting a histogram of the residuals. If the NID(0,σ^2) assumption on the errors is satisfied, this plot should look like a sample from a normal distribution centered at zero[37]. Unfortunately, with small samples, considerable fluctuation in the shape of a histogram often occurs, so the appearance of a moderate departure from normality does not necessarily imply a serious violation of the assumptions. Gross deviations from normality are potentially serious and require further analysis.

A more useful procedure is to construct a normal probability plot of the residuals. If the underlying error distribution is normal, this plot will resemble a straight line. The normal probability plot for the single factor experiment is shown in Figure 4.5[37].

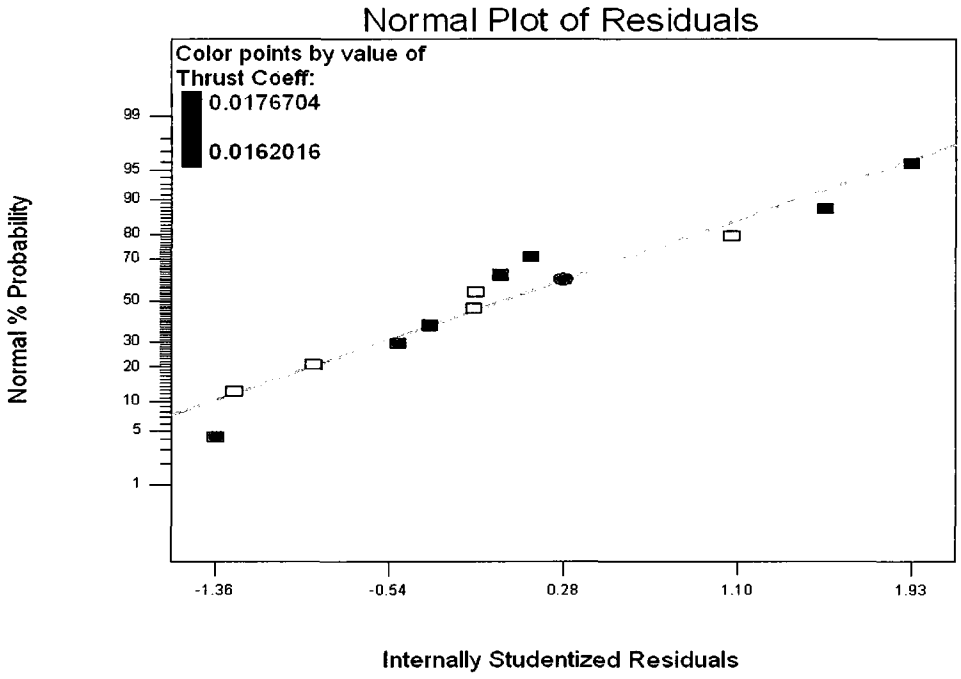

Figure 4.4 Normal Probability Plot of Residuals for Single Factor Experiment

The general impression from examining this display is that the error distribution is approximately normal. In general, moderate departures from normality are of little concern in the fixed effect analysis of variance. An error distribution that has considerably thicker or thinner tails than the normal is of more concern than a skewed distribution. It can be said that the analysis of variance is robust to the normality assumption, because the F test is only slightly affected. Departures from normality usually cause both the true significance level and the power to vary only slightly from the advertised values, with the power generally being lower.

A very common defect that often shows up on normal probability plots is one residual that is very much larger than any of the others. Such a residual is often called an outlier[37,39,40]. The presence of one or more outliers can seriously distort the analysis of variance, so when a potential outlier is located, careful investigation is called for. In our example, there is not an outlier within the normal probability plot.

4.4.2.3 Plot of Residuals in Time Sequence

Plotting the residuals versus time in order of data collection is helpful in detecting correlation between the residuals. We desire a structureless pattern of both positive and negative residuals when plotted versus time. A tendency to have runs of either positive or negative residuals indicates correlation[37,40]. This would imply that the independence assumption on the errors has been violated. This is a potentially serious problem and one that is nearly impossible to correct, so it is important to prevent the problem if possible when the data are collected. Proper randomization of the experiment is an important step in obtaining independence.

Sometimes the skill of the experimenter may change as the experiment progresses, or the process being studied may become more erratic. This will often result in a change in the error variance over time. This condition often leads to a plot of residuals versus time that exhibits more spread at one end than at the other. Nonconstant variance is a potentially serious problem that may be overcome by transformation of the response [37].

Figure 4.5 displays the residuals versus run order time. It allows checking for lurking variables that may have influenced the response during the experiment. The plot

should show a random scatter with time including positive and negative values. Trends here indicate a possible time-related variable lurking in the background. While this plot is far from ideal, the residuals are small and there is evidence of randomness, sign changing and constant variance. For this single factor experiment, it can be concluded that there is little reason to suspect any violation of the independence or constant variance assumptions but to monitor them closely.

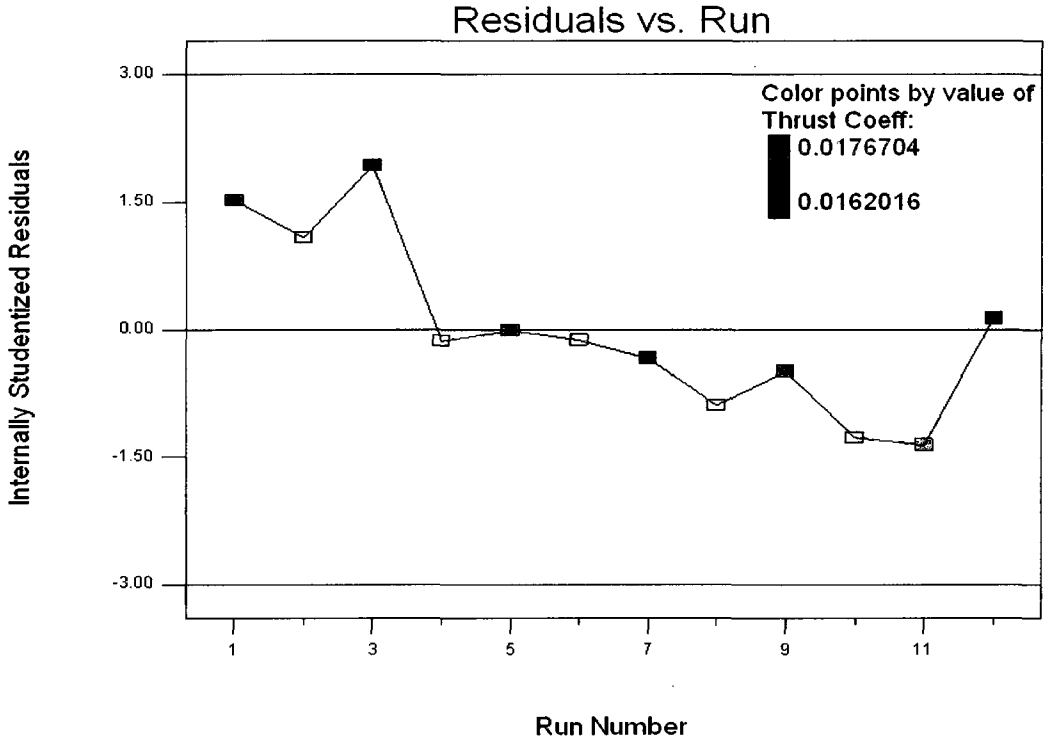

Figure 4.5 Plot of Residuals versus Run Order Time for Single Factor Experiment

4.4.2.4 Plot of Residuals versus Fitted Values

The residuals should be structureless if the model is correct and if the assumptions are satisfied. They should be unrelated to any other variable including the predicted response. A simple check is to plot the residuals versus the fitted values $\hat{y}_{ij}$. For the single factor experiment model, $\hat{y}_{ij} = \bar{y}_{i.}$, the ith treatment average. This plot should not reveal any obvious pattern. Figure 4.6 plots the residuals versus the fitted values for the 1st experiment performed.

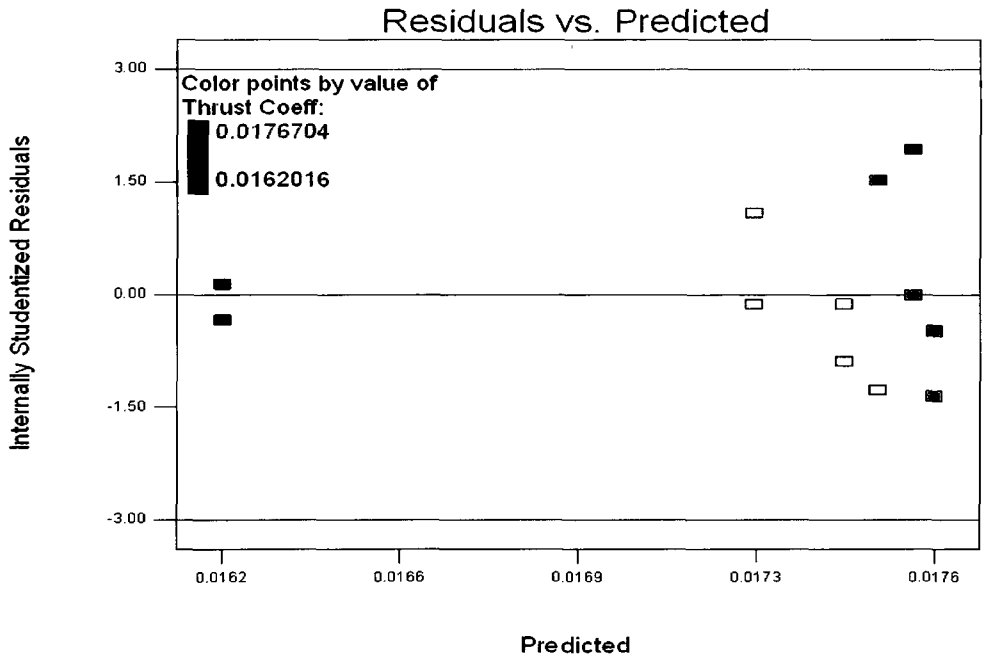

Figure 4.6 Plot of Residuals versus Fitted Values for Single Factor Experiment

As can be seen from Figure 4.7, no unusual structure is apparent although there are relatively few points. A defect that occasionally shows up on this plot is nonconstant variance. Sometimes the variance of the observations increases as the magnitude of the

observation increases. This would be the case if the error or background noise in the experiment was a constant percentage of the size of the observation. If this were the case, the plot of residuals versus $\hat{y}_{ij}$ would look like an outward-opening funnel or megaphone, and the residuals would get as large as y_{ij} gets larger[37]. Nonconstant variance also arises in cases where the data follow a non-normal, skewed distribution. It is because of these skewed distributions the variance tends to be a function of the mean. Analysis is aided by larger data sets.

4.4.2.5 Regression Model

The factors involved in an experiment can be either quantitative or qualitative. A quantitative factor can be described as one whose levels can be associated with points on a numerical scale. Some examples of quantitative factors include temperature, pressure or time. Qualitative factors are factors for which the levels can not be arranged in order of magnitude[38]. Operators and shifts are typical qualitative factors because there is no reason to rank them in any particular numerical order.

It is meaningless to consider the response for a subsequent run at an intermediate level of the factor if the factor is qualitative. The experimenter is usually interested in the entire range of values used, particularly the response from a subsequent run at an intermediate factor level with a quantitative factor. Thus, the experimenter is frequently interested in developing an interpolation equation for the response variable in the experiment. This equation is an empirical model of the process that has been studied.

The general approach to fitting empirical models is called regression analysis. Model graphs provide a nice visual summary of the experiment and with error bars allow comparison of means within the Least Significant Difference (LSD) based error. The LSD test is a statistical procedure that determines if the difference found between two treatments is due to the treatment or if the difference is simply due to random chance[37,39]. For each set of data a value is calculated at a chosen level of significance. If the difference between two treatment means is greater than this calculated value then it is said to be a 'significant difference' or a difference not due to random chance. The level of significance that is most often used and recommended by AIAA is 0.05. In other words, 95% of the time these treatments are compared this difference will occur. Figure 4.7 presents the cubic model fit for normalized vertical distance above deck (z/D) versus the thrust coefficient for the single factor experiment.

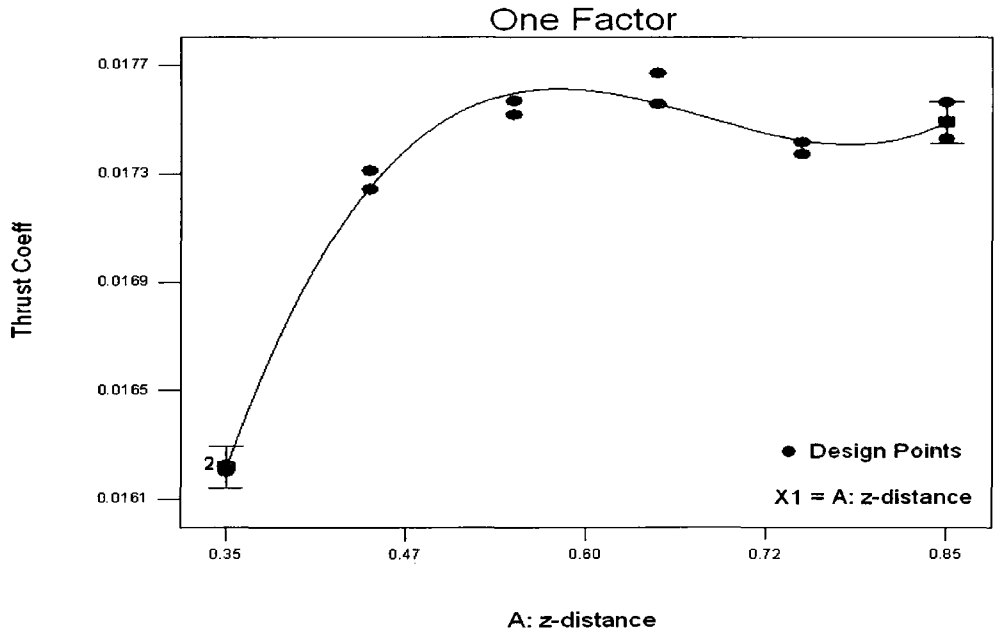

Figure 4.7 Cubic Regression Model for Single Factor Experiment

For this single factor experiment, the thrust coefficient increases with the increase of vertical distance just above the hangar door and then appears to vary with increasing vertical distance. From examining the Figure 4.7, it is clear that there is a strong relation between vertical distance and thrust coefficient. When considering the behavior above z/D = 0.47, one must factor in the uncertainty estimates provided by the aforementioned error bars. Overlapping LSD bars indicate that the differences in means are insignificant.

The subsequent 3rd order cubic regression model for thrust coefficient for the experiment was fit as follows:

$$C_T = 2.97322E\text{-}003 + 0.066993*(z/D) - 0.10048*(z/D)^2 + 0.049124*(z/D)^3$$

4.5 Statistical Analysis of the General Factorial Experiment

The experiments described in this section are referred to as general factorial designs[40]. General factorial experiments are designed to draw conclusions about more than one factor, or variable at two or more levels. The term factorial implies all possible combinations of the factors are considered. Many experiments involve the study of the effects of two or more factors. The word treatment refers a combination of level of the factors. The advantages of factorial designs over one-factor-at-a-time experiments are that they are often more run-efficient and they allow interactions to be detected, a nearly impossible feat for one-factor-at-a-time designs. An interaction is the variation among the differences between means for different levels of one factor over different levels of the other factor.

The main effect of a factor is defined to be the change in response produced by a change in the level of the factor. This is frequently called a main effect because it refers to the primary factors of interest in the experiment. This is the simple effect of a factor on a dependent variable. It is the effect of the factor alone averaged across the levels of other factors.

A main effects plus two-factor interaction regression model representation of a general factorial experiment can be written as;

$$y = \beta_0 + \sum_{i}^{k} \beta_i \chi_i + \sum \sum_{i<j} \beta_{ij} \chi_i \chi_j \qquad (4.10)$$

where k represents the number of factors and hence the number of main effects. A regression model representation of the two-factor factorial experiment could be written as;

$$y = \beta_0 + \beta_1 \chi_1 + \beta_2 \chi_2 + \beta_{12} \chi_1 \chi_2 + \varepsilon$$

where y is the response, the β's are parameters whose values are to be determined, χ_1 and χ_2 are variables representing the two factors at various levels, and ε is a random error term, and $\chi_1 \chi_2$ represents the interaction between χ_1 and χ_2.

4.5.1 A Full Factorial DOE

The 1st experiments (full-factorial DOE) were performed to investigate the feasibility of measuring significant changes in thrust coefficient due to factors:

1. Longitudinal distance (x) from base of hangar,

2. Vertical distance (z) above landing deck,

3. Presence of frigate (in/out).

A regression model with thrust coefficient as the response {C_T = f [x,z,(frigate in/out)]} was built for 2.57 m/s and 5.14 m/s in the low speed test section.

The 1st case of the 1st experiment used a rotational speed of 5,000 rpm and a freestream velocity of 2.57 m/s in order to give an advance ratio of approximately 0.0386 which replicates a full-scale frigate velocity of 13 knots and the 2nd case used a rotational speed of 5,000 rpm and a freestream velocity of 5.14 m/s in order to give an advance ratio of approximately 0.075 which replicates a full-scale frigate velocity of 32 knots.

The design points for the 2-level full-factorial 1st experiments can be seen in Figure 4.8. A grid of thrust measurement locations for this 1st experiment for both cases is Table 4.8. Two levels are chosen here as the minimum required to build a main effects plus interaction regression model for the thrust coefficient. Replication of design points provides statistical power and allows and estimate of pure error which by definition is independent of the fitted regression model. The random run order protects against systematic error and other lurking sources.

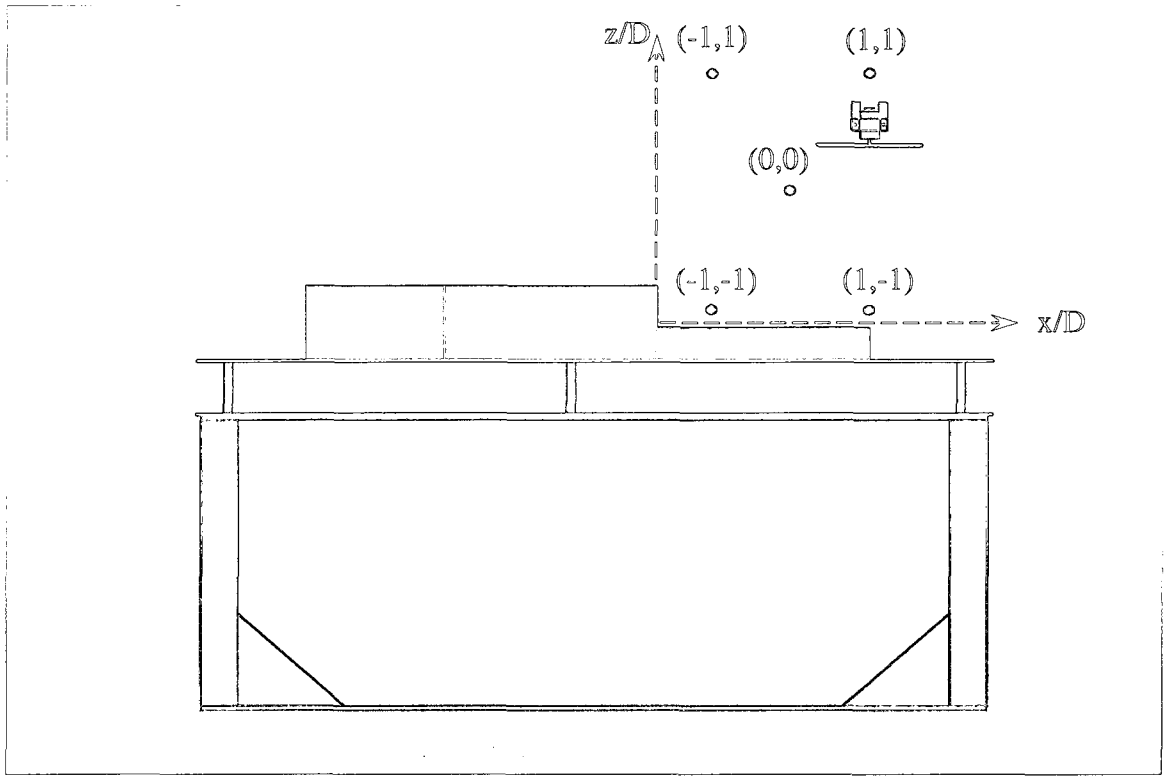

Figure 4.8 Design Points for 1st Experiments

Points	(x/D; z/D)
(0,0)	(1.25625;1.15)
(-1,-1)	(0.5125;0.25)
(1,-1)	(2;0.25)
(-1,1)	(0.5125;2.55)
(1,1)	(2;2.55)

Table 4.8 Grid of Thrust Measurement Points for 1st Experiment

The rotor position (x,z) was measured relative to the coordinate system presented in figure 3.11. The longitudinal and vertical separations are non-dimensionalized by rotor diameter (D=10 in). The longitudinal position extended from x/D=0.5125 to x/D=2, the vertical position from z/D=0.25 to z/D=2.55. The randomized run order test matrix is presented in Table 4.9 for the 1st experiment.

Run	x/D Factor A	z/D Factor B	Frigate Factor C	C_T V_∞=2.57 m/s	C_T V_∞=5.14 m/s
1	1.25625	1.15	In	0.016715	0.0171102
2	2	0.25	In	0.016785	0.0167672
3	0.5125	2.55	Out	0.016695	0.0172017
4	0.5125	0.25	In	0.018295	0.0174365
5	0.5125	0.25	Out	0.01705	0.0168156
6	1.25625	1.15	Out	0.01664	0.0172126
7	0.5125	2.55	In	0.01657	0.0170998
8	2	2.55	Out	0.016565	0.0170824
9	1.25625	1.15	Out	0.016619	0.0171926
10	1.25625	1.15	In	0.01665	0.0170268
11	2	0.25	Out	0.016995	0.0167223
12	2	2.55	In	0.016615	0.0171166

Table 4.9 Randomized Run Order Test Matrix for 1st Experiment

Design Expert ANOVA output for C_T change is presented in Figure 4.9 and 4.10. From the ANOVA report of the Design Expert commercial software, it can be seen that the model is statistically significant in both case. This is based on the confidence level of 95%. These experiments were fit with the full main effects plus 2 and 3 factor interaction models and did not reserve degrees of freedom for lack of fit testing. However, a test for the need to expand the model to include pure quadratic terms was conducted. For the cases presented here we can see that the test for curvature is significant and also that the models do not predict well, although the models themselves are significant indicating there is a change in thrust response due to changing the factors. The curvature tests suggest that a higher order model and most probably a denser spatial grid is required. While not ideal, the experiment served the intended purpose, to investigate the feasibility of going forward with a more detailed study which would include a denser spatial grid.

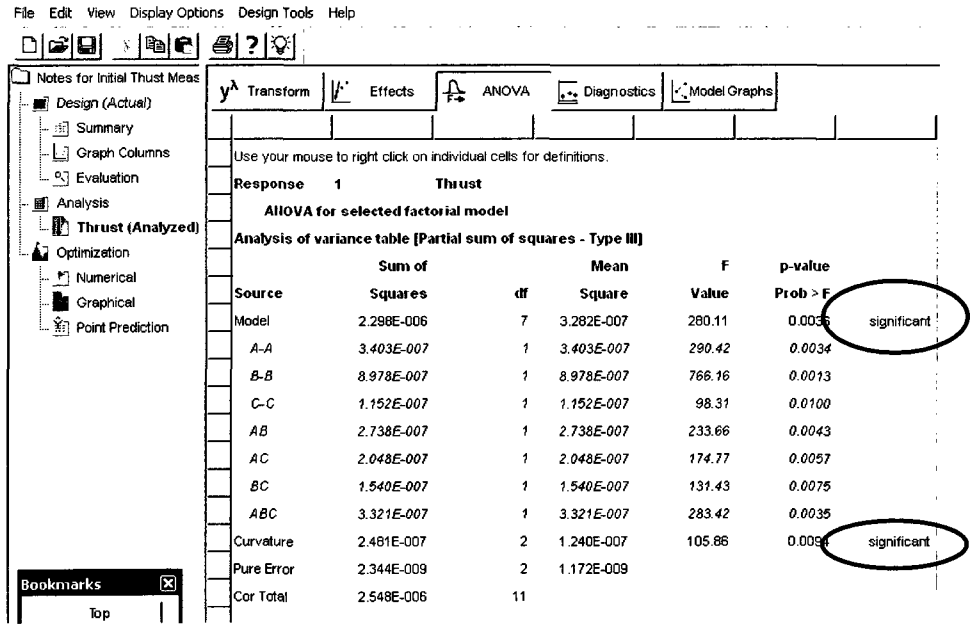

Figure 4.9 Design Expert ANOVA Report for 1st Experiment for case V_∞=2.57 m/s

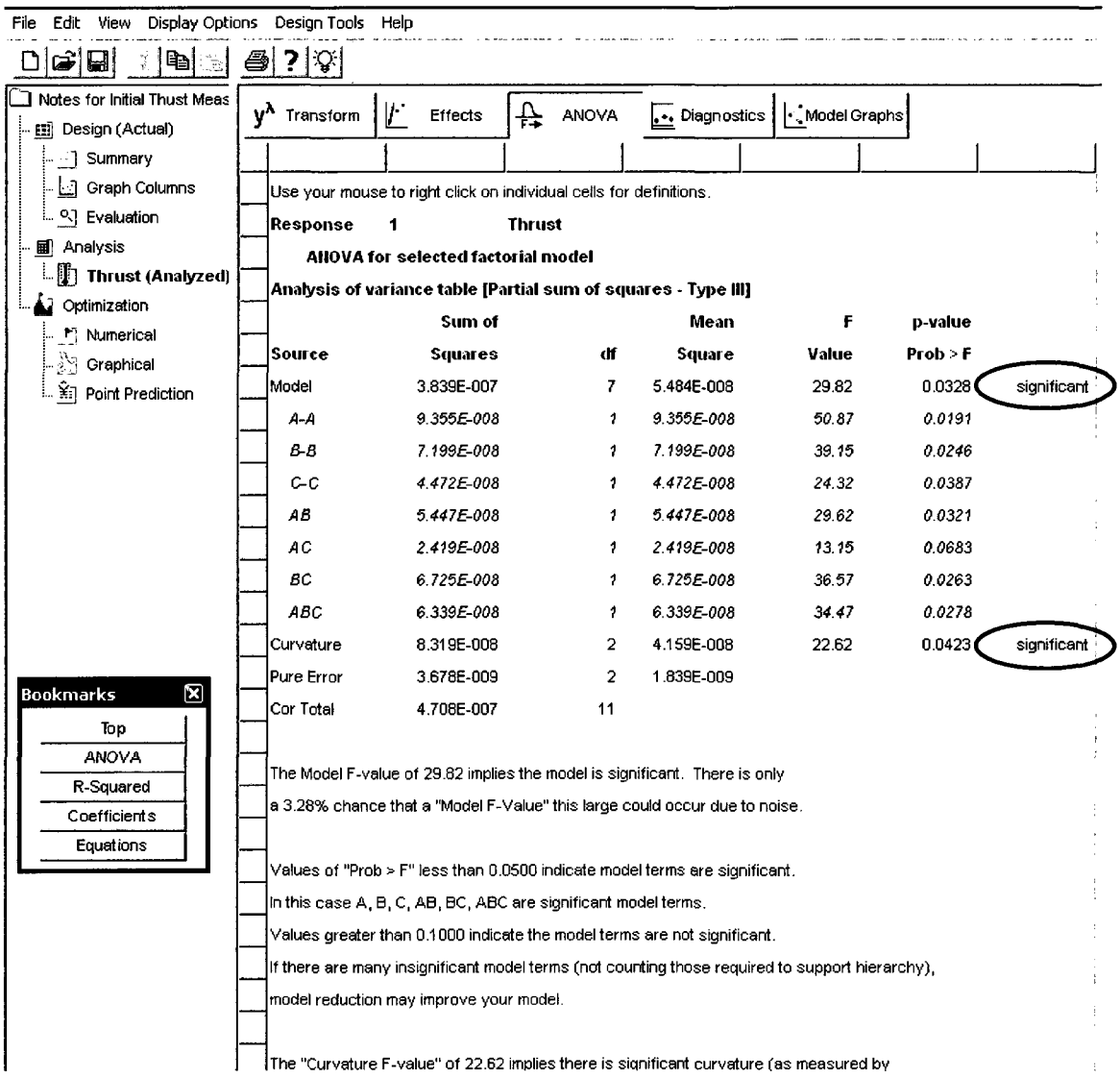

Figure 4.10 Design Expert ANOVA Report for 1st Experiment for case V_∞=5.14 m/s

The annotated ANOVA report includes an indication as to whether or not the curvature for the selected model is statistically significant or not. Curvature (2-level factorials only) compares the average response of the factorial points to the average response of the center points to test for non-linearity between the factorial points. Prob > F is the probability of seeing the observed F value if the null hypothesis is true (there is

no curvature). Small probability values call for rejection of the null hypothesis that curvature is not significant. If the Prob>F value is very small (less than 0.05) then curvature is significant. This means that the predicted value at the center point is significantly different than the value that is obtained when actually running the center point conditions. In both cases, the curvature for the model is statistically significant.

The R-squared and the adjusted R-squared values for both cases are presented in Figure 12 and Figure 4.13. Despite the seemingly high values, the fit is poor.

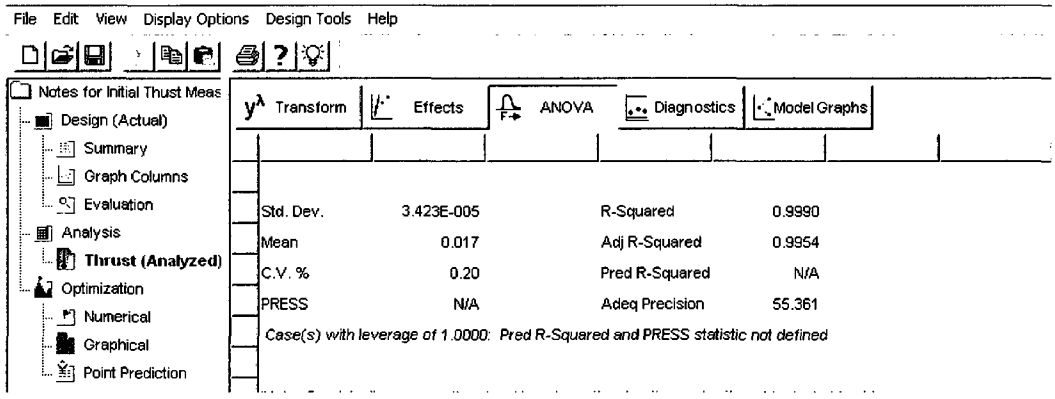

Figure 4.11 The R-Squared Values for case V_∞=2.57 m/s

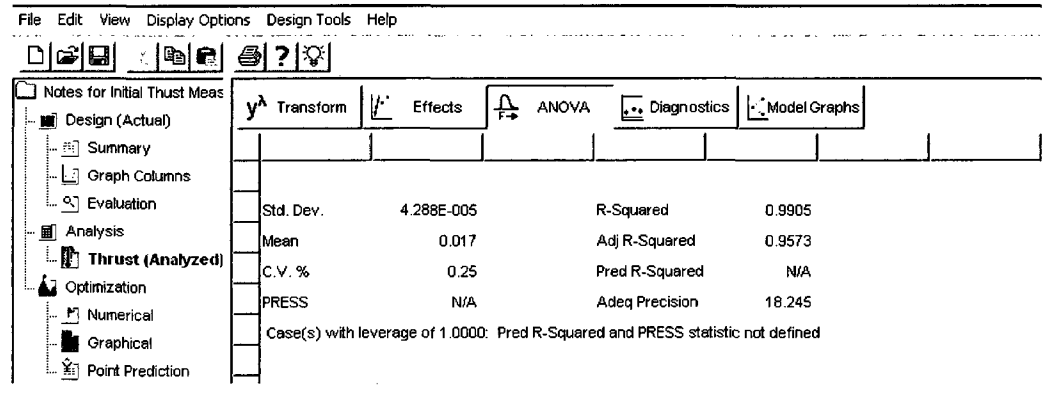

Figure 4.12 The R-Squared Values for case V_∞=5.14 m/s

4.5.1.1 The Normality Assumption

The normal probability plots for the both cases for the 1st experiments are shown in Figure 4.14 and Figure 4.15, respectively. The general impression from Figure 4.14 and Figure 4.15 is that the error distribution is approximately normal for both cases. The residuals follow the straight line.

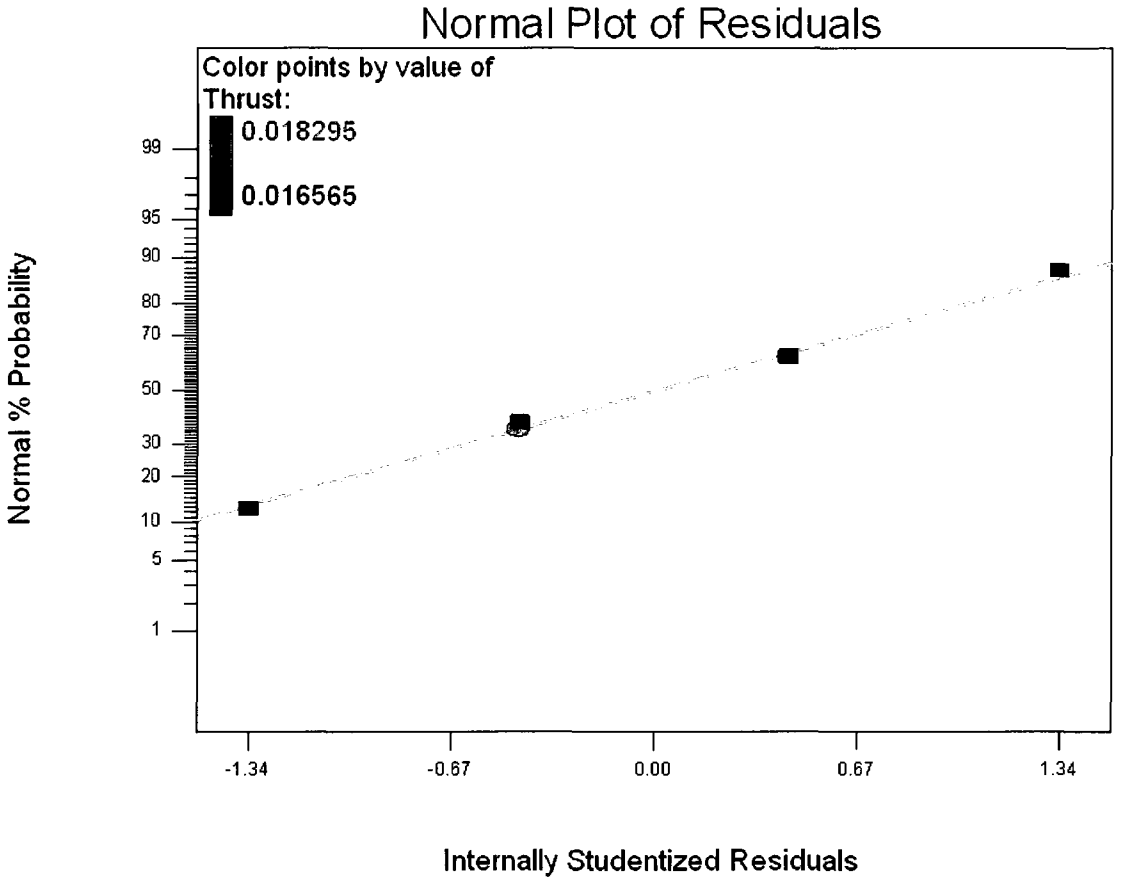

Figure 4.13 Normal Probability Plot of Residuals for case V_∞=2.57 m/s

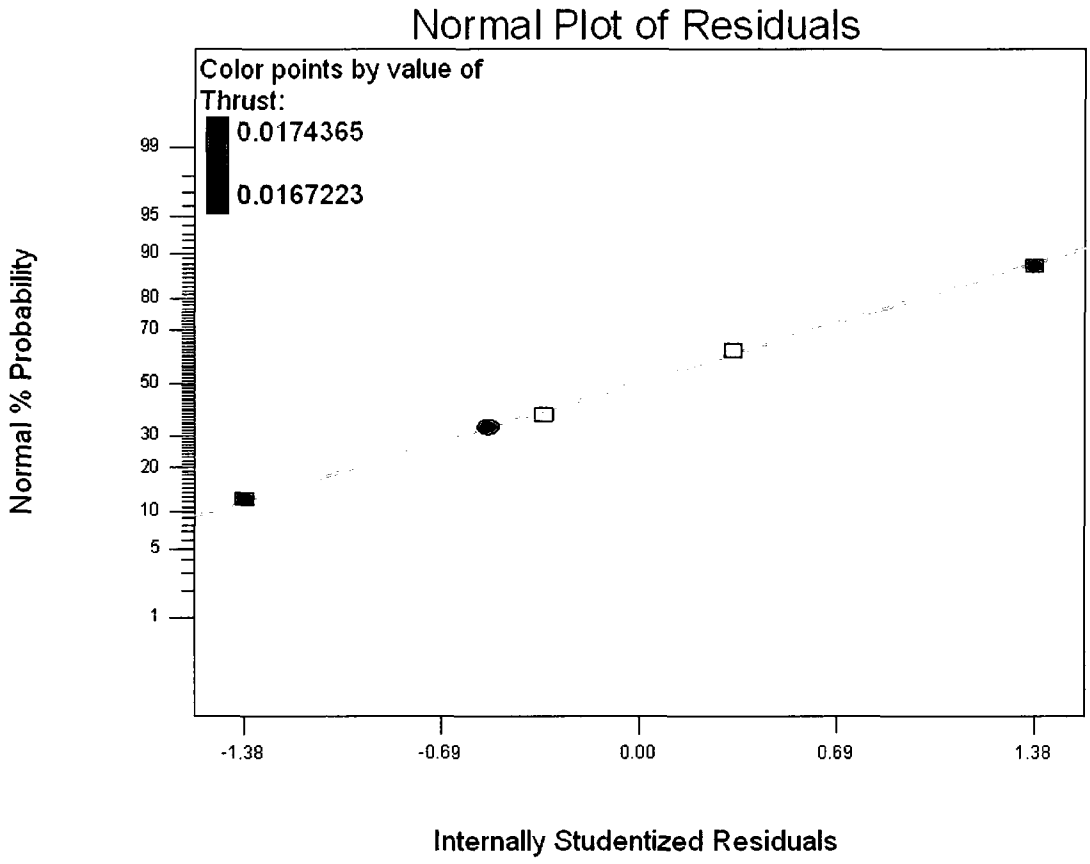

Figure 4.14 Normal Probability Plot of Residuals for case V_∞=5.14 m/s

4.5.1.2 Plot of Residuals in Time Sequence

Figure 4.16 and Figure 4.17 display the residuals versus run order time for the 1st experiment for both cases. Here the three factor interaction term is omitted from the regression model. For these full factorial experiments, it can be concluded that there is no reason to suspect any violation of the independence or constant variance assumptions.

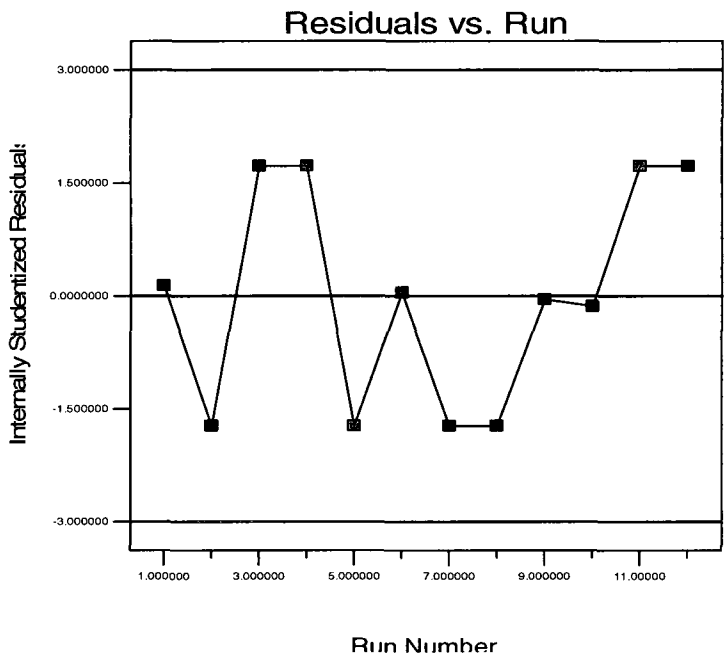

Figure 4.15 Plot of Residuals versus Run Order Time for case V_∞=2.57 m/s

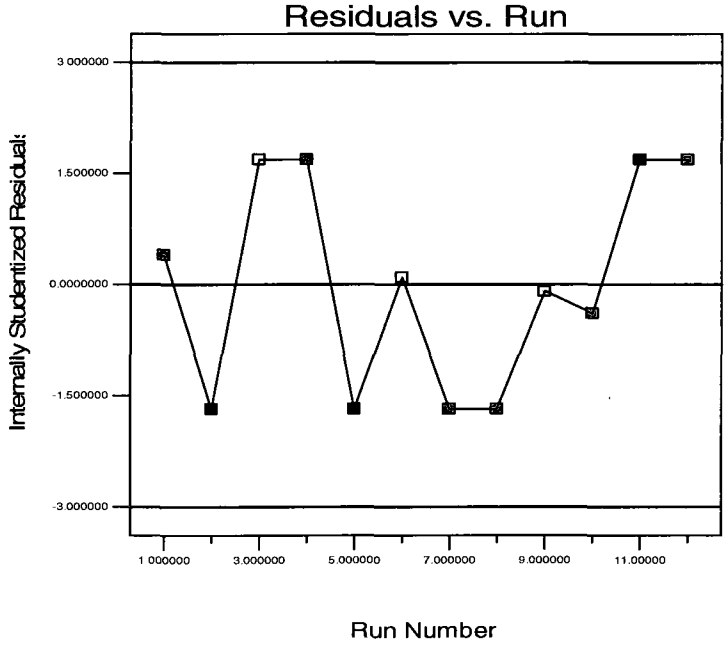

Figure 4.16 Plot of Residuals versus Run Order Time for case V_∞=5.14 m/s

5. EXPERIMENTS PERFORMED

5.1 Baseline Particle Image Velocimetry (PIV) Flowfield Surveys

The initial wind tunnel experiments at the ODU Low Speed Wind Tunnel were performed to identify the flowfield characteristics in the vicinity of a backward facing step which represented a simple frigate geometry as well as to learn and understand the 2D TSI PIV system and its limitations. Tests were performed with and without the presence of a rotary wing downwash influence on the landing deck centerline (y=0). The initial flow characterization PIV surveys were performed in the downstream 'high-speed' test section that has a cross-section of 3x4 feet, with a freestream velocity of 20 m/s and rotor speed of 8000 rpm, which gives an advance ratio of approximately 0.19.

The frigate and the 4-bladed rotor used in the initial tests is shown in Figure 5.1. For the initial PIV flowfield surveys, the rotor was placed on the frigate landing deck centerline and powered by an electrical motor which was placed under the ground board. In later PIV flowfield studies, the rotor was suspended from the ceiling via manual traverse mechanism as explained in Chapter 3.

The ship model is comprised of two rectangular boxes. With reference to Figure 5.1, these are the 'superstructure' (large box at the front) and the 'flight landing deck' (the lower box at the rear). The vertical plane and adjoining edges on the front of the model constitute the 'bow' whereas the equivalent surface and edges on the back of the model constitute the 'stern'. The rear vertical plane and adjoining edges of the superstructure perpendicular to the landing deck will be called the 'hangar'. When

referring to front and rear surfaces of the frigate, as is naval practice the directional reference is always the ship axis. For example, the front of the ship is always the bow, whether the bow is facing into or away from the onset wind.

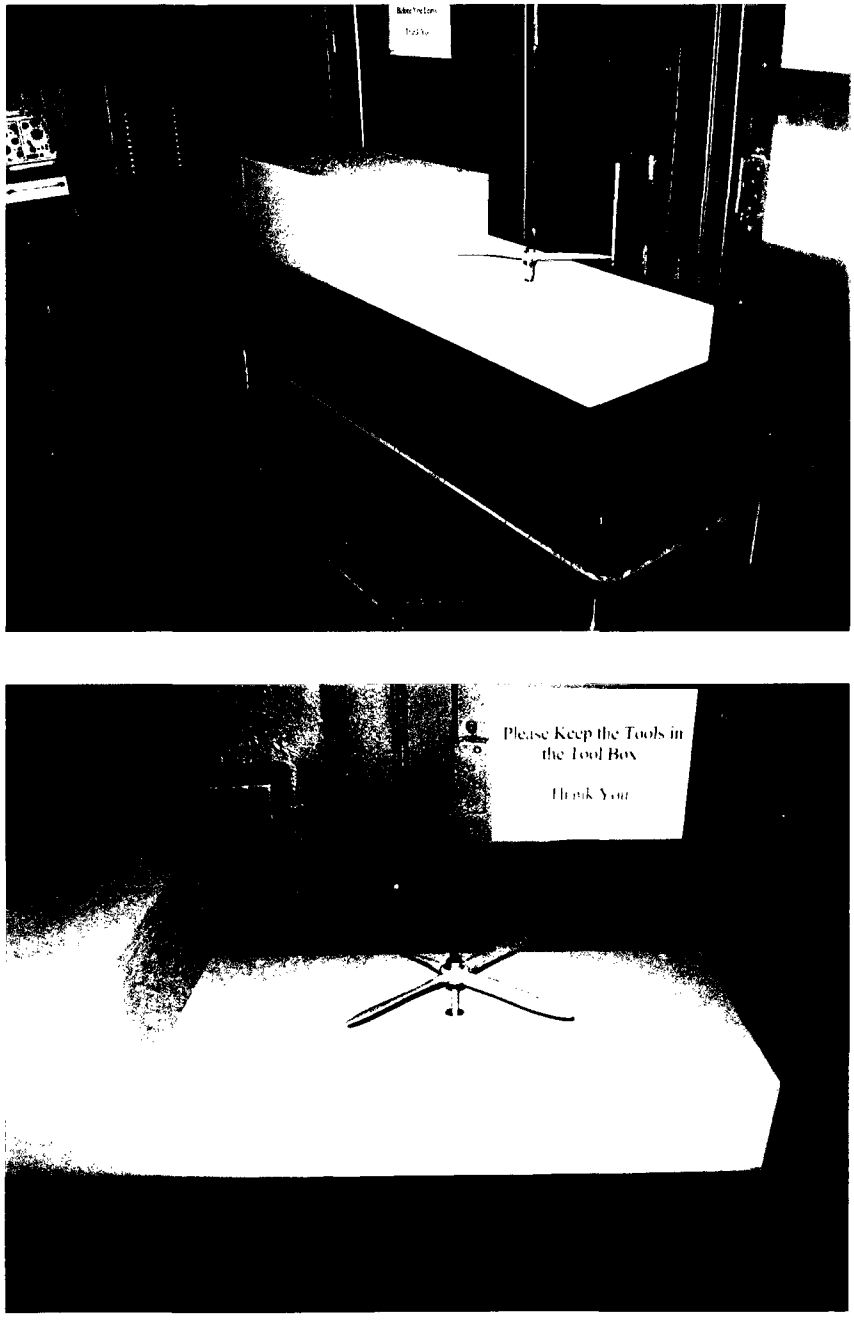

Figure 5.1 Frigate and the Rotor Used in Initial PIV Flowfield Surveys

5.1.1 Frigate Airwake Character

The flow topology over the ship follows regular, predictible patterns for bluff bodies. It is symmetric about the longitudinal centerline, when the ship is oriented directly into wind. The general features consist of flow separations and re-attachments.

As would be expected on a sharp-edged model, flow separation occurs at the bow leading edge. In smooth flow, re-attachment typically occurs about 1.6 times the body height downstream for three-dimensional rectangular bodies in the free air [31]. For the same body mounted on a solid surface, it would be expected that re-attachment would occur at a position further aft since the solid surface acts somewhat like a reflection plane.

For this study the frigate landing deck was of primary importance, rather than the superstructure portion of the frigate. Figure 5.2 shows the PIV measurements of the flow over the centerline of the frigate landing deck and aft face of the hangar. The composite image is a time average of 150 images from 2 regions. From Figure 5.2, it can be seen that the flow attached at the aft edge of the superstructure, detaches at the hangar face. A recirculation zone exists over the landing deck and behind the hangar. That is, the flow passing over the roof of the hangar flows a short distance downstream, then turns downward. This recirculation zone is an unsteady aerodynamic structure, so the instantaneous attachment location varies with time[2,5,16,19,31,43]. PIV measurements indicate a re-attachment location of 2.5 times the hangar height aft of the hangar on the centerline. Aft of the attachment locations, the flow quickly returns to the streamwise direction.

Cheney and Zan, showed that the highest pressure is found at the re-attachment point which is approximately in the center of the frigate landing deck[41]. The lowest pressure was found at the base of the hangar face which is also inside the recirculation region associated with the aft face of the hangar.

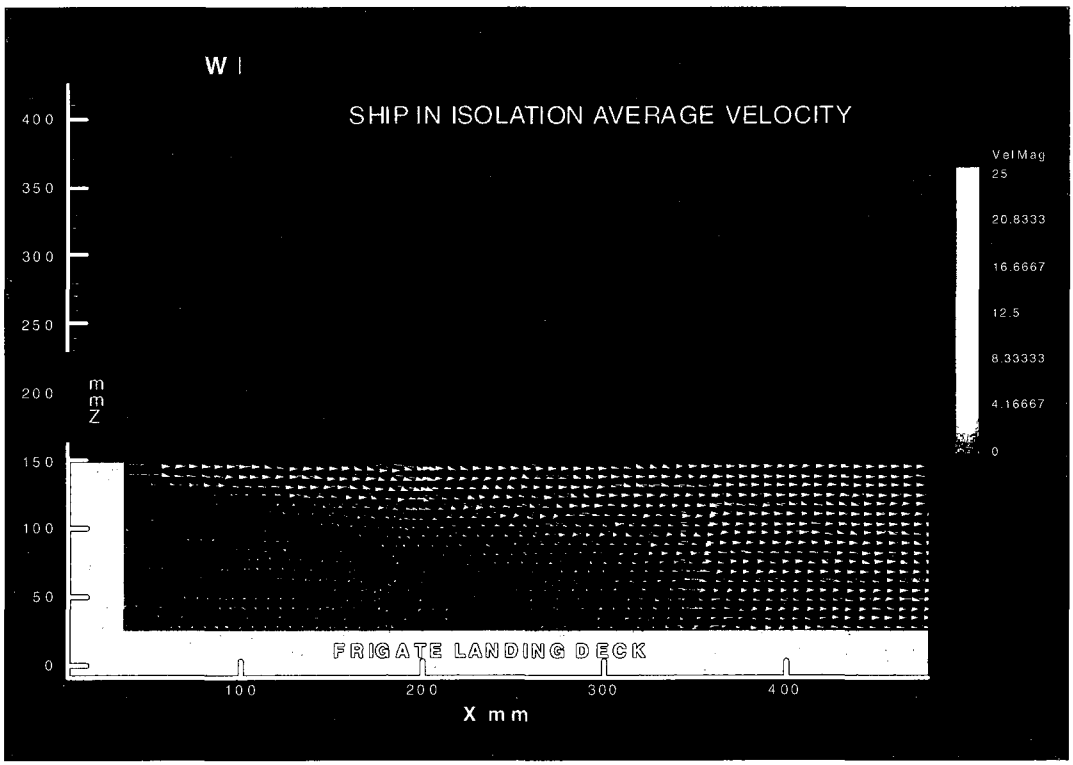

Figure 5.2 PIV Velocity Survey over Frigate Landing Deck

From the perspective of a helicopter pilot, high levels of turbulence will be encountered due to the free shear layer separating from the hangar roof[31]. The flow separating from the hangar is pulled downwards towards the flight deck by the low pressure region behind the hangar. Assuming the helicopter is facing towards the hangar door, this will reduce the angle of attack on the rotor blades as they sweep in front of the

helicopter. This results as a change in rolling moment due to gyroscopic effects and contributes to pilot workload.

5.2 Investigation of Measurement Techniques

5.2.1 Thrust Change as a Function of Presence of Frigate, Lateral and Longitudinal Distance

After performing initial PIV flowfield surveys, experiments were designed in order to investigate the feasibility of measuring significant changes in thrust coefficient due to longitudinal distance from the base of the hangar, and vertical distance above landing deck as well as presence of the frigate (in/out of tunnel). The detailed explanation of the experimental procedure, including choice of design points and the grid of thrust measurement points as well as the randomized run order test matrix with ANOVA report and summary statistics was given in Chapter 4, Section 4.5.1.

A regression model with thrust coefficient as the response {C_T=f[x,z,(frigate in/out)]} was built for freestream velocity values of 2.57 m/s and 5.14 m/s and a rotor rotation rate of 5000 rpm. To obtain the low velocity values, the experiment was performed in the low speed test section. The 1st case of the experiment gives an advance ratio of approximately 0.0386 which replicates a full-scale frigate velocity of 13 knots wheras the 2nd case gives an advance ratio of approximately 0.075, which replicates a full-scale frigate velocity of 32 knots.

From the first tests performed, it was concluded that the effect of the vertical distance change was larger than the effect of the longitudinal distance change. These

preliminary experiments showed that C_T could be measured with enough precision to identify changes due to location. Subsequent longer duration testing showed that using an advance ratio of 0.075 (V_∞=5.14 m/s, ω=5000 rpm) was necessary to prevent the motor from overheating.

5.2.2 Vertical Separation Sensitivity Study-Single Factor Experiment

Now, it was of interest to explore the effect of vertical distance on thrust coefficient and the required spatial resolution for design points. A characterization experiment was performed with one factor which is the vertical distance above the frigate landing deck. Six levels of vertical distance were chosen for this single factor experiment. The detailed explanation of the experimental procedure including design points and a grid of thrust measurements locations as well as the ANOVA report and summary statistics can be found in Chapter 4, Section 4.4.2.

From the second experiment, it was found that there is a strong non-linear relationship between vertical distance and thrust coefficient. The thrust coefficient increases with the increase of vertical distance until just above the hangar door and then appears to vary only slightly with increasing vertical distance.

5.2.3 Identification of Regions of Airwake Influence

An acceptable design point density was established after the 1st and 2nd tests were conducted. The 3rd experiments focused on more clearly identifying regions where the influence of the ship airwake was found to be statistically significant with regards to changing the thrust coefficient (versus no airwake). Two experiments were compared in

order to find the regions where airwake influence was statistically significant, one with freestream flow V_∞=5.14 m/s, and the other with V_∞=0.

The two factors for the 3rd experiments are longitudinal distance (x) and vertical distance (z). The longitudinal and vertical separations are specified in terms of rotor diameter. The longitudinal position extended from x/D=0.5125 to x/D=2 where the vertical position extended from z/D=0.35 to z/D=0.85. The 3rd experiments were conducted for the same rotor speed of 5,000 rpm and freestream velocity of 5.14 m/s in order to give an advance ratio of approximately 0.075. A subset of the design points of the 3rd experiments for both cases are presented in Figure 5.3 (Design Expert v7) where the airwake case is on the left and the no-airwake case on the right.

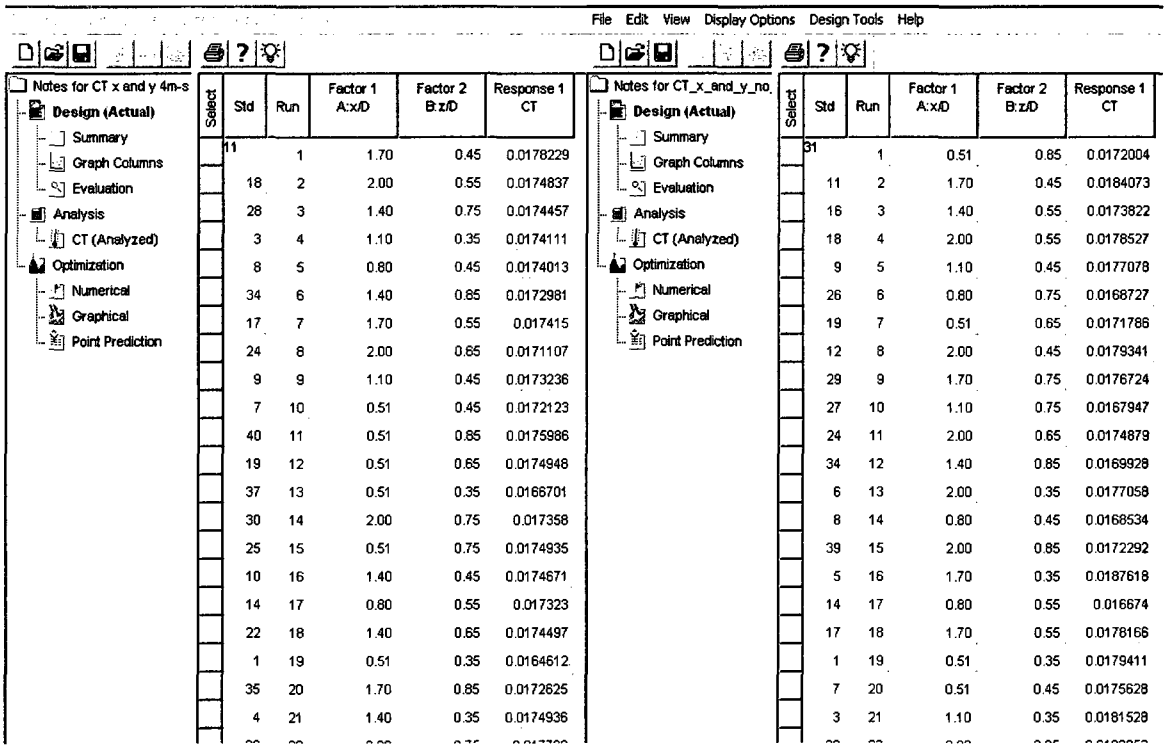

Figure 5.3 Full Factorial Designs for the 3rd Experiments (Airwake case left)

Design Expert ANOVA analysis results for thrust coefficient (C_T) changes for the 3rd two-factor factorial experiments are presented in Figure 5.4 and Figure 5.5, respectively.

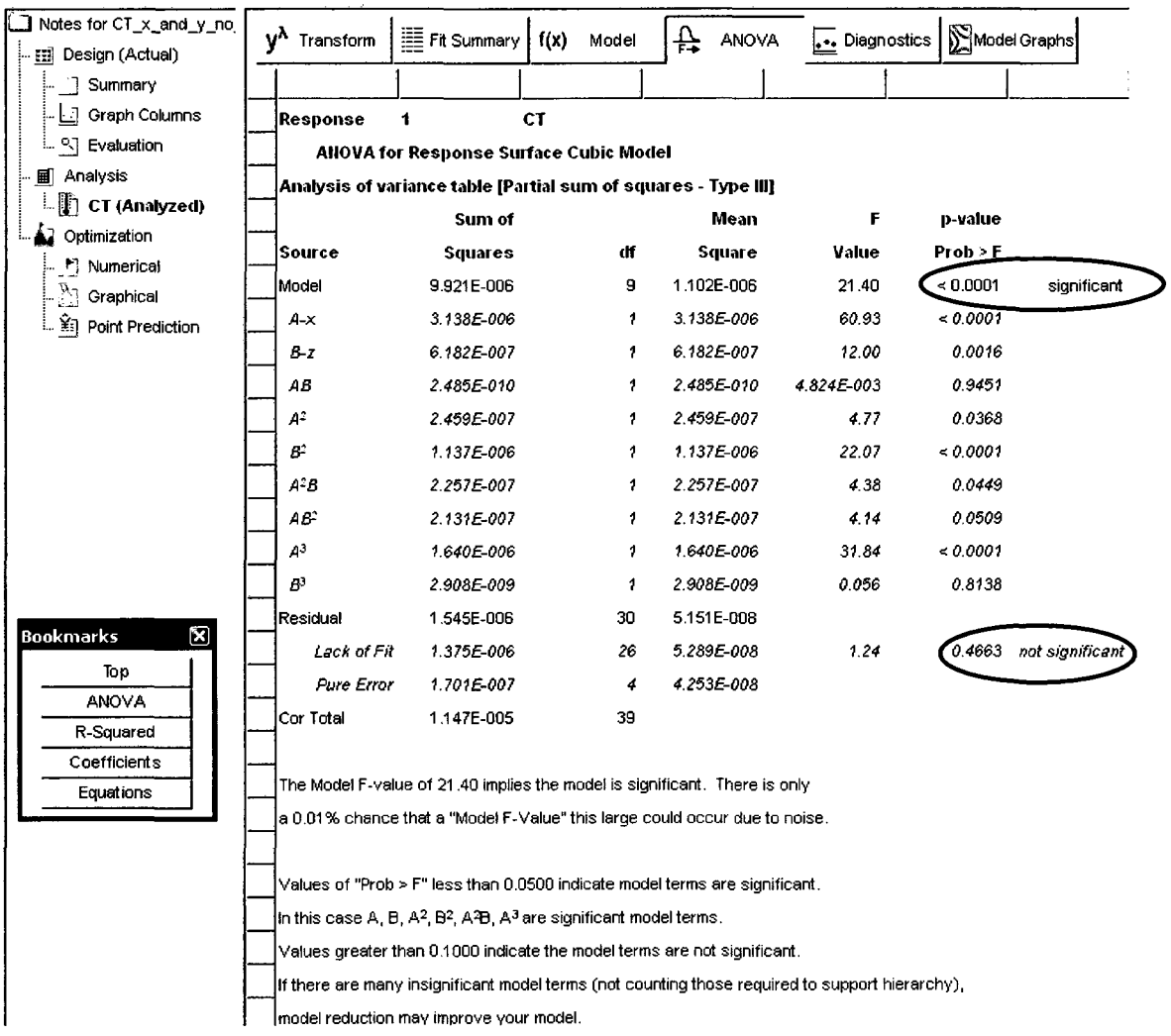

Figure 5.4 Design Expert ANOVA Report for V_∞=0 m/s Case

From the ANOVA report in Figure 5.4, it can be seen that the model is statistically significant and the lack of fit test for the model is statistically insignificant meaning that the polynomial coefficients chosen, well represent the data. The p-value of $P < 0.0001$

associated with the model indicates there is less than a 0.01 % probability that the regression model was chosen in error.

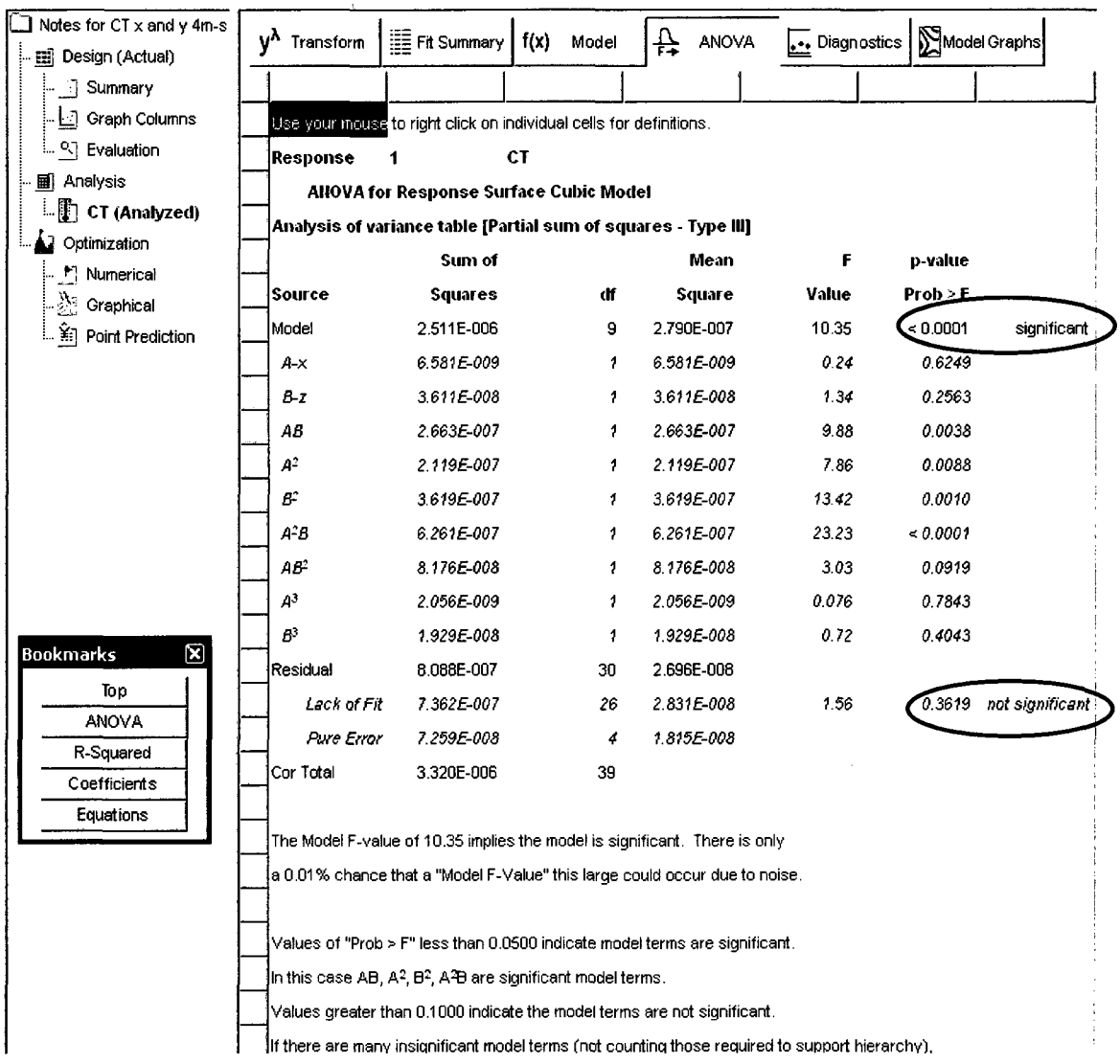

Figure 5.5 Design Expert ANOVA Report for V_∞=5.14 m/s Case

The ANOVA report in Figure 5.5 shows that the model is statistically significant for the 3rd experiment using the freestream velocity V_∞=5.14 m/s case and the lack of fit test for the model is statistically insignificant.

5.2.3.1 The Normality Assumption

The normal probability plot of residuals of the 3rd experiment for the V_∞=5.14 m/s and V_∞=0 cases are presented in Figure 5.6 and Figure 5.7, respectively.

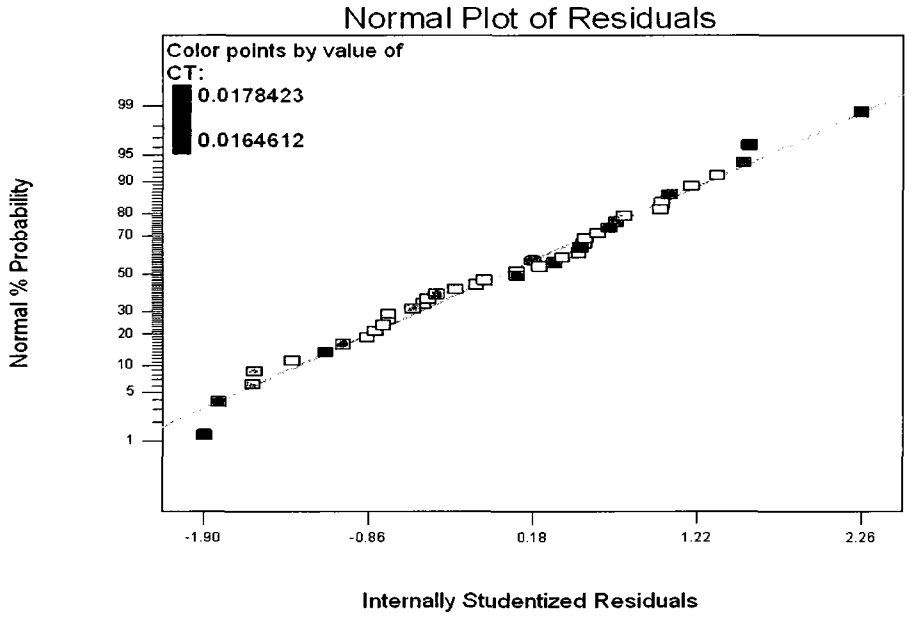

Figure 5.6 Normal Probability Plot of Residuals for V_∞=5.14 m/s Case

The normal probability plot does not reveal anything particularly troublesome, although the largest negative residual does stand out somewhat from the others for the V_∞=5.14 m/s case.

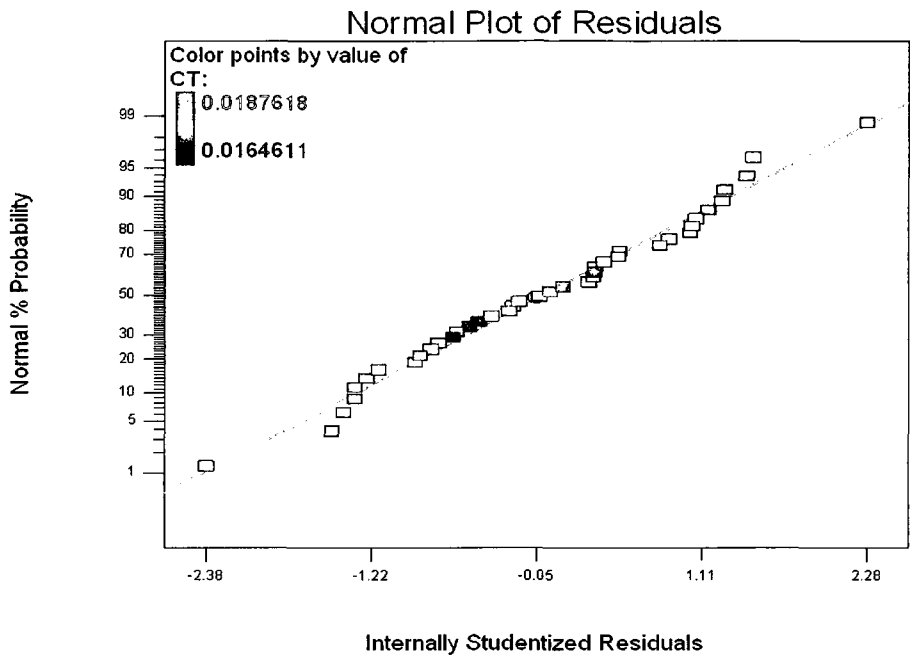

Figure 5.7 Normal Probability Plot of Residuals for V_∞=0 m/s Case

The general impression from the normal probability plot of residuals from Figure 5.7 is that the error distribution is approximately normal. This is determined subjectively by observing that the residuals form a band around the line. The ANOVA procedure is rather robust to small departures from normality.

5.2.3.2 Plot of Residuals in Time Sequence

Figure 5.8 and Figure 5.9 display the residuals versus run order time for the 3rd experiment for both the V_∞=5.14 m/s and V_∞=0 cases. For the 3rd experiments, it can be concluded that there is no reason to suspect any violation of the independence or constant variance assumptions for both cases.

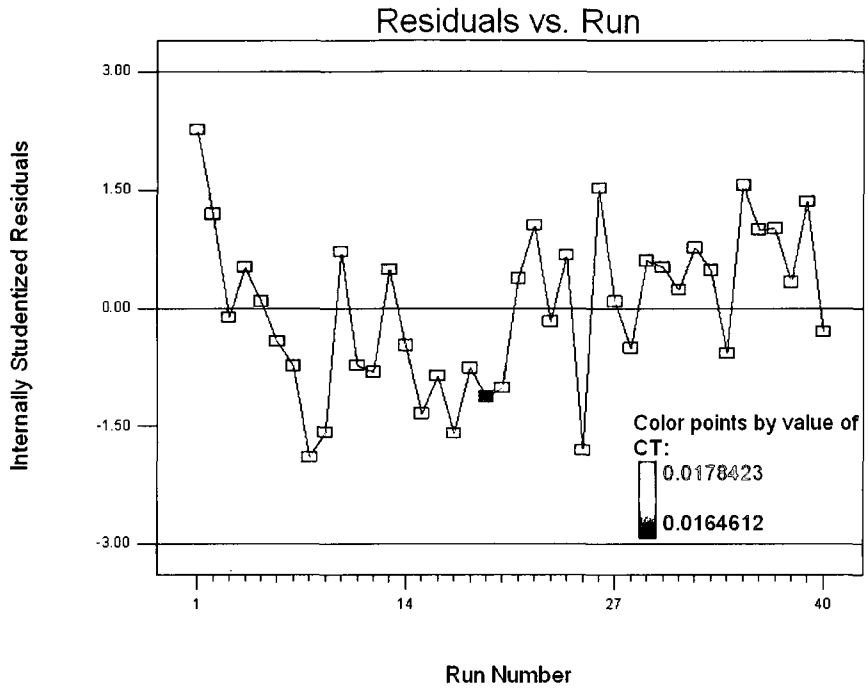

Figure 5.8 Plot of Residuals versus Run Order Time for V_∞=5.14 m/s Case

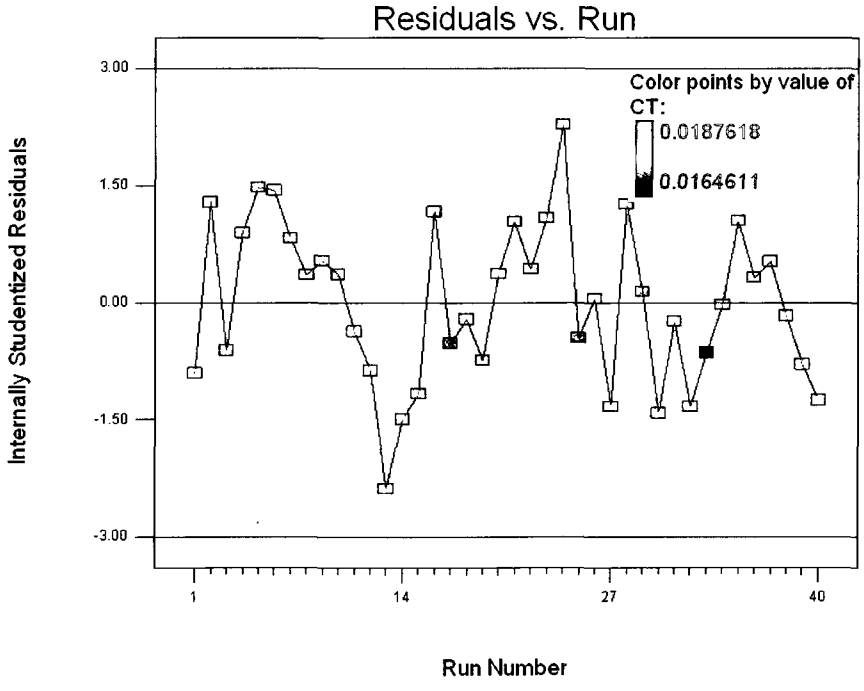

Figure 5.9 Plot of Residuals versus Run Order Time for V_∞=0 m/s Case

5.2.3.3 Plot of Residuals versus Fitted Values

Figure 5.10 and Figure 5.11 plot the residuals versus the fitted values for the 3rd experiments performed for both cases of V_∞=5.14 m/s and V_∞=0 m/s, respectively. As can be seen from both Figure 5.10 and Figure 5.11, no unusual structure is apparent.

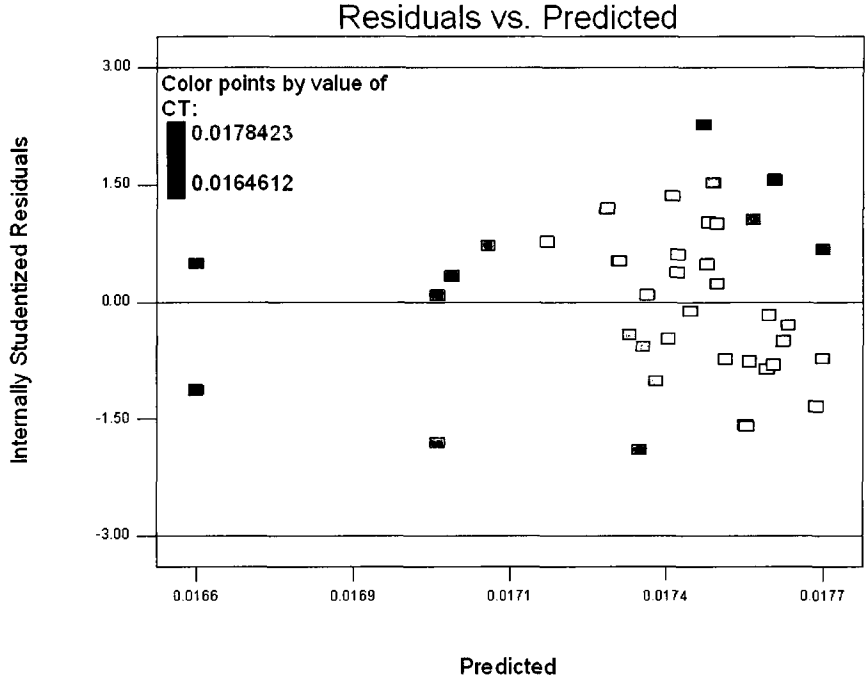

Figure 5.10 Plot of Residuals versus Fitted Values for V_∞=5.14 m/s Case

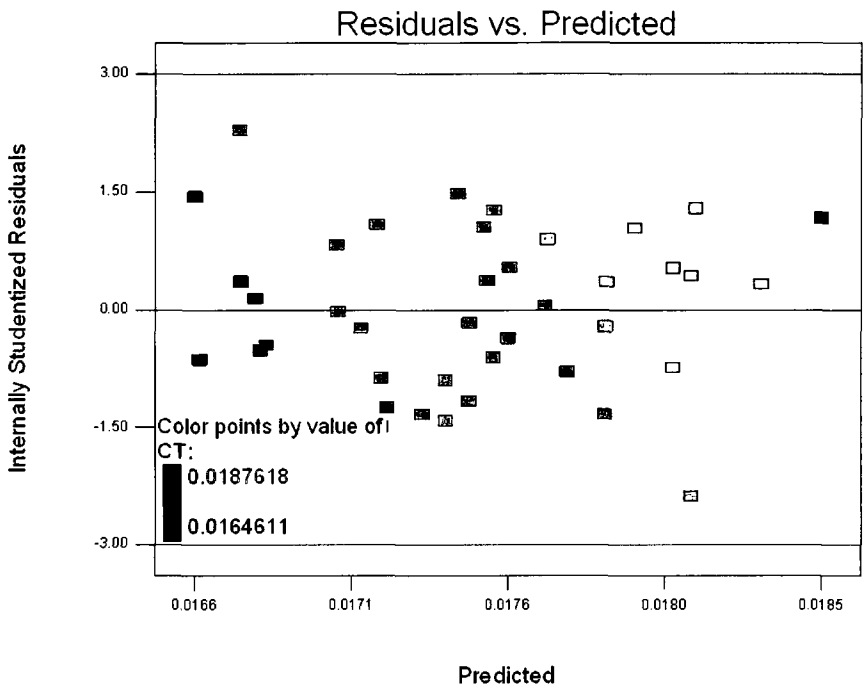

Figure 5.11 Plot of Residuals versus Fitted Values for V_∞=0 m/s Case

5.2.3.4 Regression Model and Uncertainty Estimates

Figure 5.12 and Figure 5.13 present contour plots of thrust coefficient (C_T) versus normalized vertical distance above deck (z/D) and normalized longitudinal distance along the landing deck for the third experiments. The red filled symbols indicate the location of the design points.

Response surface plots of thrust coefficient (C_T) of the normalized vertical distance above deck (z/D) and normalized longitudinal distance along the landing deck versus the thrust coefficient for the 3rd experiments for both cases of V_∞=5.14 m/s and V_∞=0 m/s (no ship airwake) are presented in Figure 5.14 and Figure 5.15, respectively.

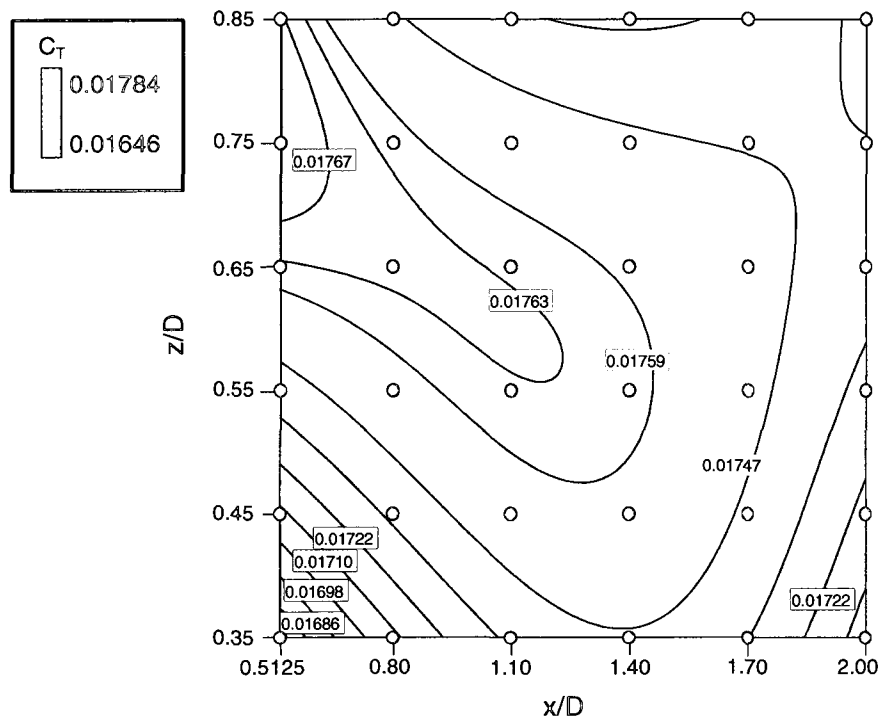

Figure 5.12 Thrust Coefficient Contour Plot for V_∞=5.14 m/s Case

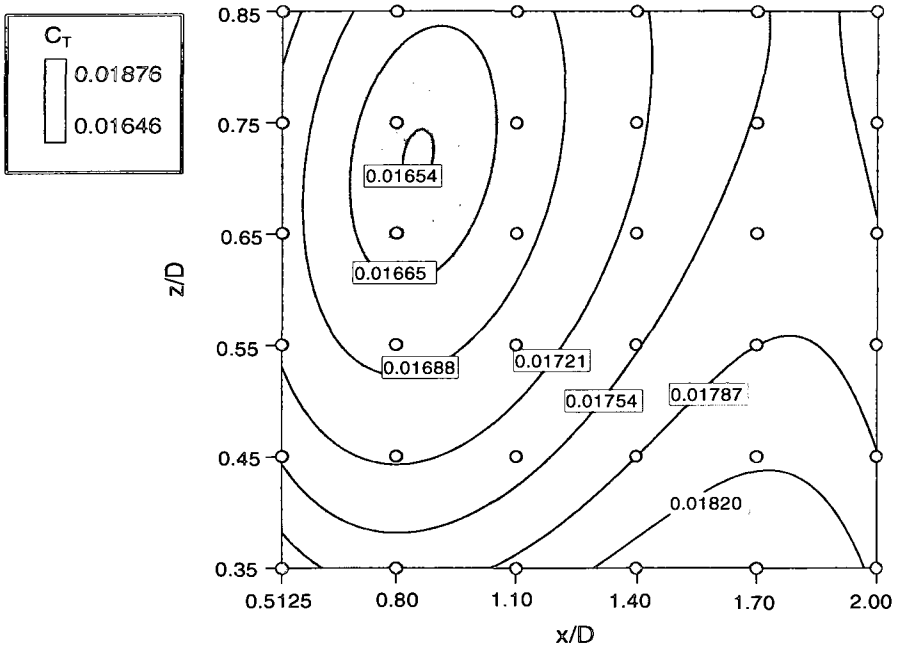

Figure 5.13 Thrust Coefficient Contour Plot for V_∞=0 m/s Case

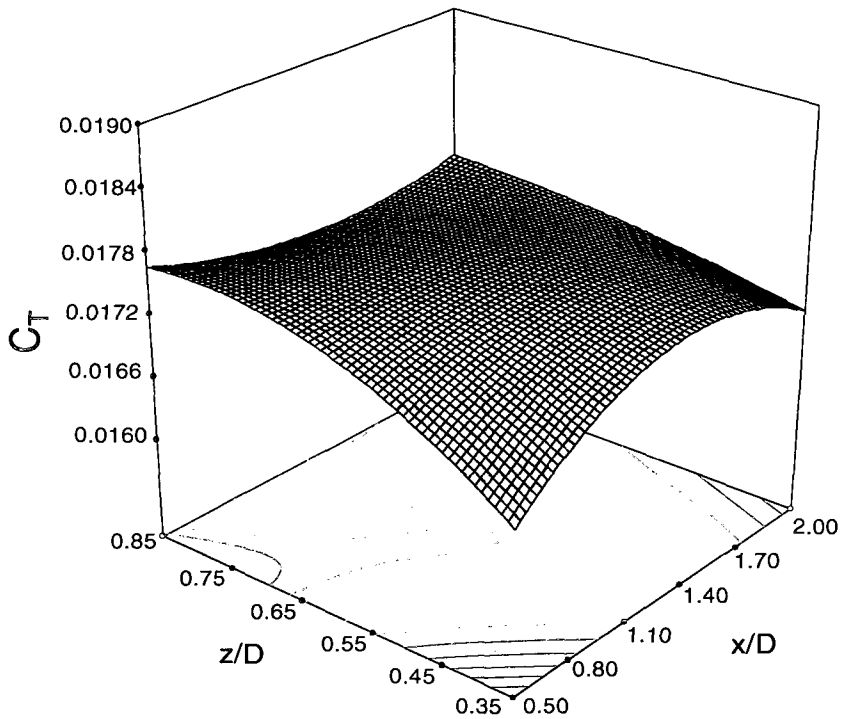

Figure 5.14 Response Surface Plot for V_∞=5.14 m/s Case

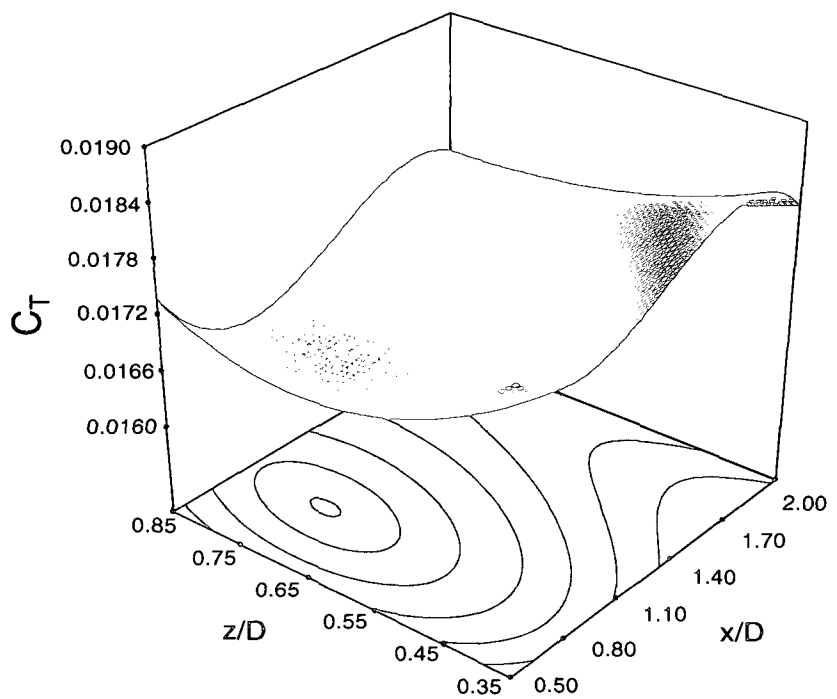

Figure 5.15 Response Surface Plot for V_∞=0 m/s Case

The subsequent 3rd order cubic regression model for thrust coefficient for the 3rd experiment, V_∞=5.14 m/s case (ship airwake) was fit as follows:

$$C_T = 0.01102+0.007044*x/D+0.01505*z/D-0.01249*x/D*z/D$$

$$-0.002199*x/D^2-0.007763*z/D^2+0.003124*x/D^2*z/D$$

$$+0.003198*x/D*z/D^2 \qquad \text{(LSD based CI half width = 0.00021)}$$

The subsequent 3rd order cubic regression model for thrust coefficient for the 3rd experiment for V_∞=0 m/s case (no ship airwake) was fit as follows:

$$C_T = + 0.02484 - 0.009764*x/D - 0.01549*z/D+0.001818*x/D*z/D$$

$$+ 0.008337*x/D^2 + 0.01327*z/D^2 + 0.001806*x/D^2*z/D$$

$$- 0.005277*x/D*z/D^2 - 0.002406*x/D^3 \quad \text{(LSD based CI half width = 0.00029)}$$

5.2.3.5 Determining Airwake Influence

Regions in the design space where thrust coefficient C_T differs (with quantifiable statistical significance) due to freestream velocity changes from V_∞=0 m/s and V_∞=5.14 m/s represent regions where including the wake interaction is important. Confidence intervals (C.I.) were used for C_T associated with both experiments in order to determine airwake interaction. Confidence intervals measure the precision of our estimates and were based on LSD calculations.

A simple comparison test was made to determine airwake interaction by determining whether confidence intervals overlap or do not overlap. If the confidence intervals overlap, no airwake influence occurs within the bounds of the experimental

error. If confidence intervals do not overlap then airwake (versus no-airwake) influence occurs. It should be remembered that this simple comparison test was performed on time averaged flowfields and represents a first step at eventually developing a method to determine the need for modeling coupling of the rotor and ship airwakes. It is not a test for identifying coupling. Confidence intervals were computed at a 5% significance level using Least Significant Difference (LSD) bounds[37]. Figure 5.16 presents significant interaction points of the region.

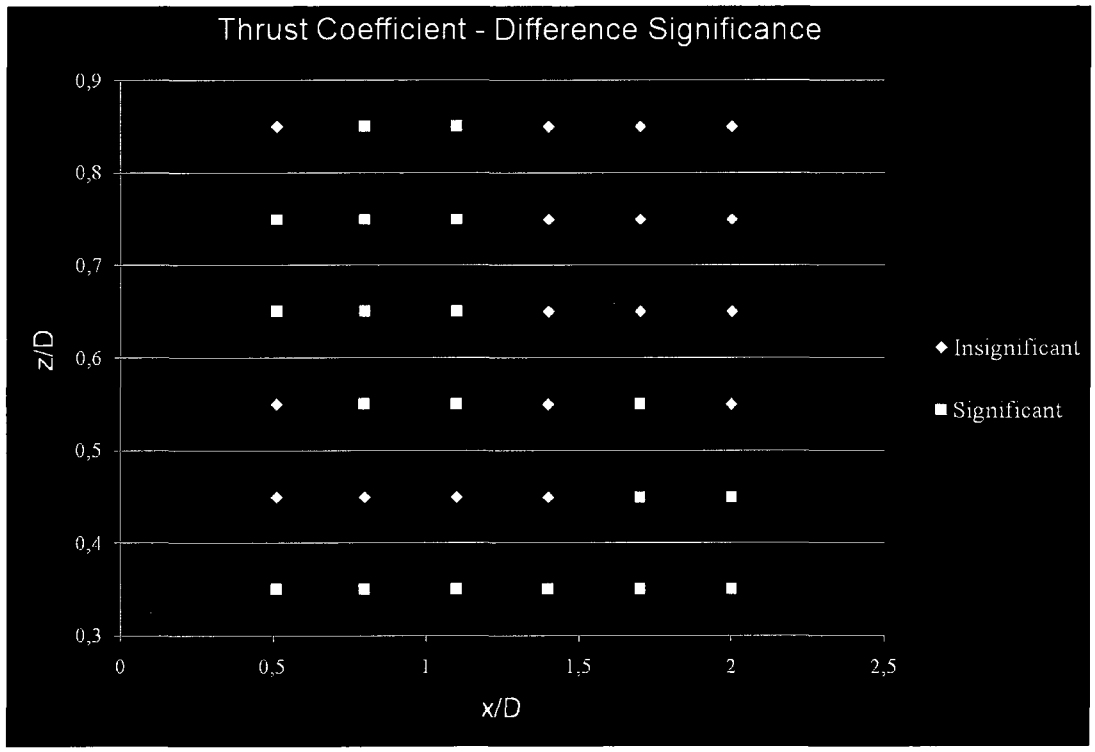

Figure 5.16 Thrust Coefficient-Difference Significance

5.2.4 Detailed PIV Surveys

The next phase of the study was aimed at correlating flowfield features with changes in C_T, for instance, analysis of recirculation regions with attention to re-ingestion in the rotor flowfield and modified downwash due to airwake inflow

The PIV flowfield surveys were conducted for longitudinal and lateral planes as well as for the ship in isolation, rotor in isolation and ship/rotor cases. Some sample results for a longitudinal and lateral case (V_∞=5.14 m/s; ω=5000 rpm) are given in Figure 5.17 and Figure 5.18, respectively. It should be noted that all longitudinal surveys were conducted for y = 0 (center plane) and the rotor rotational direction is counterclockwise when viewed from above. Surveys in the lateral plane were conducted for various x locations. The dashed lines in the figures represent the approximate outline of the hangar door. The coordinates in the captions are the location of the center of the rotor disk and the thrust coefficients specified are from the measurements of the third experiment.

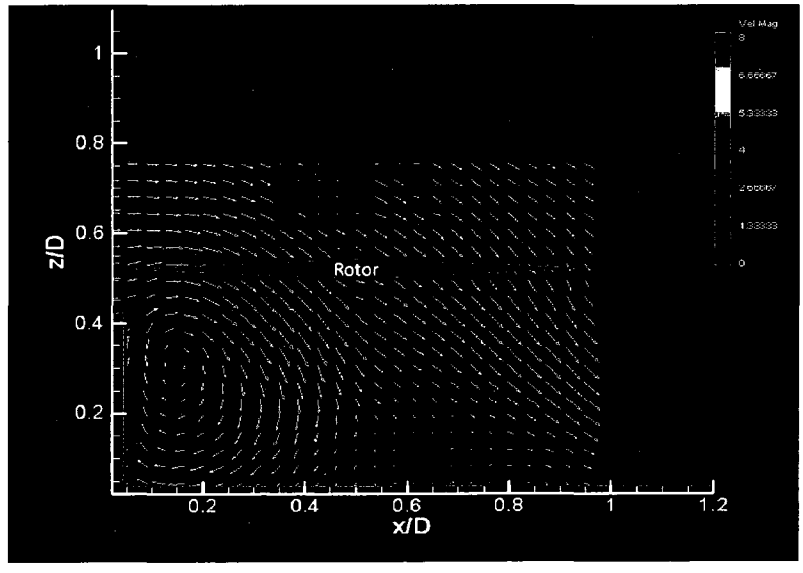

Figure 5.17 PIV Survey for Longitudinal Plane (x/D=0.5; z/D=0.55)

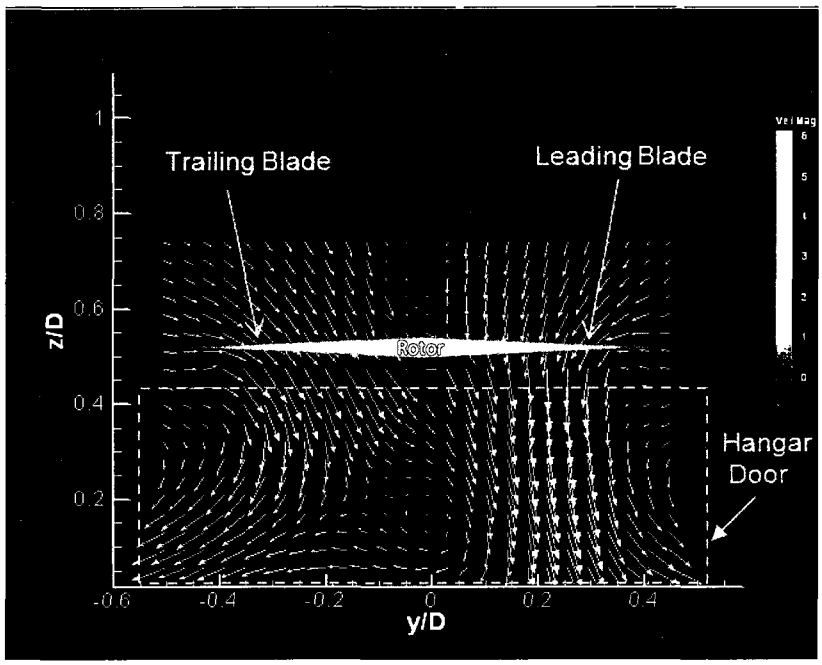

Figure 5.18 PIV Survey for Lateral Plane (x/D=0.5; z/D=0.55)

5.2.5 Initial Coupling Experiments

5.2.5.1 Investigation of the Feasibility of Identifying Coupled Regions

The thrust measurement test conducted previously showed the regions in the design space where thrust coefficient C_T differs due to changes in the freestream velocities V_∞=5.14 m/s and V_∞=0 m/s (no-airwake). NAVAIR CFD modelers define coupling as the region of the dynamic interface where the downwash of the rotor has an impact on the inflow to the rotor due to the presence of a nearby surface. In regions with coupling, a full time-accurate solution is required for flight simulations, whereas in regions without coupling, a superposition of an isolated rotor velocity field with an isolated ship airwake velocity field will suffice for flight simulations.

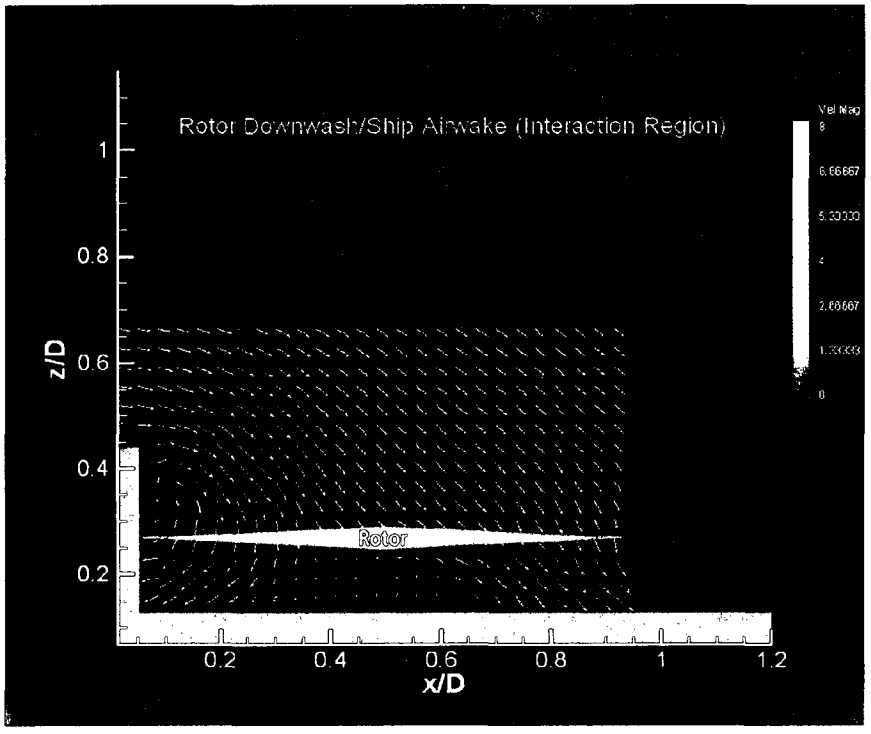

Figure 5.19 PIV Survey in Region of Interaction (x/D=0.5; z/D=0.55)

5.2.5.2 Isolated Ship and Rotor PIV Surveys

Thrust measurements and PIV flowfield surveys for both isolated ship (no rotor downwash) and isolated rotor (no ship airwake) cases were performed in order to investigate coupling. The rotor in isolation surveys were performed for various cases like rotor in isolation without ground board as well as rotor in isolation with ground board and rotor in isolation with ship model. A detailed test matrix and the results for each case will be presented in Chapter 6.

A sample case for the PIV survey for the case of a ship in isolation (V_∞=5.14 m/s) is given in Figure 5.20 where Figure 5.21 presents the case for the rotor in isolation (ω=5000 rpm).

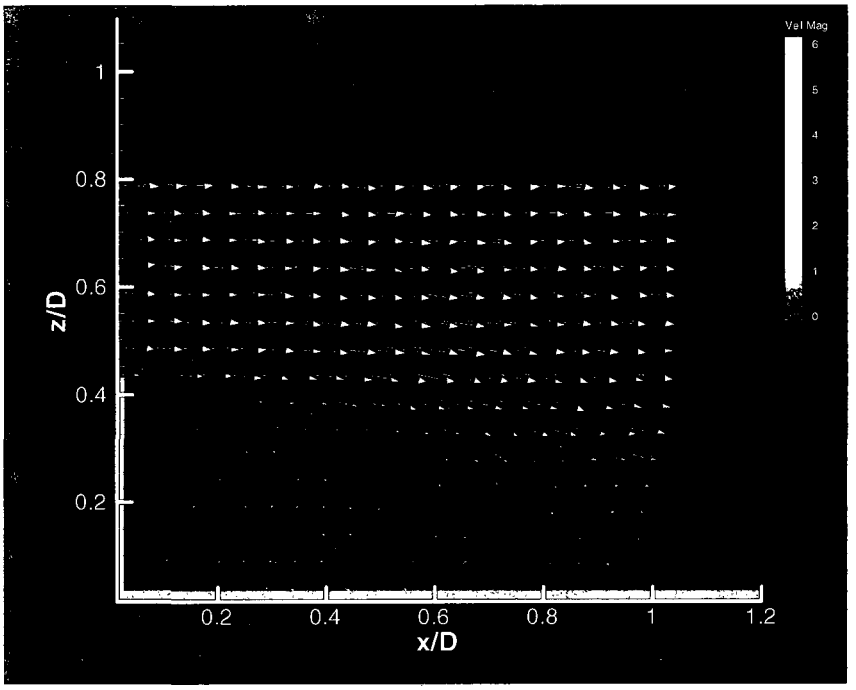

Figure 5.20 PIV Survey for Ship in Isolation Case

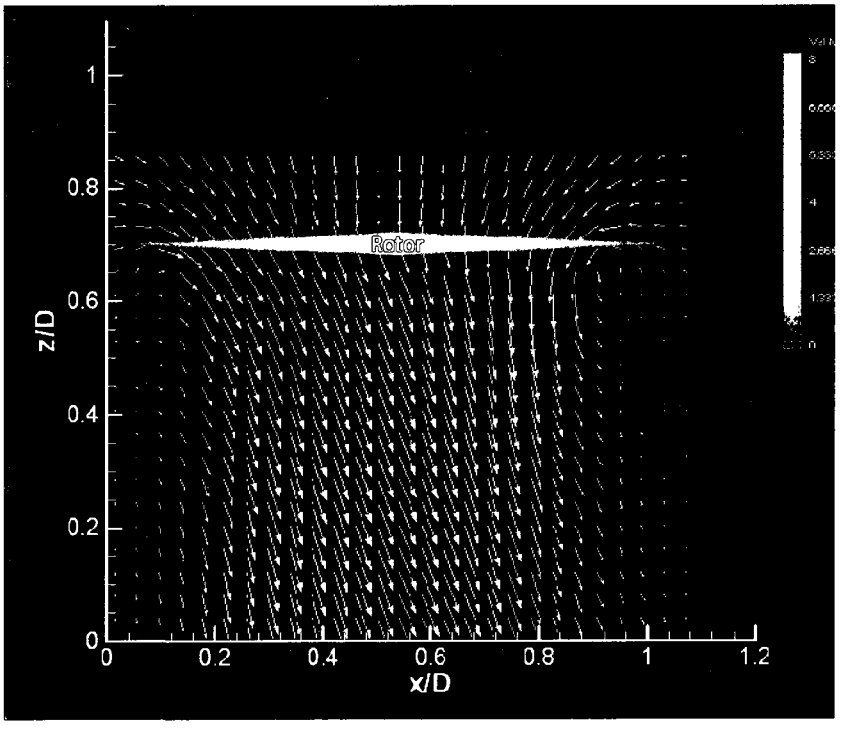

Figure 5.21 PIV Survey for Rotor in Isolation Case

5.2.5.3 Comparison of Ship Airwake/Rotor Downwash Combined Measurements with the Rotor Velocity Fields Superposed on Ship Airwake

One long range goal of this research program is to help understand the ship airwake/rotor downwash coupling and how it might affect CFD modeling. For this reason, the PIV flowfield survey was conducted with the ship in isolation, rotor in isolation and the combined ship/rotor cases in order to compare superposed individual velocity fields to a combined measurement. The two dimensional average velocities in both longitudinal (U) and vertical (V) directions for the rotor in isolation case and the ship in isolation case were superposed in order to compare to the measured velocity field of the combined rotor and ship airwake. Figure 5.22 presents the superposition of the time averaged velocities for the rotor in isolation and the ship in isolation cases. More results and comparisons are detailed in Chapter 6.

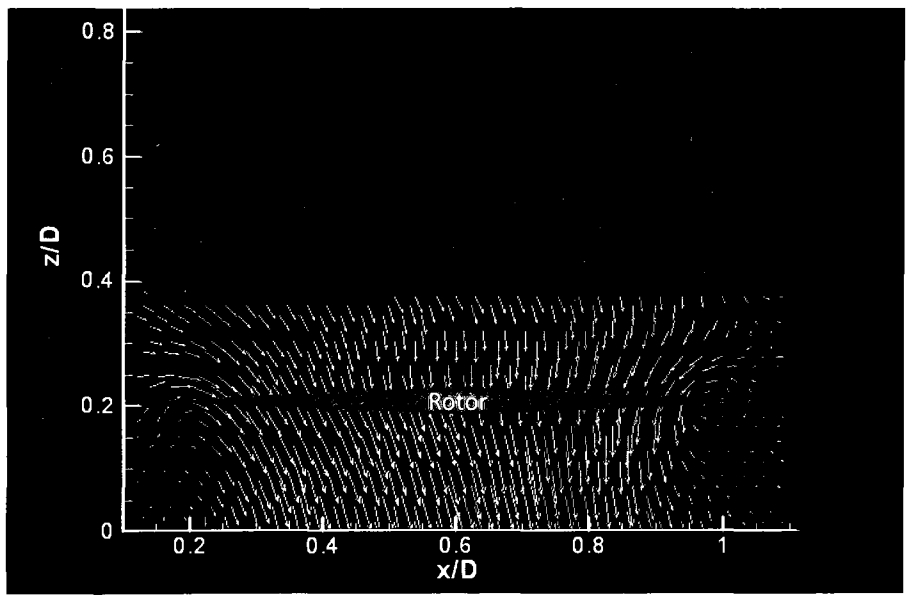

Figure 5.22 Superposition of Rotor Downwash/Ship Airwake

6. RESULTS

6.1 Introduction

In this chapter the experimental results and brief explanations of the flowfields will be presented including interpretation of the overall effects on rotor thrust. Results include PIV flowfield surveys which are performed with the ship in isolation, the rotor in isolation, and the rotor downwash with the ship airwake in the longitudinal plane as well as the lateral plane. In addition some of the design points which are detailed in Chapter 5 are chosen for analysis. Each of the PIV velocity field plots is a time average of 150 images sampled at approximately 3.5 Hz. The x-axis is aligned with the ship longitudinal centerplane. The y-axis is positive to starboard and lies in a lateral plane. The z-axis is positive upwards. The coordinate system may be seen in figure 3.11. The experimental cases are summarized in table 6.1 with x/D and z/D, given as the location of the rotor disk center. All cases are for zero yaw (WOD=0), rotor at 5000 RPM, and advance ratio of 0.075.

Rotor downwash with ship airwake (Longitudinal Plane, V_∞= 5.14 m/s)		**Rotor downwash with ship airwake (Lateral Plane, V_∞= 5.14 m/s)**	
x/D	**z/D**	**x/D**	**z/D**
0.5	0.25	0.5	0.35
0.5	0.55	0.5	0.55

0.5	0.75	0.5	0.75
0.8	0.45	1	0.35
0.8	0.65	1	0.55
0.8	0.85	1	0.5
1.1	0.35	1.5	0.35
1.1	0.55	1.5	0.55
1.1	0.75	1.5	0.75
1.4	0.45		
1.4	0.65		
1.4	0.85		
1.7	0.35		
1.7	0.55		
1.7	0.75		
2	0.45		
2	0.65		
2	0.85		

Table 6.1 Experimental Cases

Ship in Isolation Case (Longitudinal Plane V_∞= 5.14 m/s):

1. Ship in isolation **a** (from hangar door to the middle of the landing deck)
2. Ship in isolation **b** (from middle of the landing deck to the end of the landing deck)

Rotor in Isolation Case:

1. Rotor in isolation (5000 RPM)
2. Rotor in isolation (5000 RPM) with V_∞= 5.14 m/s

6.2 Ship in Isolation Case

For this PIV flowfield survey case, the focus was on understanding the ship airwake characteristics over the landing deck without the presence of a rotary wing downwash influence. The PIV measurements of the flow in the longitudinal center plane of the frigate landing deck and aft face of the hangar are presented in Figure 6.1 and Figure 6.2, respectively. Figure 6.1 presents averaged velocity vectors whereas Figure 6.2 presents contour plots. The flow is essentially that over a backward facing step of finite width. The flow is divided into a region of recirculation and that of an inclined flowfield with near freestream conditions. The longitudinal dividing streamline extends approximately from the top of the hangar to a point at approximately the center of the landing deck.[2,12,31,41,43]

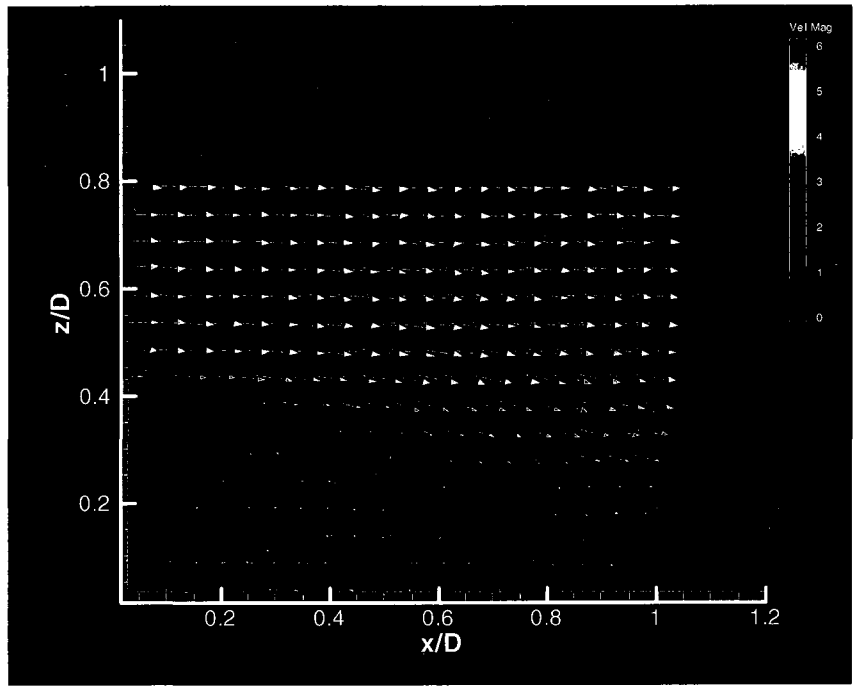

Figure 6.1 Velocity Vectors (m/s) over Frigate Landing Deck in the x-z plane

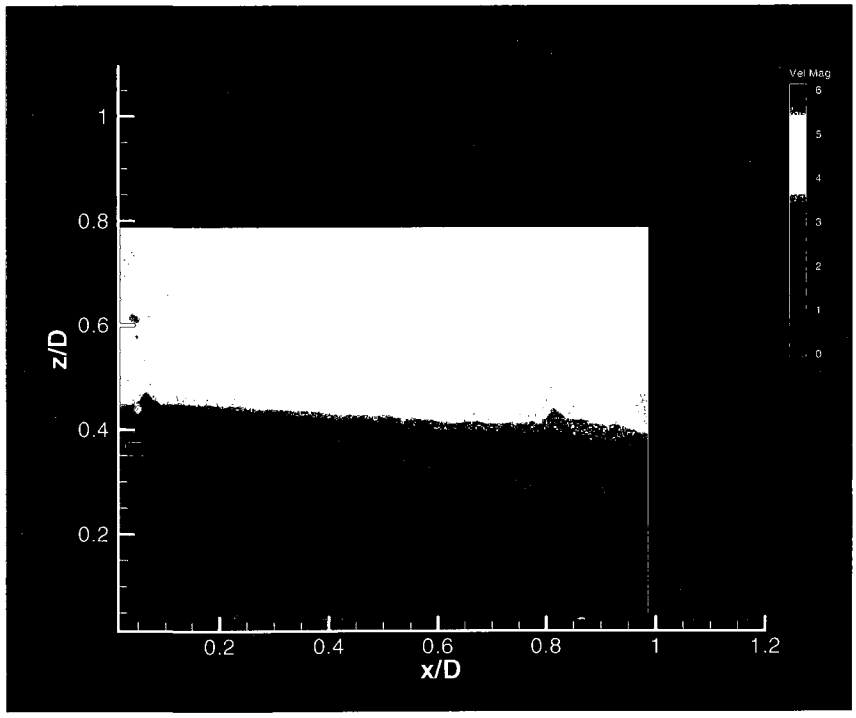

Figure 6.2 Contour Plot over Frigate Landing Deck in the x-z plane

6.3 Rotor in Isolation

The rotor in isolation case was performed for both wind-off and wind-on conditions. In both cases the rotor was rotating at 5000 RPM. The PIV flowfield survey was conducted to investigate the rotor downwash with and without the presence of the freestream velocity. The averaged velocity vectors for the wind-off condition are presented in Figure 6.3, where the contour plot is presented in Figure 6.4.

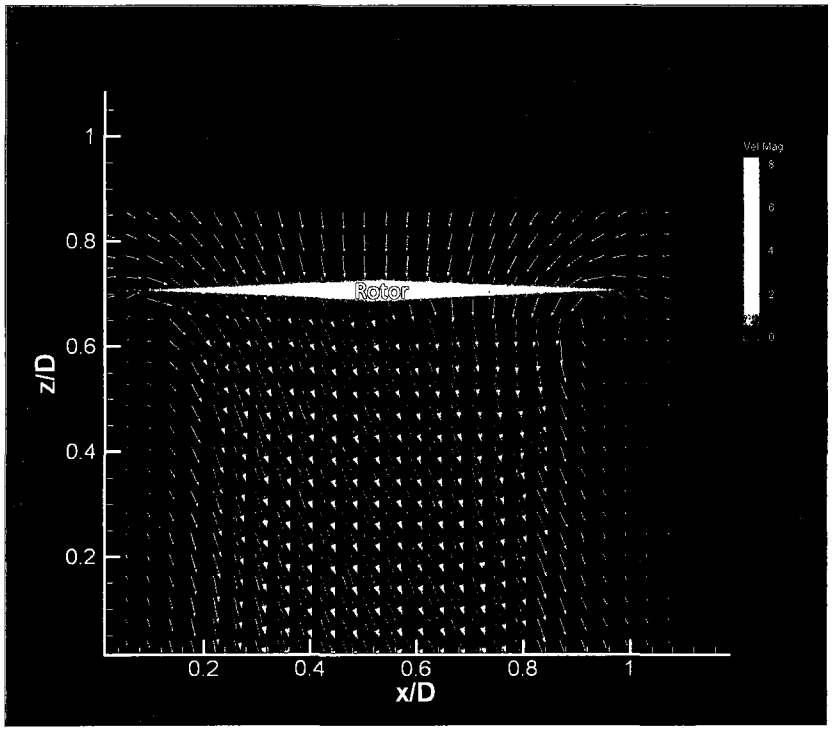

Figure 6.3 Velocity Vector (m/s) for Rotor in Isolation Case (C_T=0.01087)

The quiescent air is accelerated by the rotor blades and directed down the rotational axis of the rotor as can be seen in Figure 6.3.

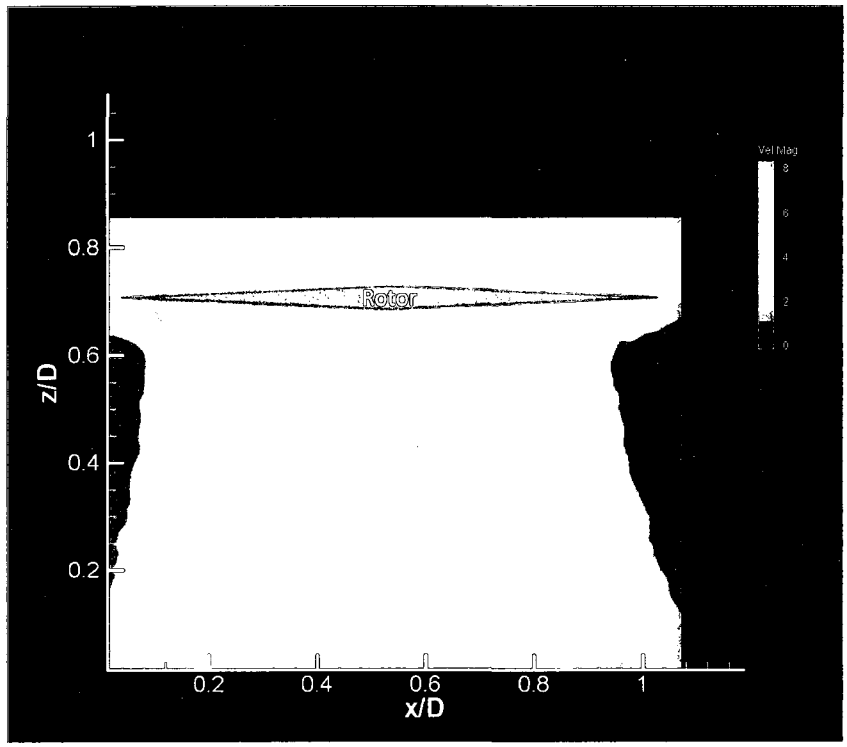

Figure 6.4 Contour Plot for Rotor in Isolation Case

Figure 6.5 and Figure 6.6 present the PIV flowfield survey for the wind-on case. The effect of the freestream velocity on the rotor downwash can be seen clearly in both the velocity vectors and velocity contour plots. The combined flowfield appears asymmetric with respect to the rotational axis and is inclined at approximately 45° from the vertical. The magnitude of this angle, called the wake skew angle, is in keeping with established rotor theory for an advance ratio of 0.075 and measured thrust coefficient of 0.011.[44]

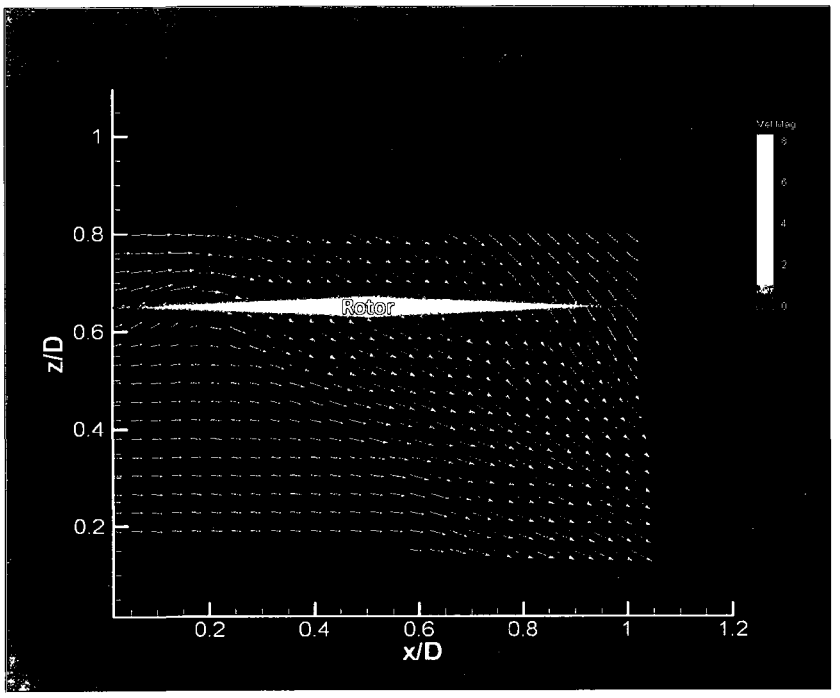

Figure 6.5 Rotor in Isolation with V_∞= 5.14 m/s Case (C_T=0.01145)

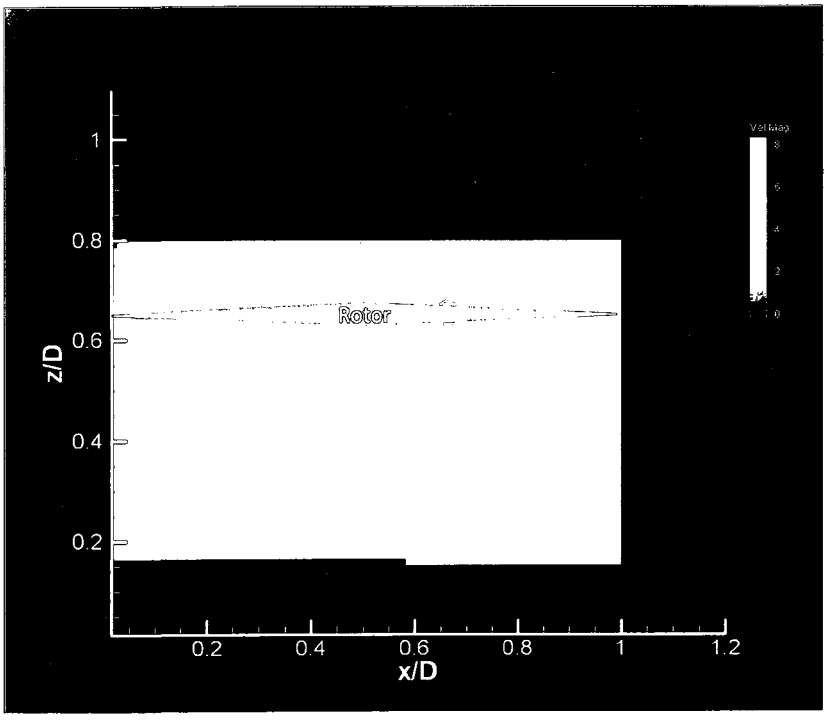

Figure 6.6 Rotor in Isolation with V_∞=5.14 m/s Case (Contour Plot)

6.4 Rotor Downwash with Ship Airwake in the Longitudinal Plane

PIV flowfield surveys were conducted over the region defined by the design points first shown in the factorial designs of Chapter 5. Images were captured from the port side of the frigate in the x-z plane. The reported thrust coefficients are taken from the measurements of experiment 3 shown in section 5.2.3. All survey results are for a freestream velocity V_∞= 5.14 m/s and a rotor speed of 5000 rpm. Results for a rotor location of approximately 0.5D away from the hangar door and 0.25D above the centerline of the landing deck are presented in Figure 6.7 and Figure 6.8, respectively.

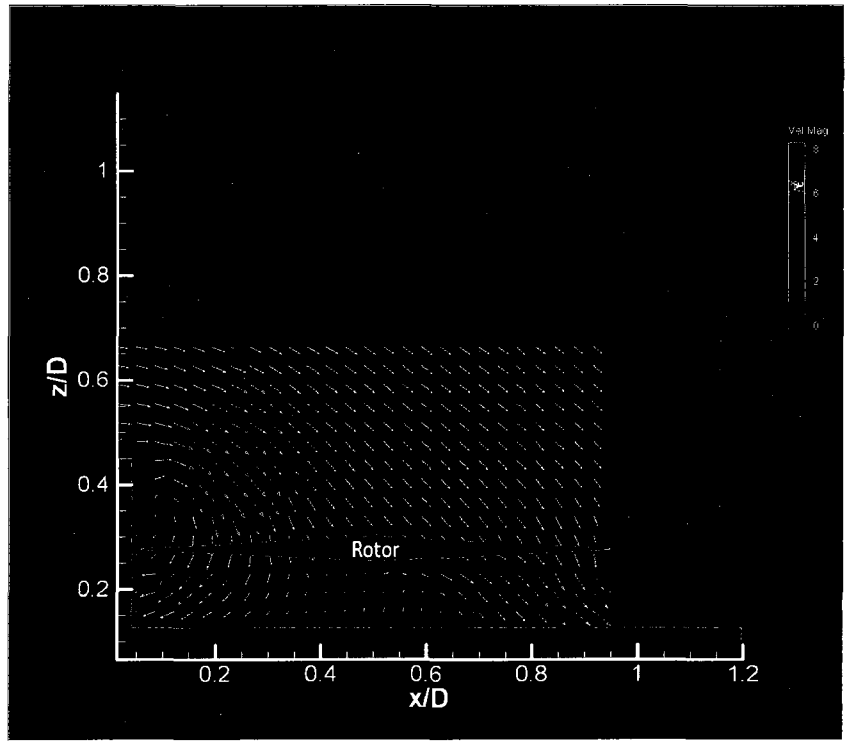

Figure 6.7 Rotor with ship airwake V_∞=5.14 m/s (x/D=0.5; z/D=0.25) (C_T=0.01638)

When the rotor is below the top of the hangar door, the recirculation region has a powerful interaction with the rotor wake. The rotor thrust is a balance of several

influences, the deleterious effect of reingestion, downwash, and the relatively low streamwise flow components and the positive influence of ground effect.[42] The result is that the thrust coefficient is much higher than the isolated rotor case. The flow passing over the top of the hangar turns downward with the downwash effect of the rotor and recirculation zone and continues downstream to the stern of the ship. The recirculation zone appears to be smaller and stronger than that of the ship in isolation.[42]

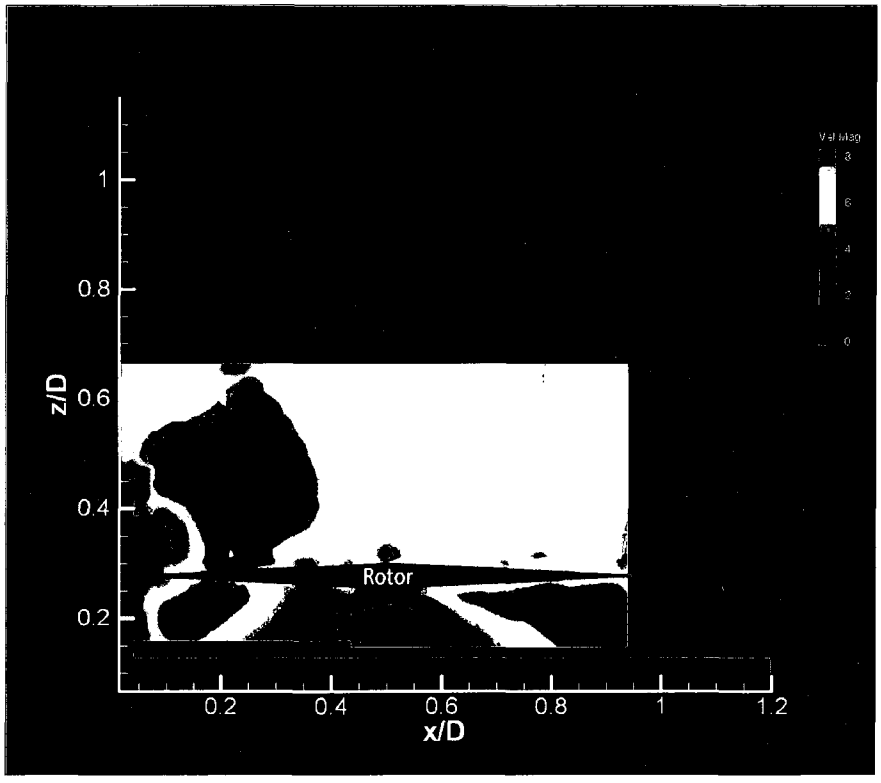

Figure 6.8 Rotor with ship airwake V_∞=5.14 m/s (x/D=0.5; z/D=0.25) (Contour Plot)

An increasingly larger recirculation zone develops behind the hangar door with increasing rotor height above the deck. Figure 6.9 presents the PIV flowfield survey for x/D=0.5 and z/D=0.55 as velocity vectors where Figure 6.10 presents the velocity contour plot for the same location. In general, it is noted that the effect of the rotor on the

recirculation zone which exists aft of the hangar eventually decreases, with increasing vertical distance above the landing deck. Recirculation zones are inherently unsteady and thus give rise to the unsteady component of the airwake. As the rotor height increases to a level above that of the hangar door, the thrust coefficient increases due to the increased streamwise flow contribution.[42,43]

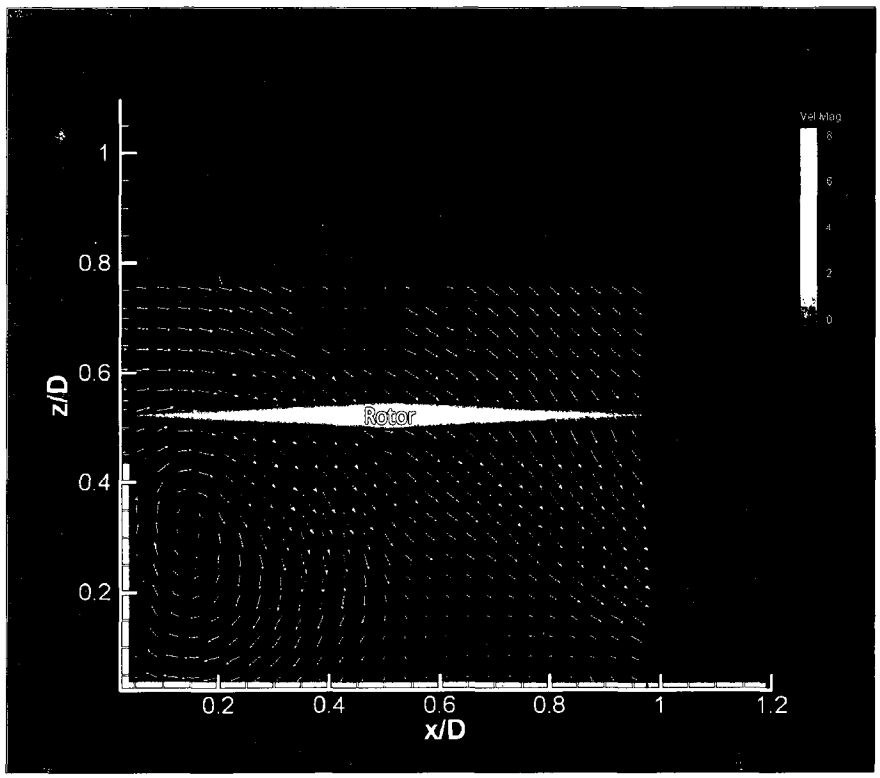

Figure 6.9 Rotor with ship airwake V_∞=5.14 m/s (x/D=0.5; z/D=0.55) (C_T=0.0174)

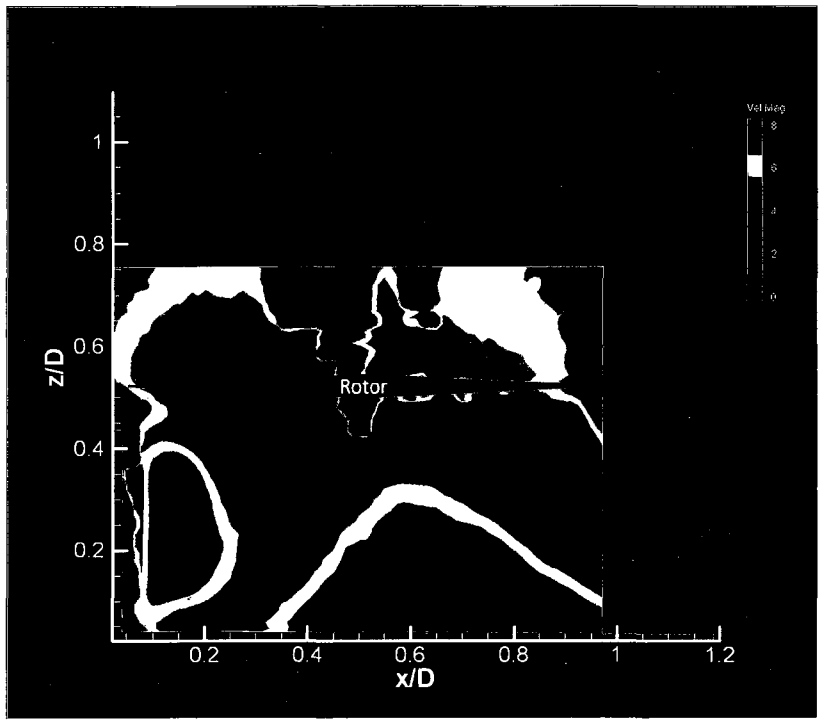

Figure 6.10 Rotor with ship airwake V_∞=5.14 m/s (x/D=0.5;z/D=0.55) (Contour Plot)

The general appearance of the velocity field just below the rotor for the design point x/D=0.5 and z/D=0.75 looks similar to the rotor in isolation, with the exception of the area just aft of the hangar door which is affected with rotor downwash and a recirculation zone. The rotor downwash causes a stagnation line to exist at about x/D=0.5. The measured thrust coefficient was again greater than that at x/D=0.5, z/D=0.55 owing to the greater freestream contribution. The velocity vector and velocity contour plots are presented in Figure 6.11 and Figure 6.12, respectively.

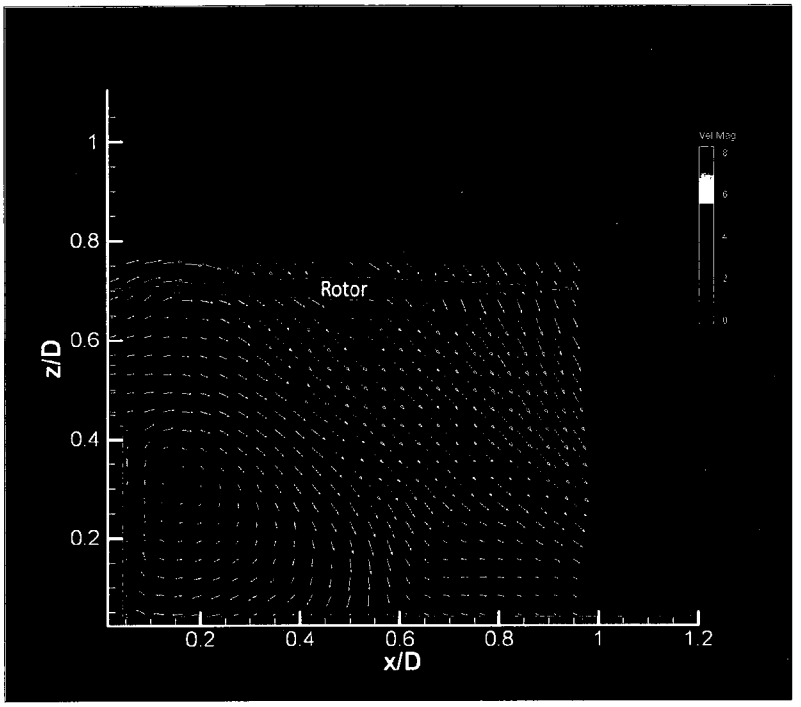

Figure 6.11 Rotor with ship airwake V_∞=5.14 m/s (x/D=0.5; z/D=0.75) (C_T=0.0177)

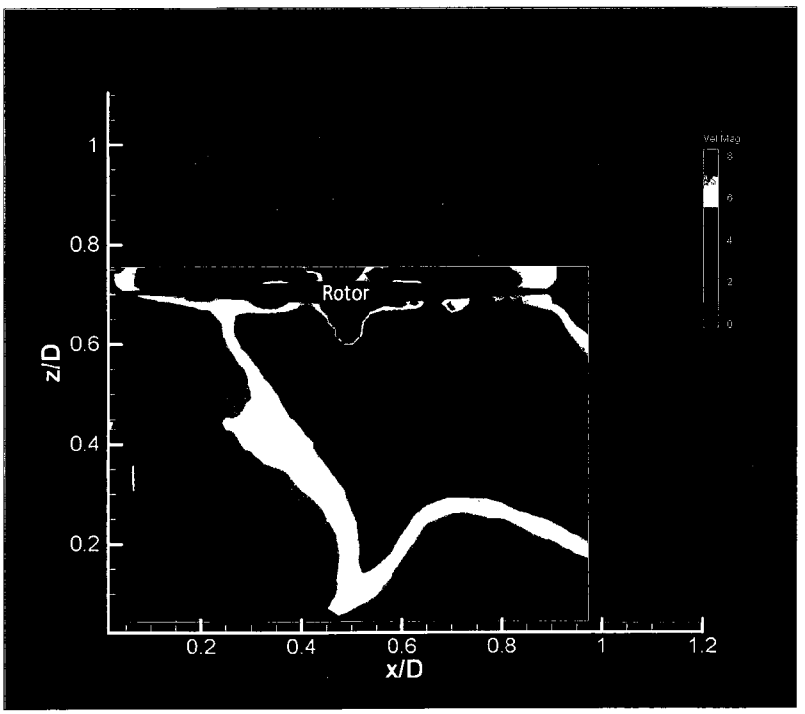

Figure 6.12 Rotor with ship airwake V_∞=5.14 m/s (x/D=0.5;z/D=0.75) (Contour Plot)

The rotor downwash effect with increased height is consistent as the rotor is moved aft. The recirculation zone gets weaker as the rotor is moved vertically away from the deck. The thrust coefficient increase with height is not as profound as the rotor is moved away from the hangar door. The stagnation line moves aft along the longitudinal axes of the landing deck from the hangar door towards the stern of the frigate. These trends can be seen for the location x/D=0.8 as presented by Figures 6.13 - 6.16.

A trend similar to the rotor in isolation can be seen for the point x/D=0.8 and z/D=0.85 presented in Figure 6.17 and Figure 6.18 because of the increased vertical distance above the landing deck..

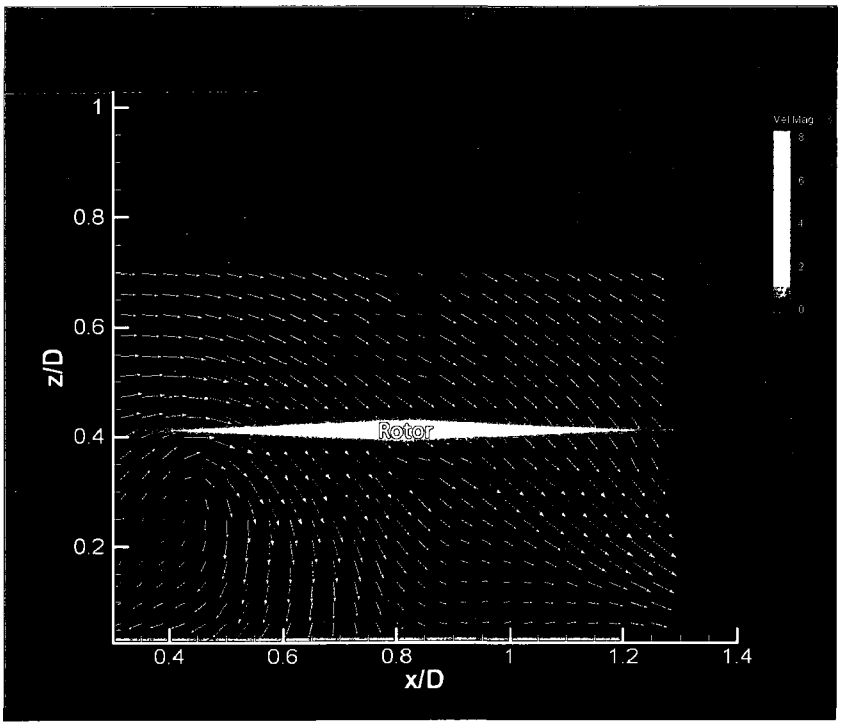

Figure 6.13 Rotor with ship airwake V_∞=5.14 m/s (x/D=0.8; z/D=0.45) (C_T=0.0174)

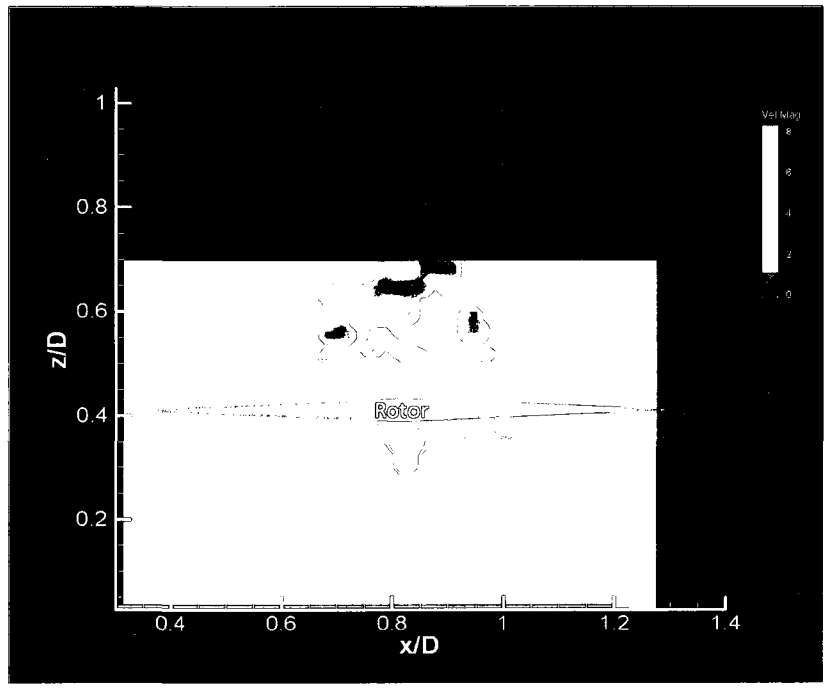

Figure 6.14 Rotor with ship airwake V_∞=5.14 m/s (x/D=0.8;z/D=0.45) (Contour Plot)

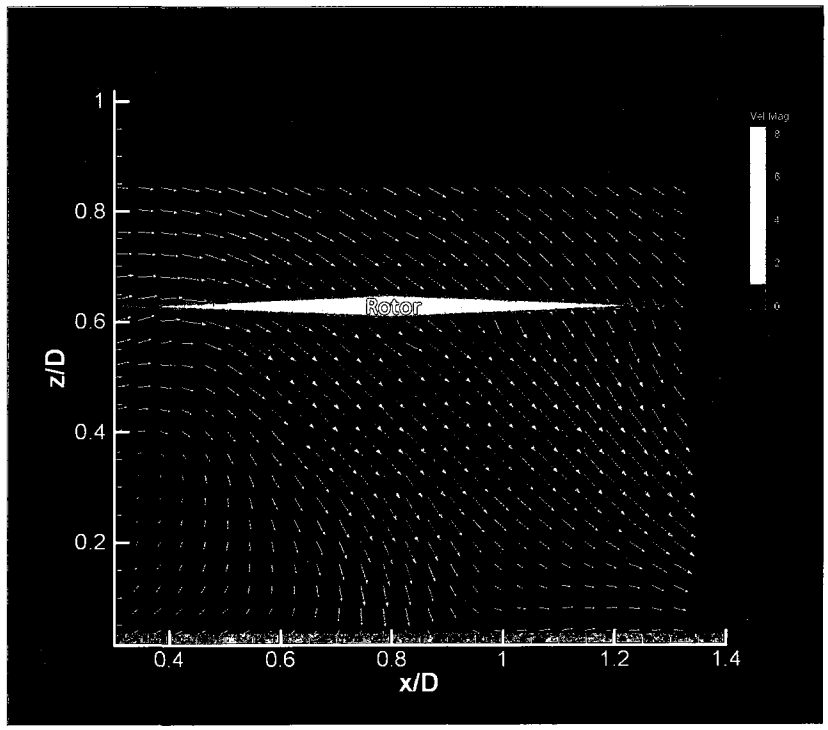

Figure 6.15 Rotor with ship airwake V_∞=5.14 m/s (x/D=0.8; z/D=0.65) (C_T=0.0176)

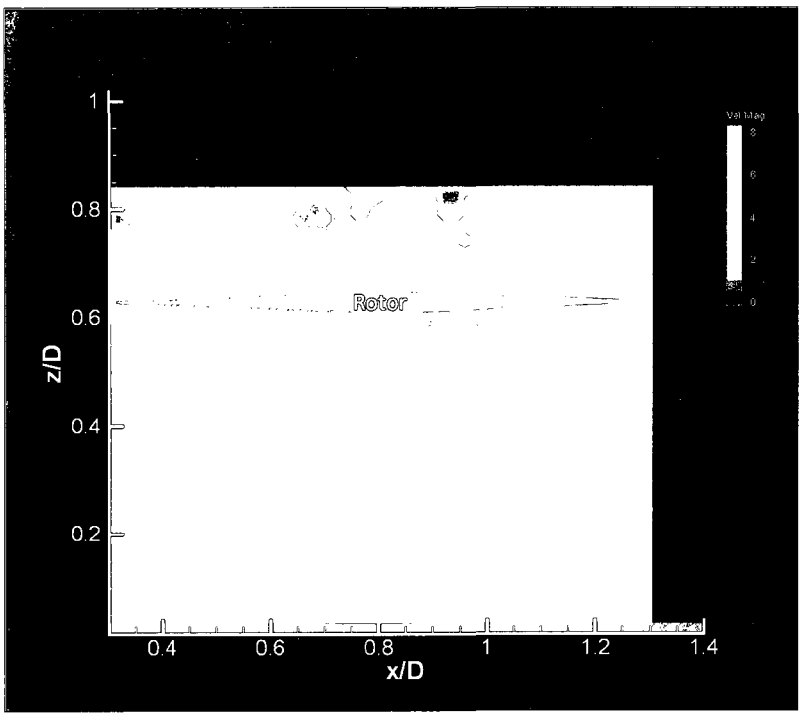

Figure 6.16 Rotor with ship airwake V_∞=5.14 m/s (x/D=0.8;z/D=0.65) (Contour Plot)

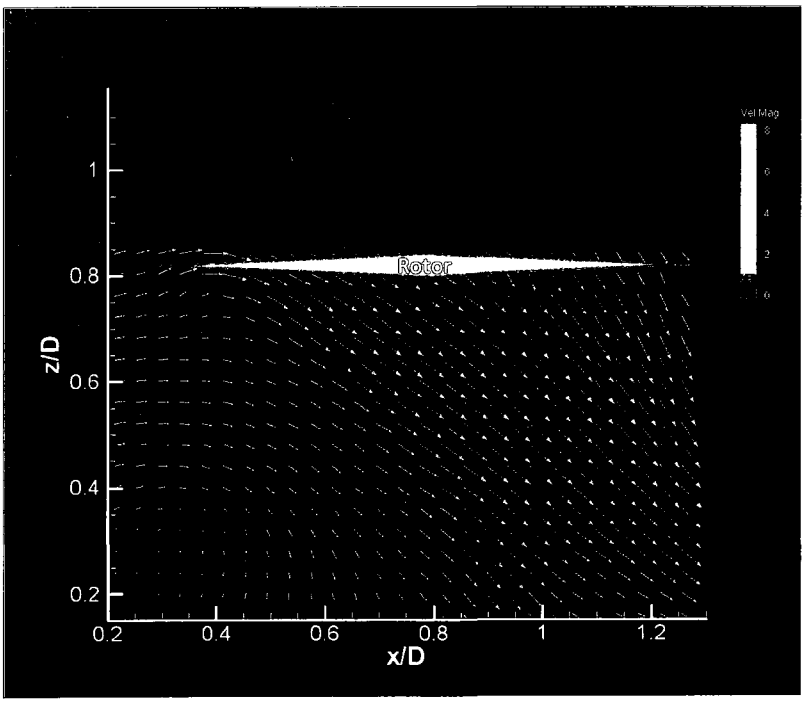

Figure 6.17 Rotor with ship airwake V_∞=5.14 m/s (x/D=0.8; z/D=0.85) (C_T=0.0175)

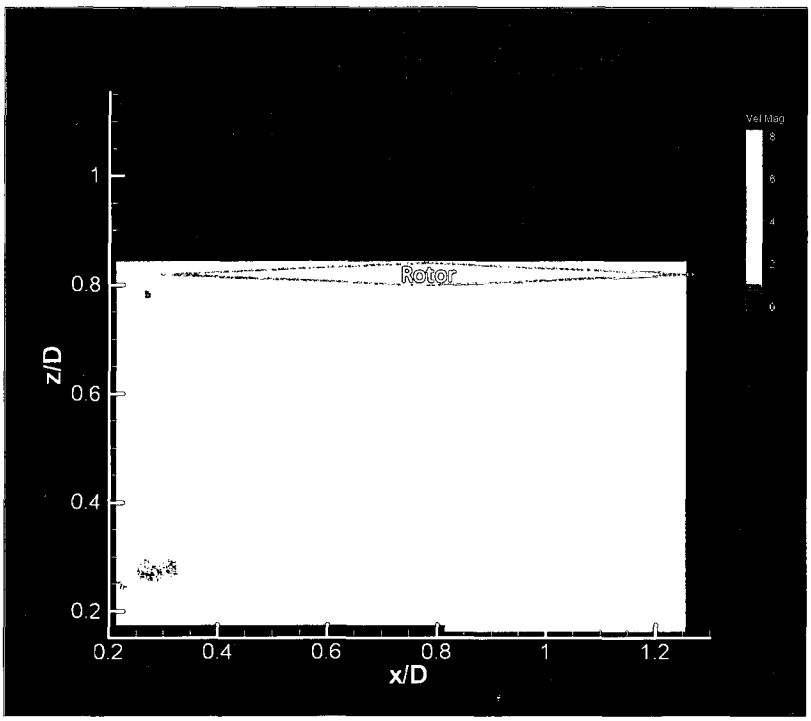

Figure 6.18 Rotor with ship airwake V_∞=5.14 m/s (x/D=0.8;z/D=0.85) (Contour Plot)

The two stations along the longitudinal axes of the landing deck located at x/D=1.1 and x/D=1.4 show a similar velocity flowfield for corresponding design points (3 vertical design points on 2 longitudinal stations). These design points are x/D=1.1,z/D=0.35; x/D=1.1,z/D=0.55; x/D=1.1, z/D=0.75; x/D=1.4, z/D=0.45; x/D=1.4, z/D=0.65; and x/D=1.4, z/D=0.85. The velocity vector and contour plots are presented in figures 6.19 through Figure 6.30.

Again, in general the rotor downwash effect is stronger and has a major interaction with ship airwake when the rotor is close to landing deck and gets weaker when the rotor vertical distance above the landing deck increases. A recirculation zone exists for all cases even it is small compared with previous forward rotor positions

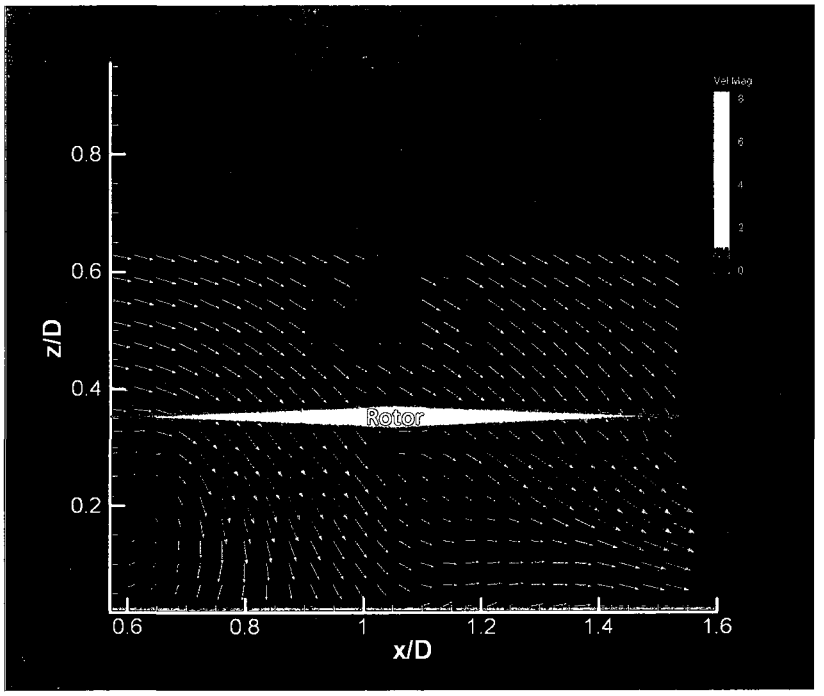

Figure 6.19 Rotor with ship airwake V_∞=5.14 m/s (x/D=1.1; z/D=0.35) (C_T=0.0174)

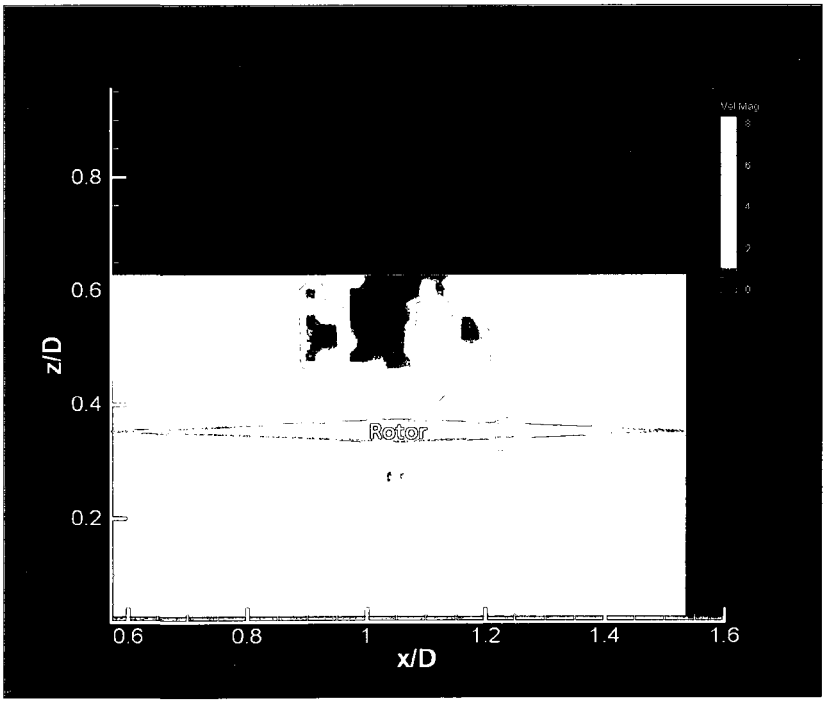

Figure 6.20 Rotor with ship airwake V_∞=5.14 m/s (x/D=1.1;z/D=0.35) (Contour Plot)

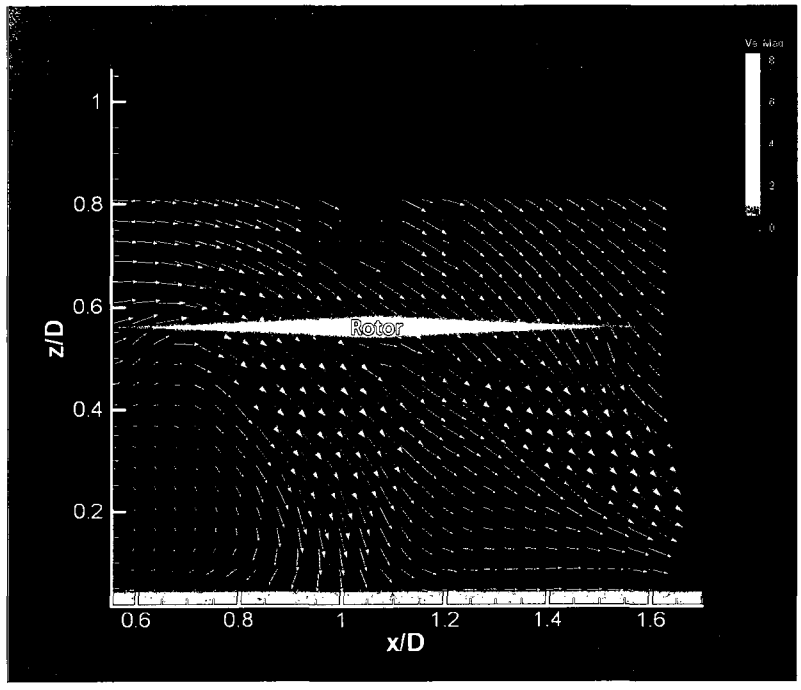

Figure 6.21 Rotor with ship airwake V_∞=5.14 m/s (x/D=1.1; z/D=0.55) (C_T=0.0176)

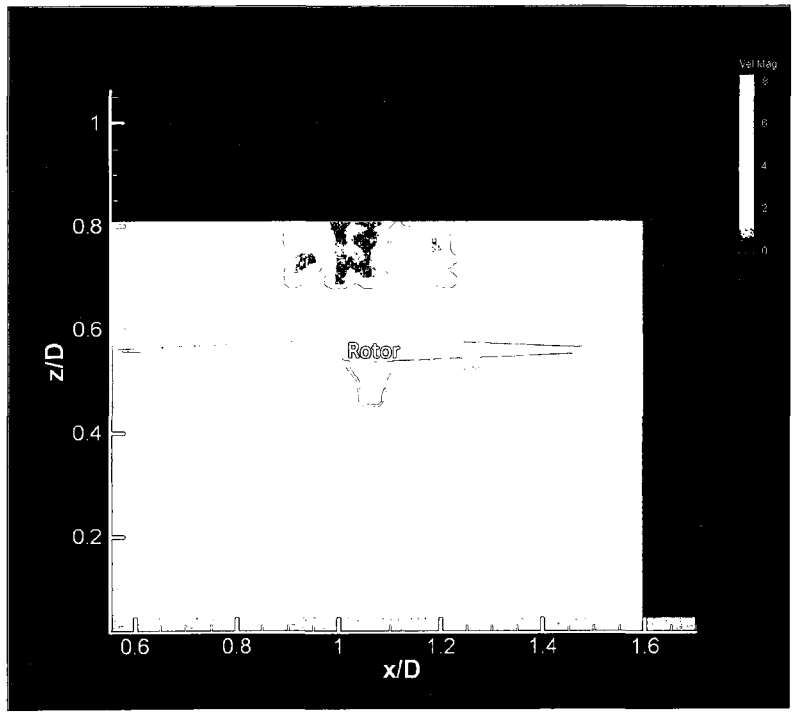

Figure 6.22 Rotor with ship airwake V_∞=5.14 m/s (x/D=1.1;z/D=0.55) (Contour Plot)

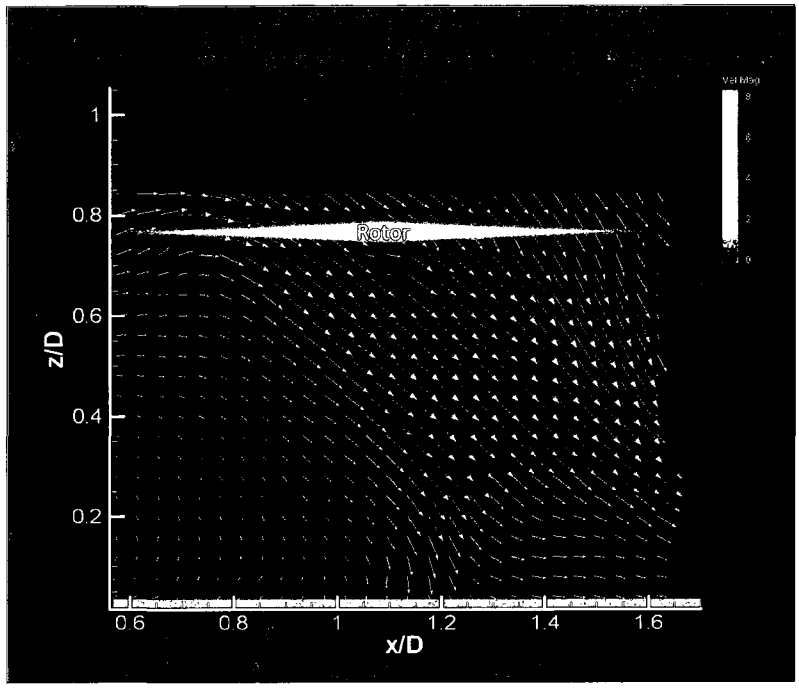

Figure 6.23 Rotor with ship airwake V_∞=5.14 m/s (x/D=1.1; z/D=0.75) (C_T=0.0175)

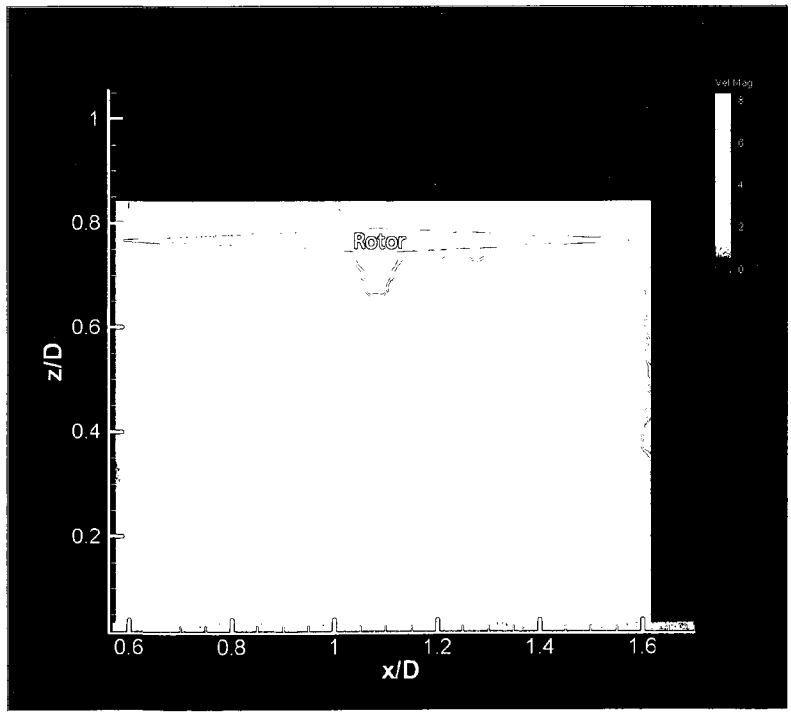

Figure 6.24 Rotor with ship airwake V_∞=5.14 m/s (x/D=1.1;z/D=0.75) (Contour Plot)

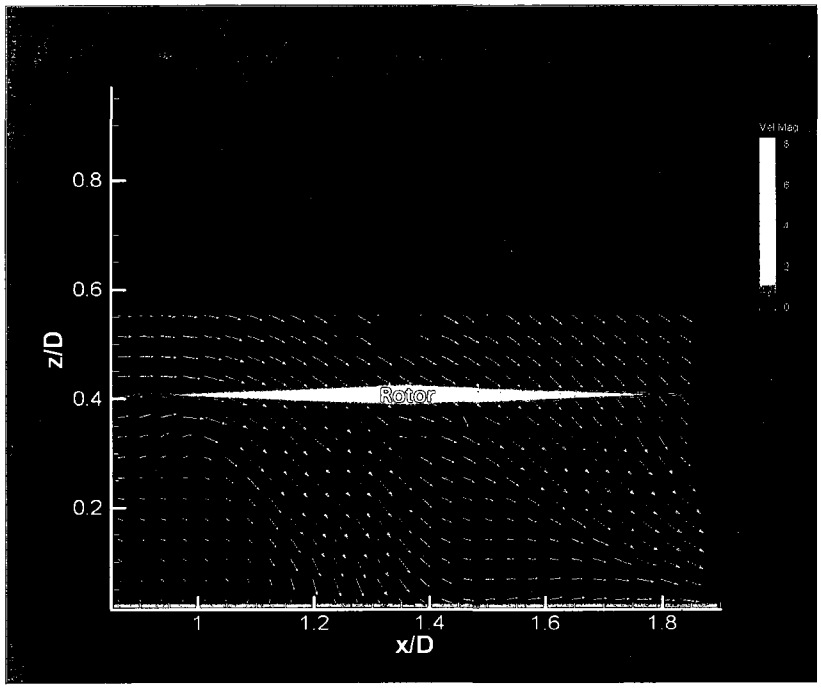

Figure 6.25 Rotor with ship airwake V_∞=5.14 m/s (x/D=1.4; z/D=0.45) (C_T=0.0176)

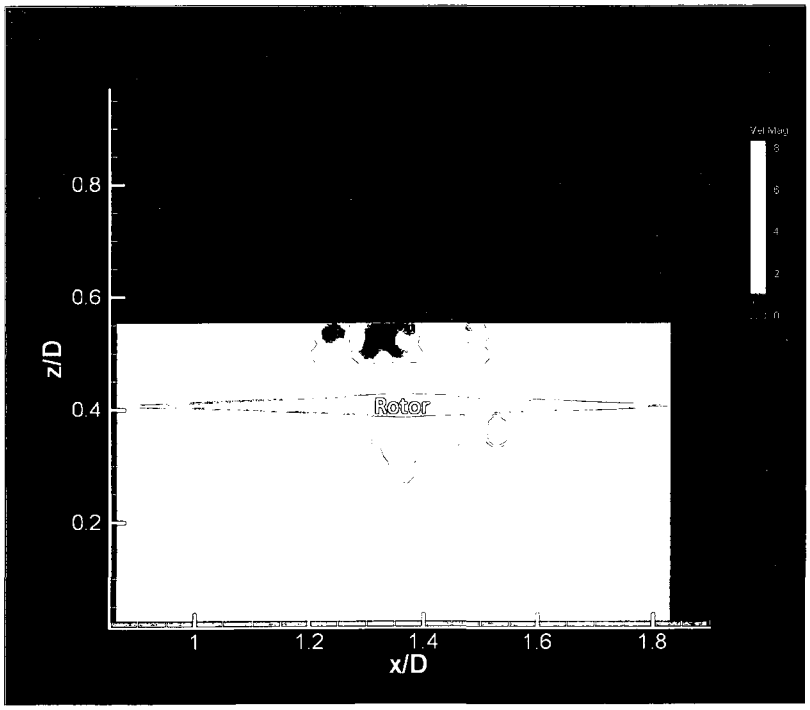

Figure 6.26 Rotor with ship airwake V_∞=5.14 m/s (x/D=1.4;z/D=0.45) (Contour Plot)

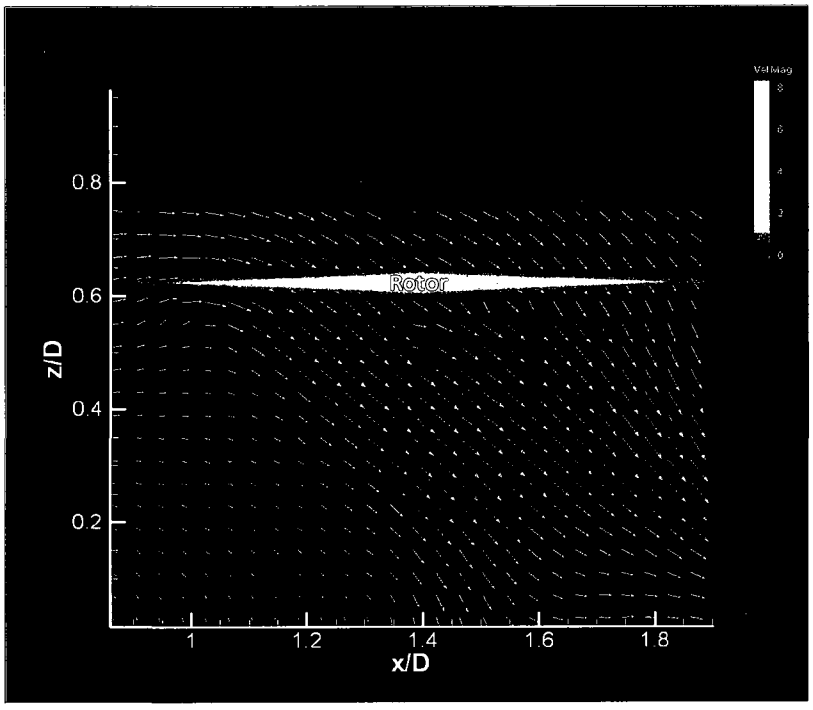

Figure 6.27 Rotor with ship airwake V_∞=5.14 m/s (x/D=1.4; z/D=0.65) (C_T=0.0176)

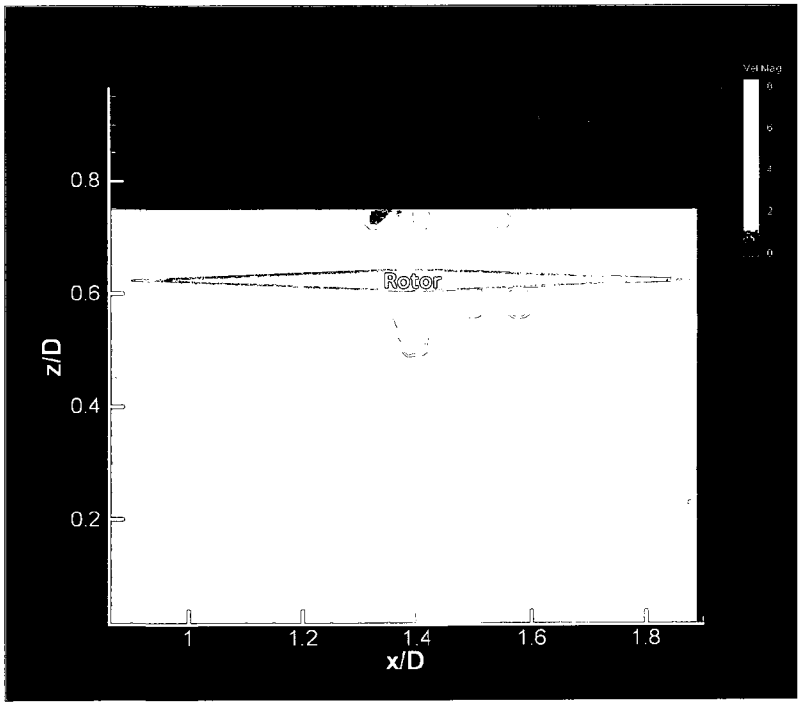

Figure 6.28 Rotor with ship airwake V_∞=5.14 m/s (x/D=1.4;z/D=0.65) (Contour Plot)

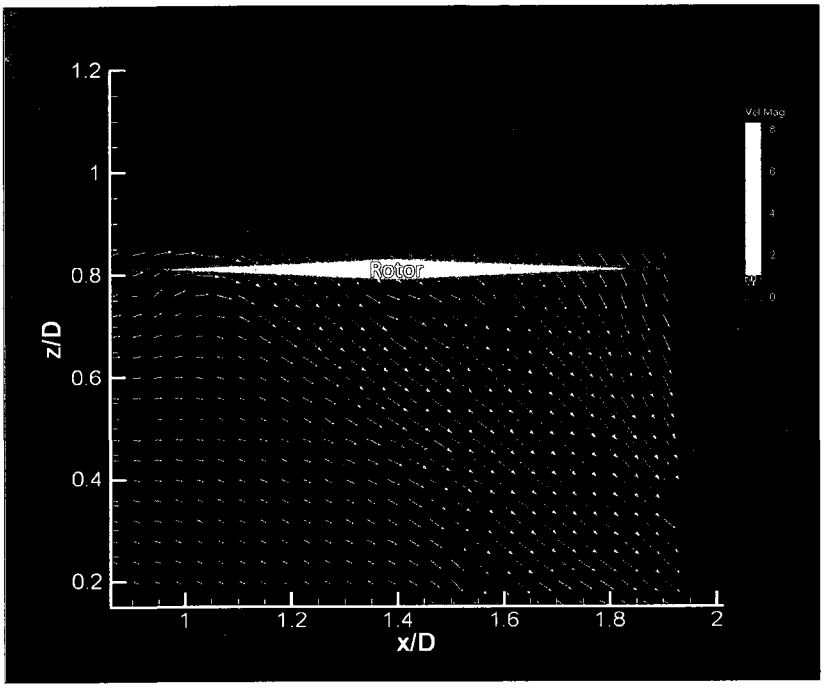

Figure 6.29 Rotor with ship airwake V_∞=5.14 m/s (x/D=1.4; z/D=0.85) (C_T=0.0173)

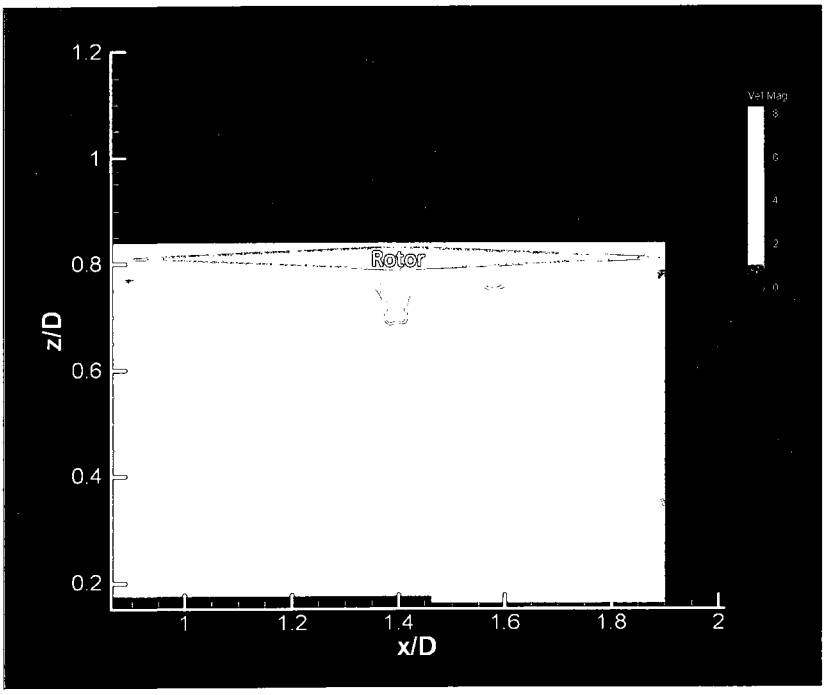

Figure 6.30 Rotor with ship airwake V_∞=5.14 m/s (x/D=1.4;z/D=0.85) (Contour Plot)

Rotor thrust coefficients appear to be relatively constant in the aft locations of the surveys. The recirculation zone and the upflow through the upstream side of the rotor get weaker while proceeding aft in the longitudinal direction. These effects can be seen by the design points on the landing deck for longitudinal axis points x/D=1.7 and x/D=2. There are again 3 vertical design points on 2 longitudinal stations for these cases. These design points are x/D=1.7; z/D=0.35, x/D=1.7; z/D=0.55, x/D=1.7; z/D=0.75, x/D=2; z/D=0.45, x/D=2; z/D=0.65 and x/D=2; z/D=0.85 in. Figures 6.31 - 6.42 present PIV flowfield surveys as velocity vectors as well as velocity contour plots for these stations. It should be noted that the recirculation zone behind the hangar door can't be seen because these design points are very close to the stern of the frigate and the maximum camera image area would not allow for coverage.

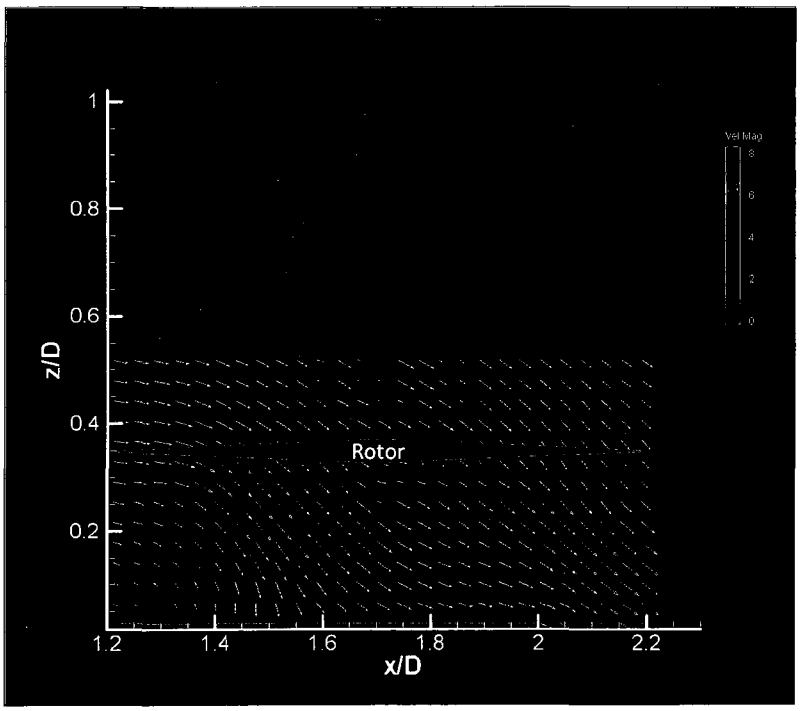

Figure 6.31 Rotor with ship airwake V_∞=5.14 m/s (x/D=1.7; z/D=0.35) (C_T=0.0173)

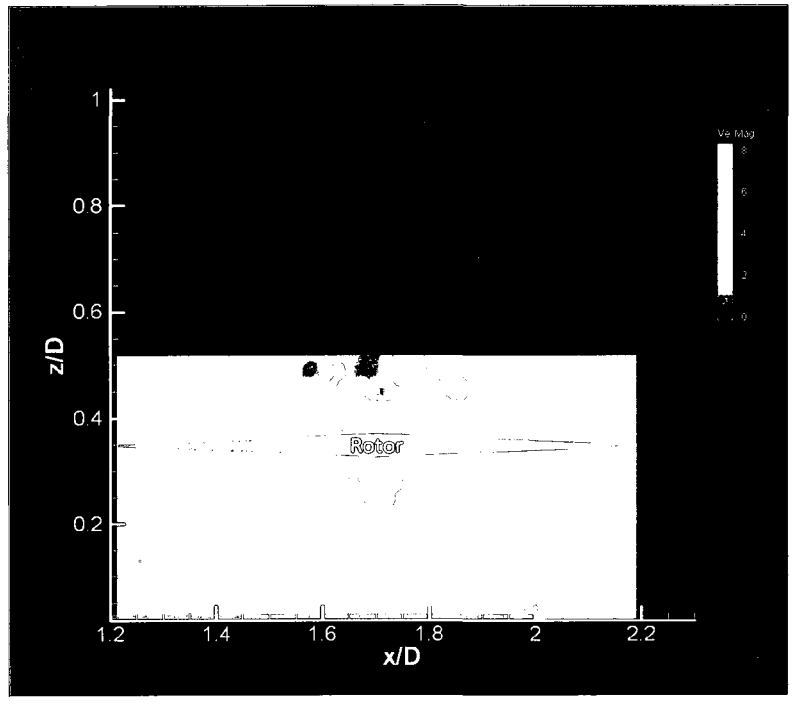

Figure 6.32 Rotor with ship airwake V_∞=5.14 m/s (x/D=1.7;z/D=0.35) (Contour Plot)

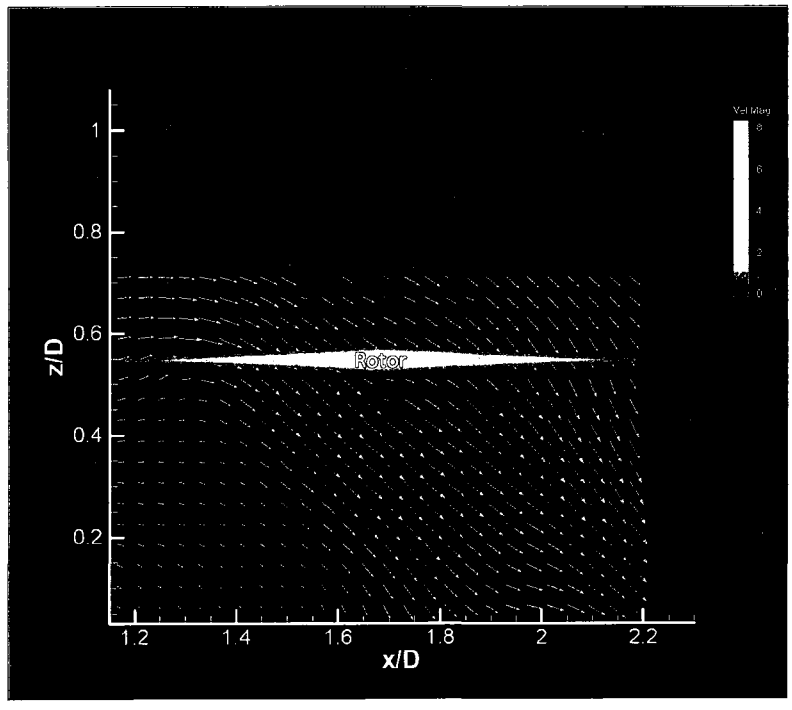

Figure 6.33 Rotor with ship airwake V_∞=5.14 m/s (x/D=1.7;z/D=0.55) (C_T=0.0175)

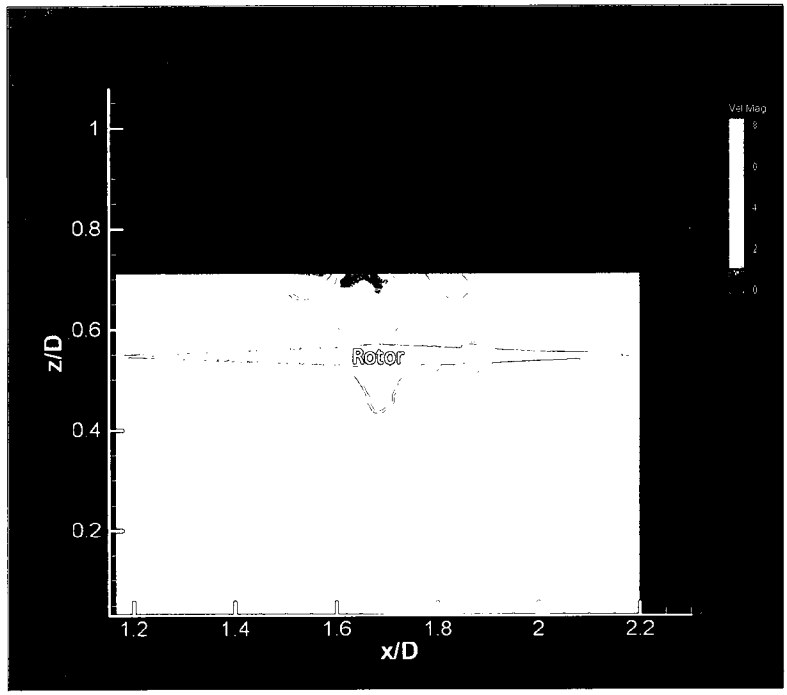

Figure 6.34 Rotor with ship airwake V_∞=5.14 m/s (x/D=1.7;z/D=0.55) (Contour Plot)

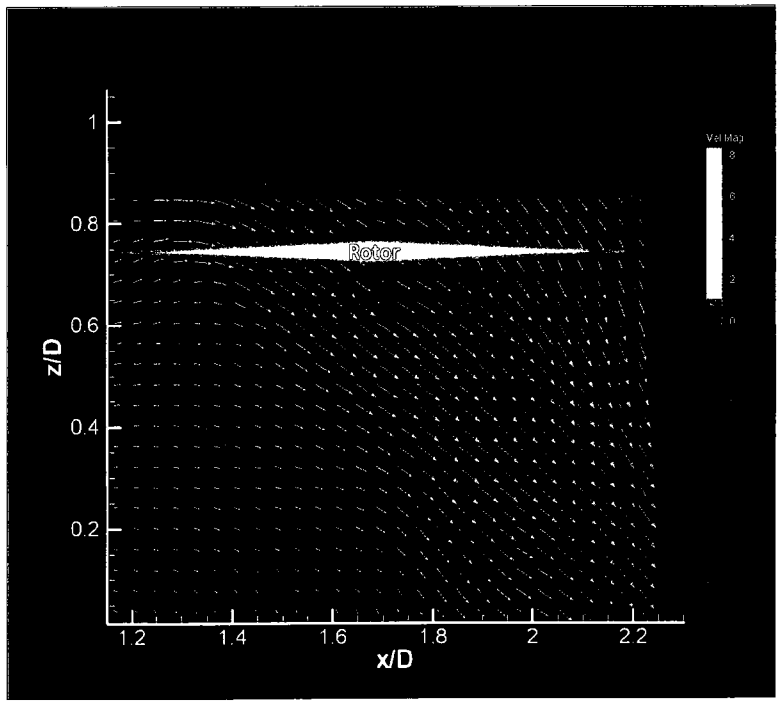

Figure 6.35 Rotor with ship airwake V_∞=5.14 m/s (x/D=1.7; z/D=0.75) (C_T=0.0175)

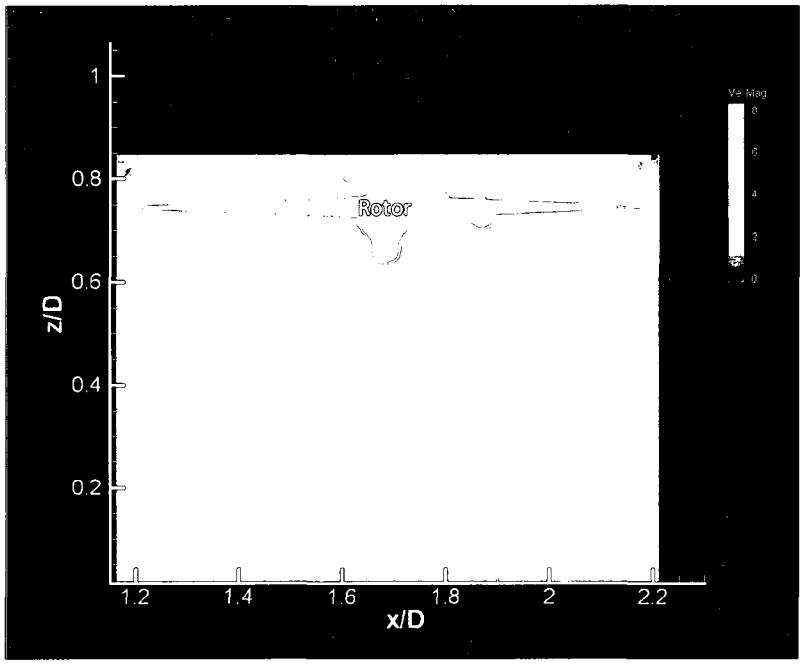

Figure 6.36 Rotor with ship airwake V_∞=5.14 m/s (x/D=1.7;z/D=0.75) (Contour Plot)

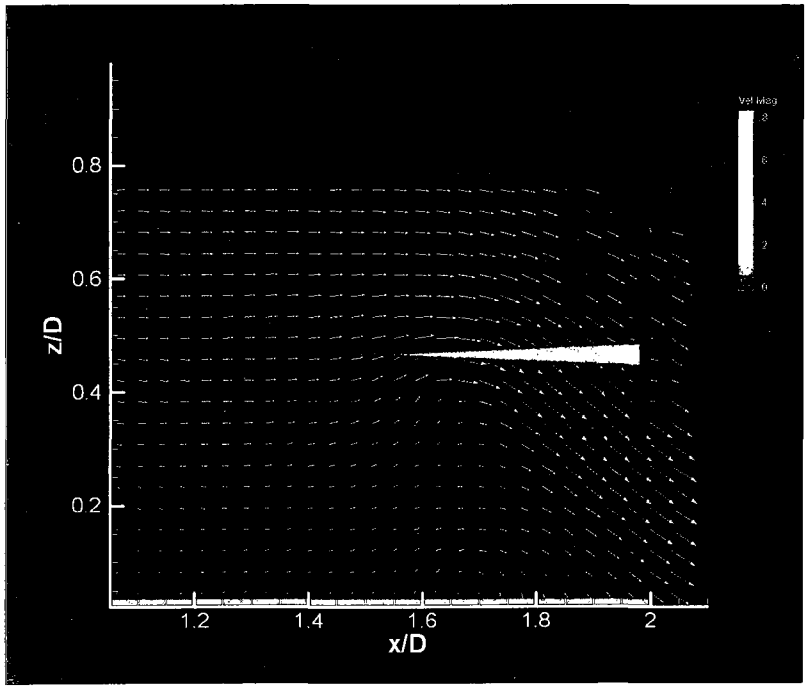

Figure 6.37 Rotor with ship airwake V_∞=5.14 m/s (x/D=2; z/D=0.45) (C_T=0.0172)

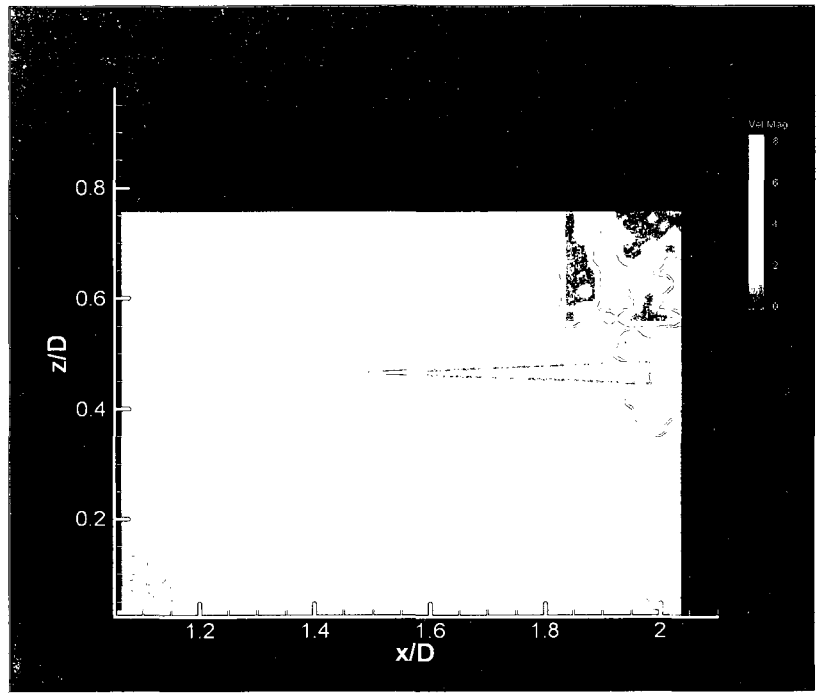

Figure 6.38 Rotor with ship airwake V_∞=5.14 m/s (x/D=2; z/D=0.45) (Contour Plot)

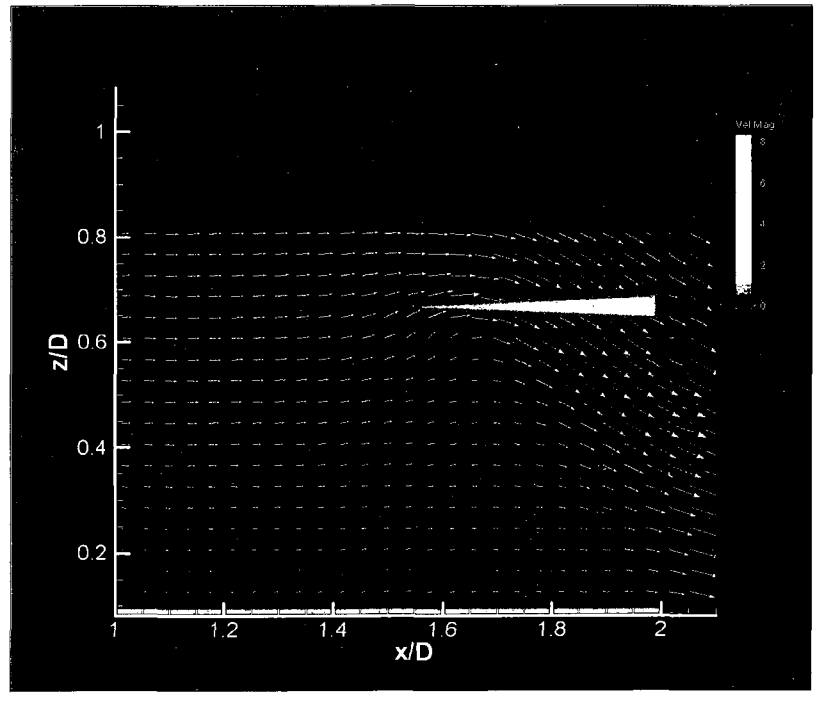

Figure 6.39 Rotor with ship airwake V_∞=5.14 m/s (x/D=2; z/D=0.65) (C_T=0.0174)

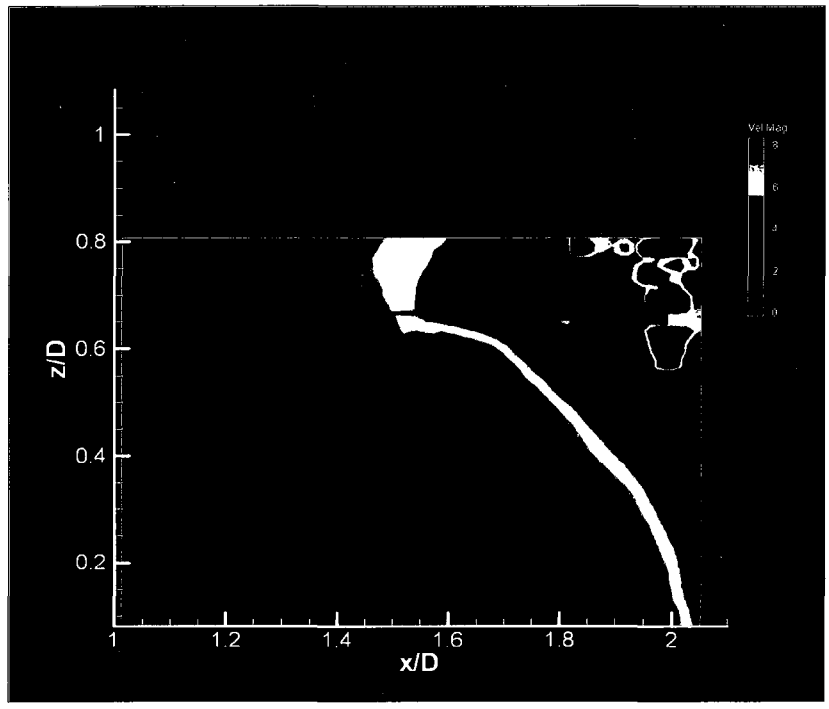

Figure 6.40 Rotor with ship airwake V_∞=5.14 m/s (x/D=2; z/D=0.65) (Contour Plot)

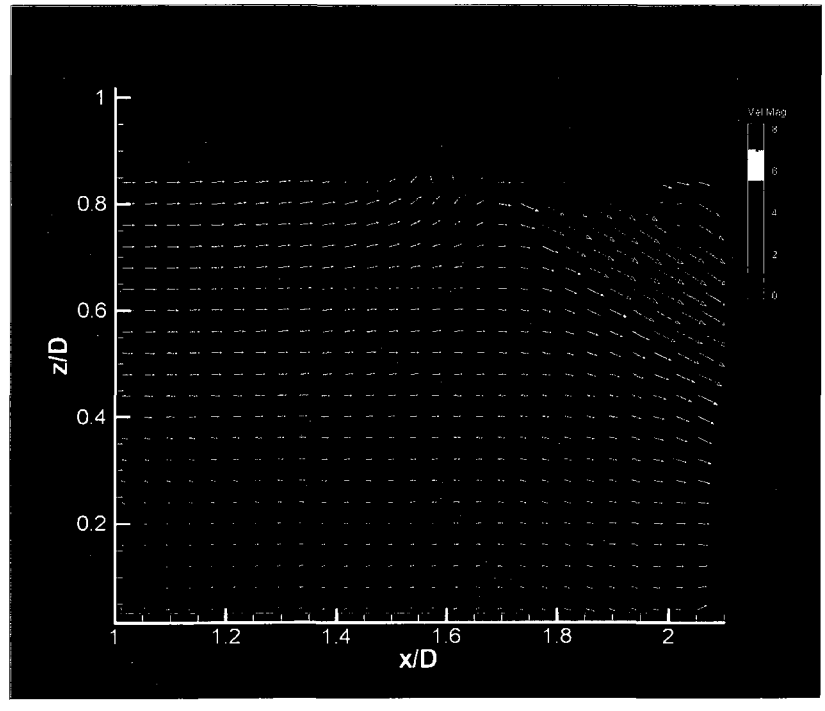

Figure 6.41 Rotor with ship airwake V_∞=5.14 m/s (x/D=2; z/D=0.85) (C_T=0.0175)

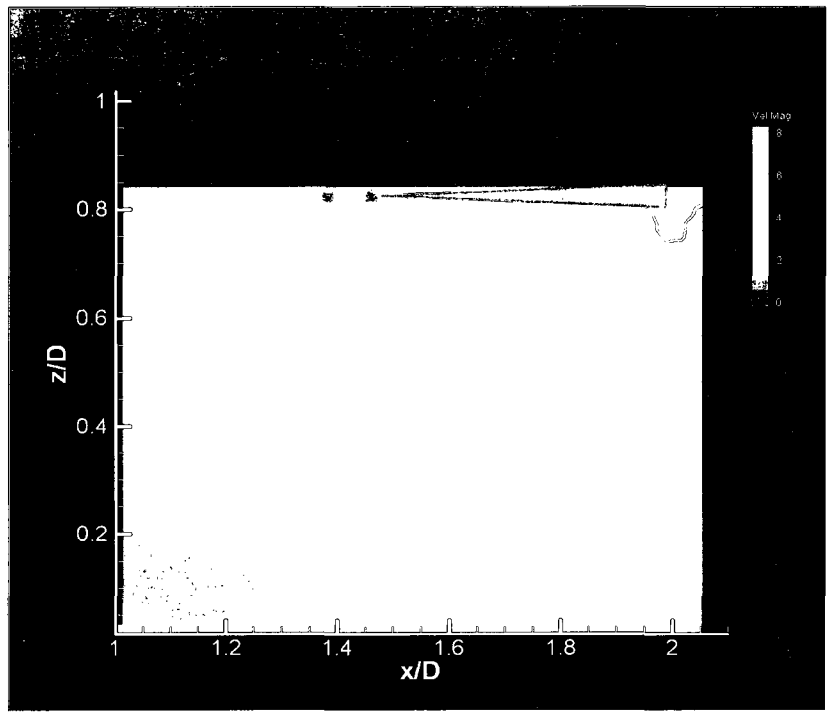

Figure 6.42 Rotor with ship airwake V_∞=5.14 m/s (x/D=2; z/D=0.85) (Contour Plot)

6.5 Rotor Downwash with Ship Airwake in the Lateral Plane

A PIV flowfield survey was conducted for nine different stations on lateral planes. Figures 6.43 to Figure 6.60 present velocity vectors (m/s) and contour plots in y-z plane for three x-locations for the same flow conditions rotor velocity (5000 RPM) as presented in section 6.4.

The first design point is x/D=0.5; z/D=0.35. The velocity vector field and the contour plot for this station are presented in Figure 6.43 and 6.44, respectively. A near-symmetric velocity flowfield can be seen from the Figure 6.43. Because the rotor was located below the hangar door vertical limit and very close to the landing deck and

hangar door longitudinally, the freestream flowfield is not seen to interact resulting in a relatively symmetric flowfield.

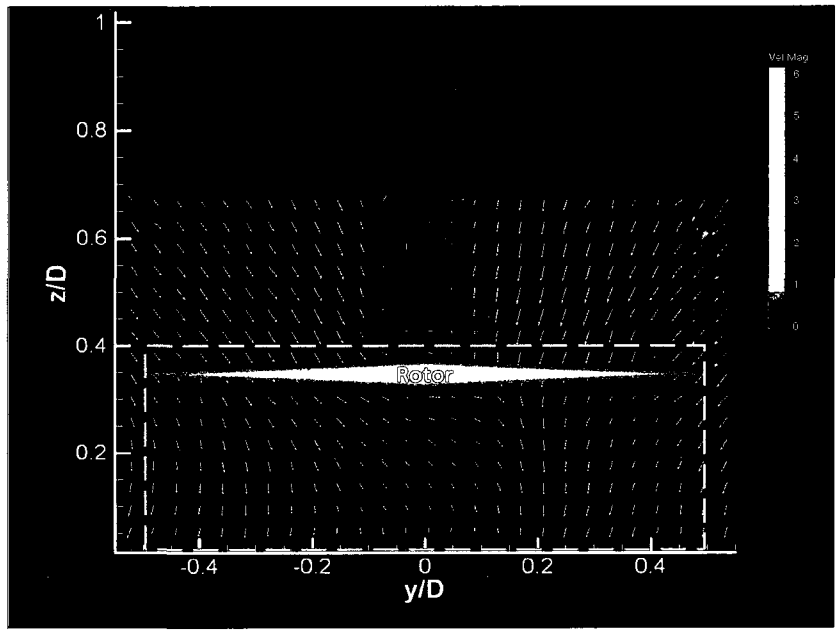

Figure 6.43 Rotor with ship airwake V_∞=5.14 m/s (x/D=0.5; z/D=0.35) (C_T=0.0166)

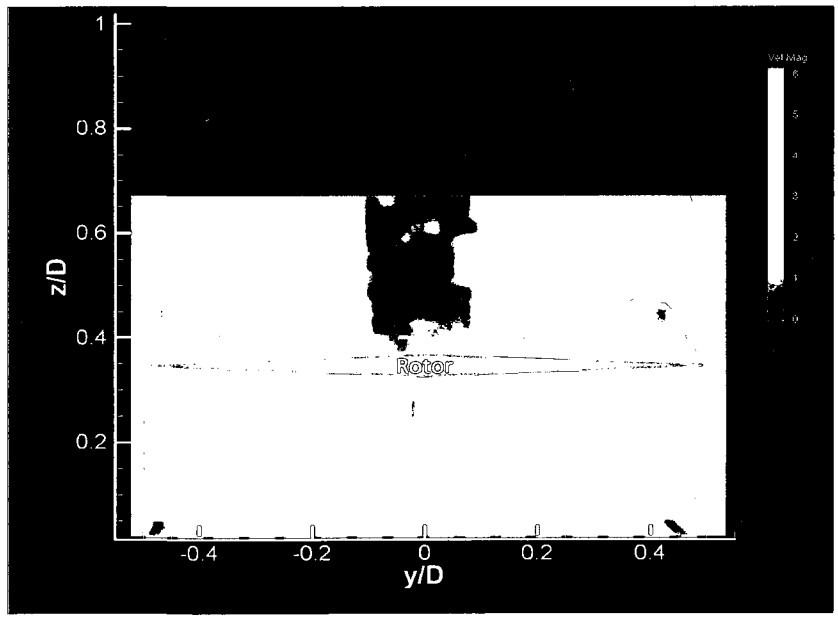

Figure 6.44 Rotor with ship airwake V_∞=5.14 m/s (x/D=0.5;z/D=0.35) (Contour Plot)

With increasing vertical distance above the landing deck, the symmetric velocity field becomes increasingly asymmetric due to the effect of the relative velocity change in the leading and trailing blades. Flow is accelerated more under the leading (starboard) which results in the asymmetric velocity flowfield. The figures show that the starboard side has a higher velocity field magnitude with a more vertical direction compared to the port side. There is little difference in the flow for design points x/D=0.5; z/D=0.55 and x/D=0.5; z/D=0.75 as seen in figures 6.45 - 6.48. The velocity deficit seen in the center of the lateral plane survey images below the rotor is felt to be the result of the wake of the motor located directly above. There is also data loss above the rotor which may be attributed to the same cause. The blue "ghost" in the contour plot of figure 6.46 clearly shows the motor location.

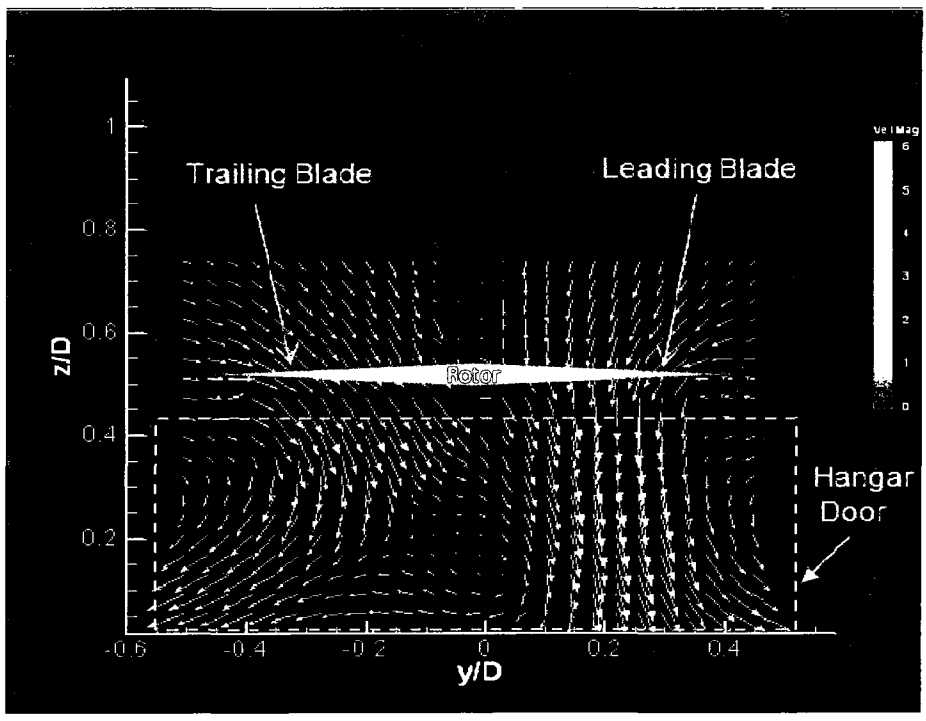

Figure 6.45 Rotor with ship airwake V_∞=5.14 m/s (x/D=0.5;z/D=0.55) (C_T=0.0174)

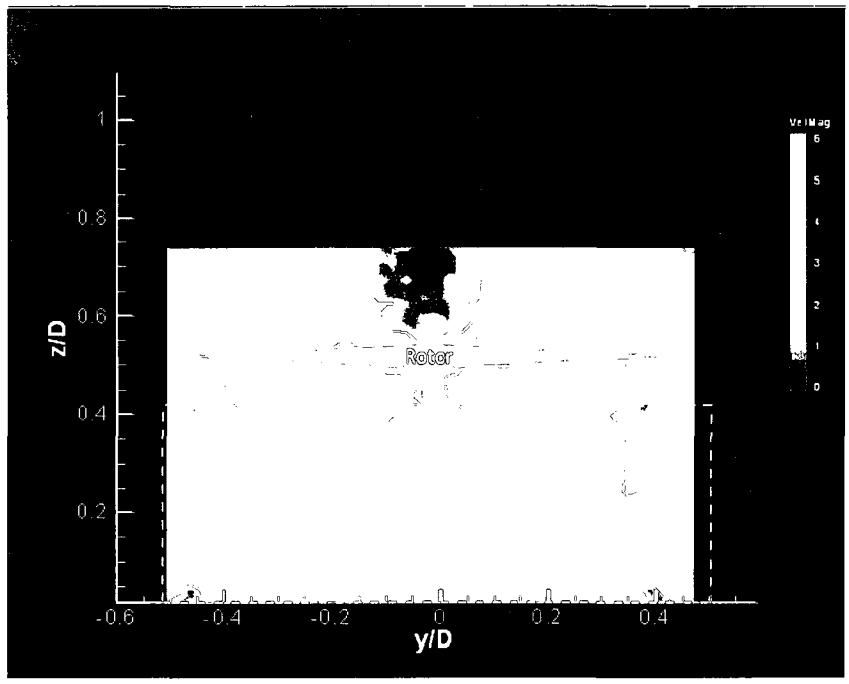

Figure 6.46 Rotor with ship airwake V_∞=5.14 m/s (x/D=0.5;z/D=0.55) (Contour Plot)

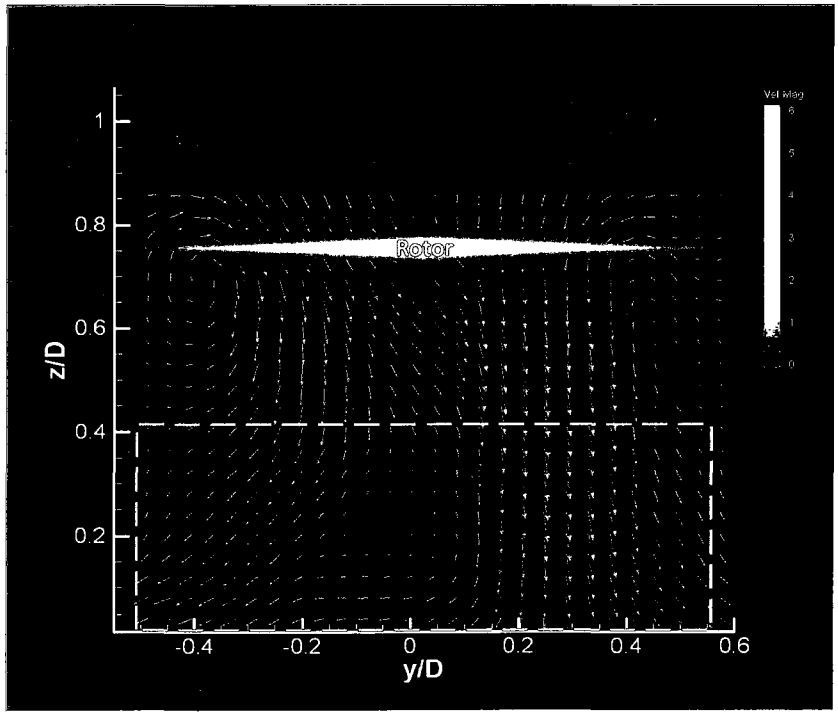

Figure 6.47 Rotor with ship airwake V_∞=5.14 m/s (x/D=0.5; z/D=0.75) (C_T=0.0177)

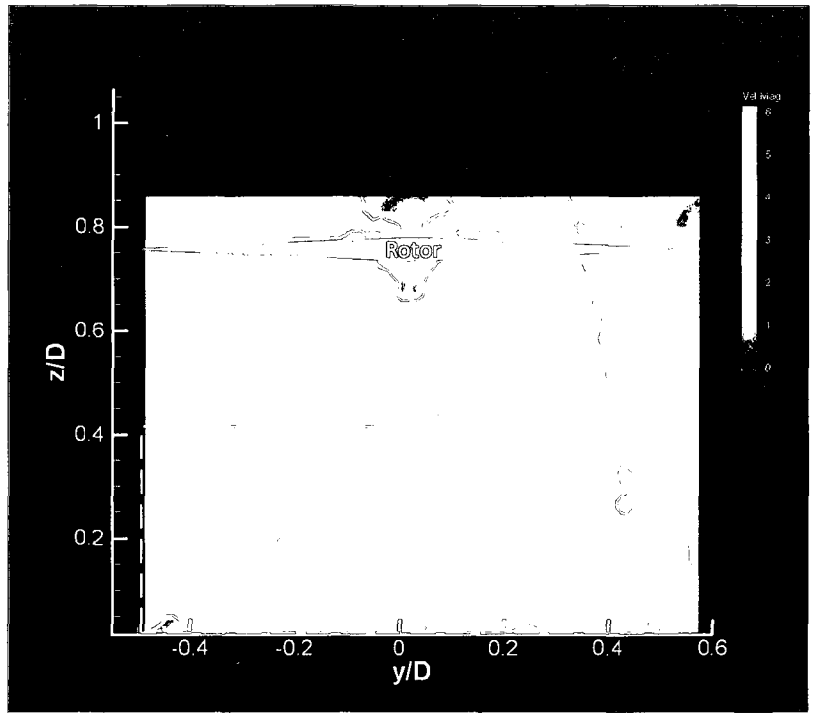

Figure 6.48 Rotor with ship airwake V_∞=5.14 m/s (x/D=0.5;z/D=0.75) (Contour Plot)

By proceeding downstream along the longitudinal axis of the landing deck (x) from the hangar door towards the stern of the frigate, a near-symmetric velocity flowfield can be seen with a recirculation zone. This recirculation zone is not symmetric and created just a little to the right of the longitudinal centerline of the landing deck. These effects and the recirculation zone are presented in Figure 6.49 as velocity vectors and in Figure 6.50 as contour plot.

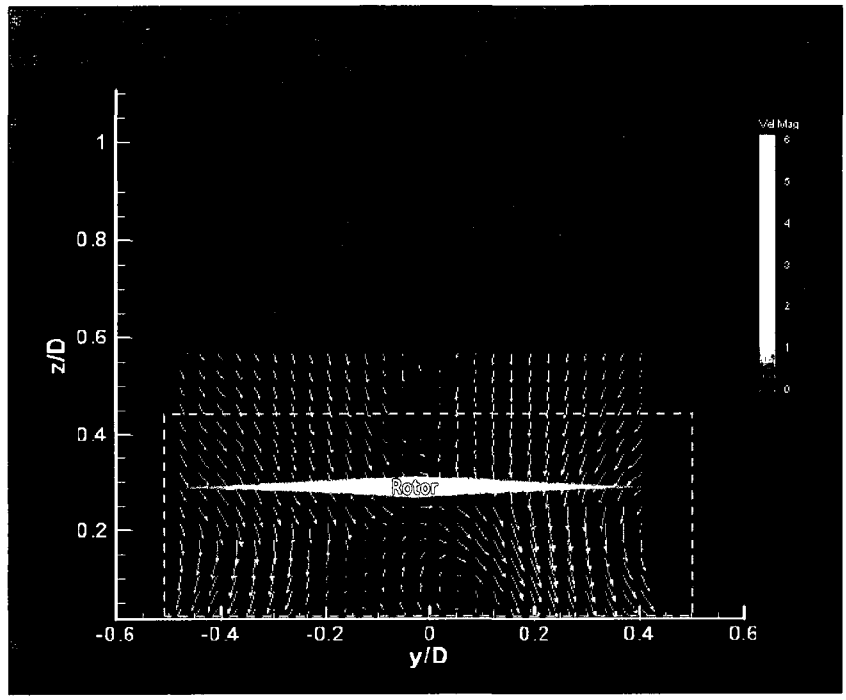

Figure 6.49 Rotor with ship airwake V_∞=5.14 m/s (x/D=1; z/D=0.35) (C_T=0.0174)

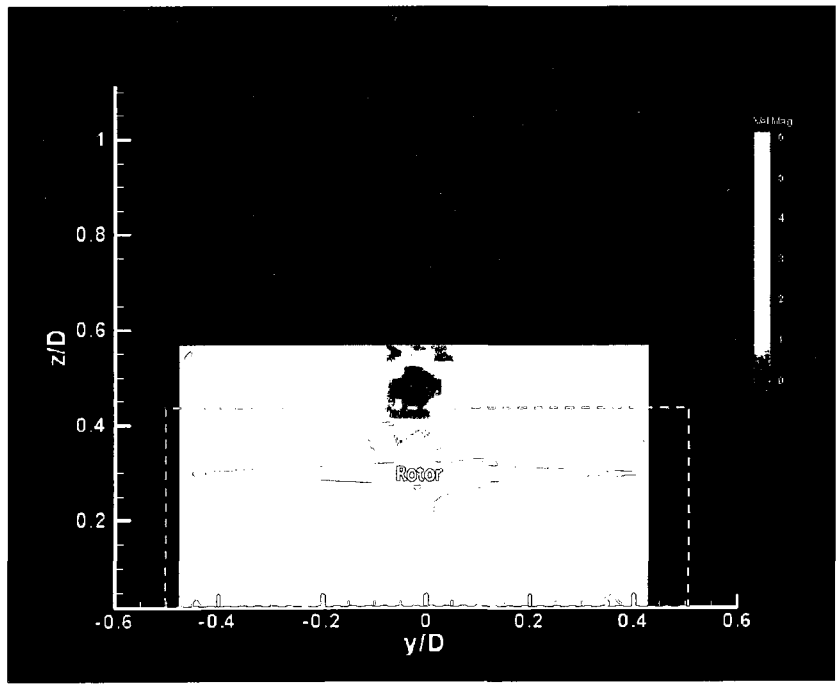

Figure 6.50 Rotor with ship airwake V_∞=5.14 m/s (x/D=1; z/D=0.35) (Contour Plot)

With increasing vertical distance above the landing deck, the largely symmetric velocity field changes to a definitively asymmetric velocity field as in the previous cases discussed above. The downwash of the rotor is affected by the freestream velocity because the rotor is above the hangar level. The recirculation zone moves to longitudinal centerline of the frigate when compared with the position of the rotor which is shown by Figure 6.49.

For the design point x/D=1; z/D=0.75, the recirculation zone vanishes because the rotor downwash effect decreases with increasing vertical distance above landing deck. These PIV surveys are presented in figures 6.51 - 6.54.

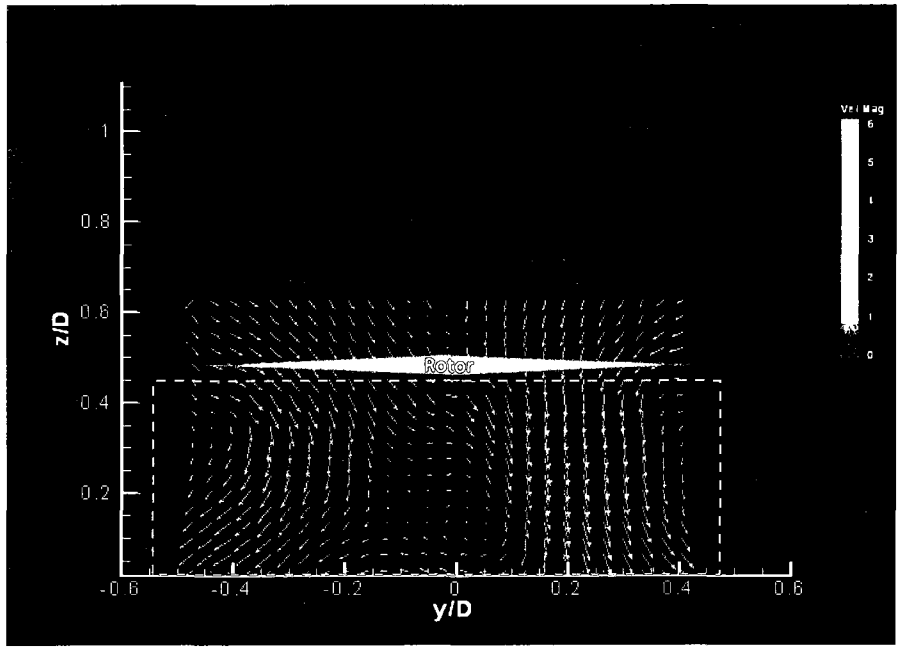

Figure 6.51 Rotor with ship airwake V_∞=5.14 m/s (x/D=1; z/D=0.55) (C_T=0.0176)

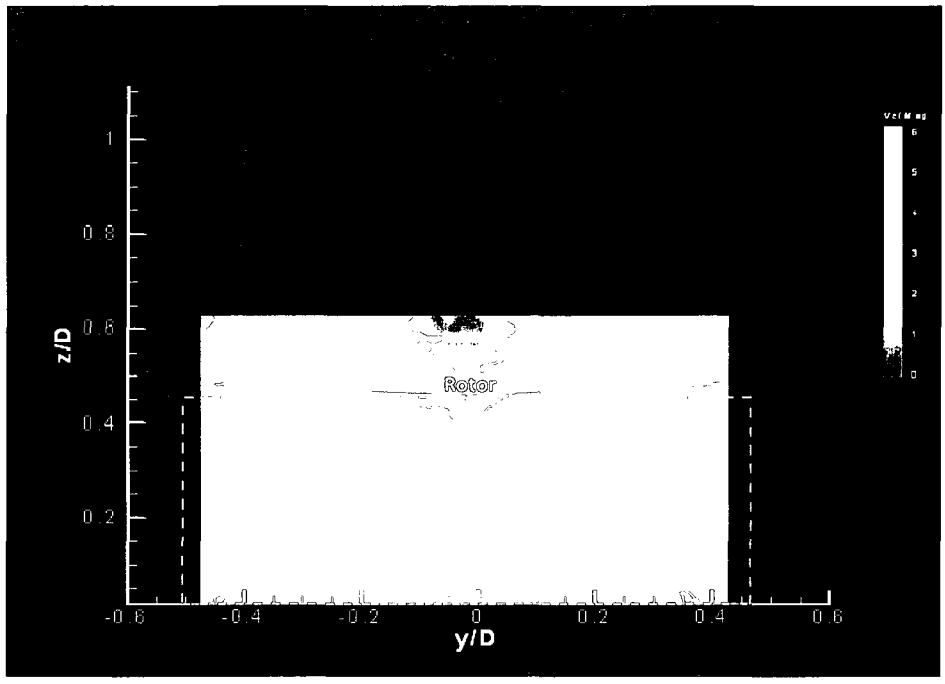

Figure 6.52 Rotor with ship airwake V_∞=5.14 m/s (x/D=1; z/D=0.55) (Contour Plot)

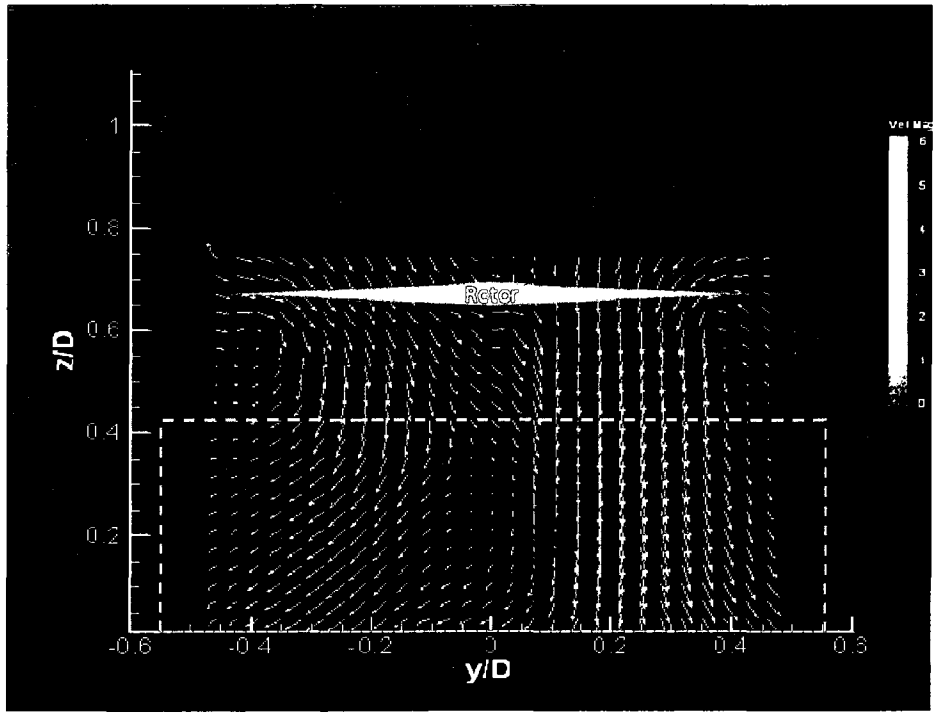

Figure 6.53 Rotor with ship airwake V_∞=5.14 m/s (x/D=1; z/D=0.75) (C_T=0.0175)

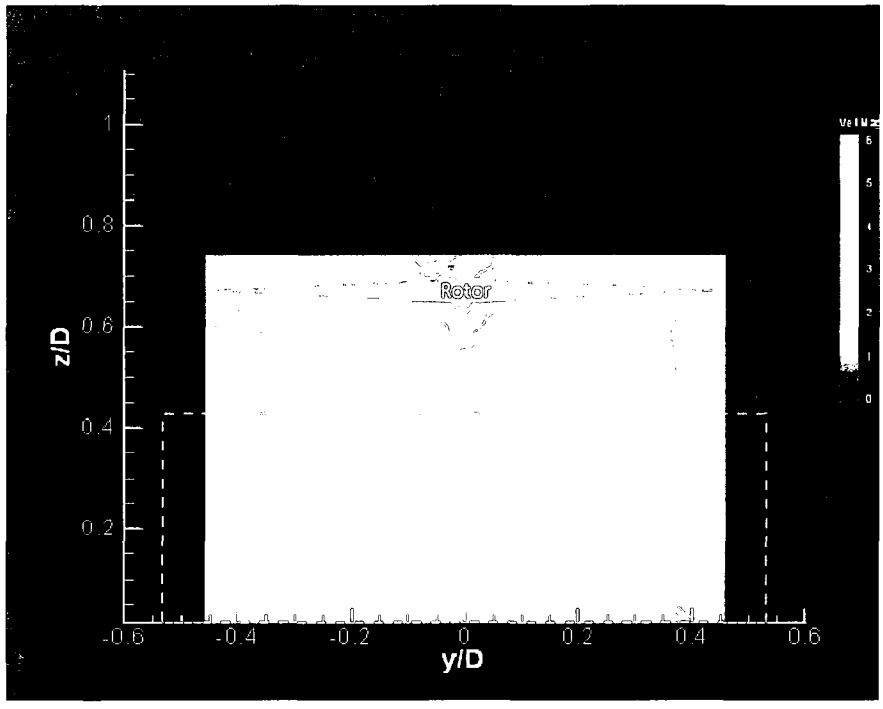

Figure 6.54 Rotor with ship airwake V_∞=5.14 m/s (x/D=1; z/D=0.75) (Contour Plot)

Similar trends for the velocity fields can be seen for the new design points on the x/D =1.5 station. Again, the near-symmetric velocity flowfield existed with a recirculation zone. This recirculation zone is not symmetric and formed slightly to the right of the longitudinal centerline of the landing deck when the rotor vertical distance is below the hangar door as presented in Figure 6.55 and Figure 6.56.

With increasing vertical distance above the landing deck, the near-symmetric velocity field changes to an asymmetric velocity field and the recirculation zone moves to the longitudinal centerline of the frigate as presented in Figure 6.57 and 6.58, respectively. Again, it is felt that the recirculation zone below the rotor may be the wake of the motor located just above the rotor.

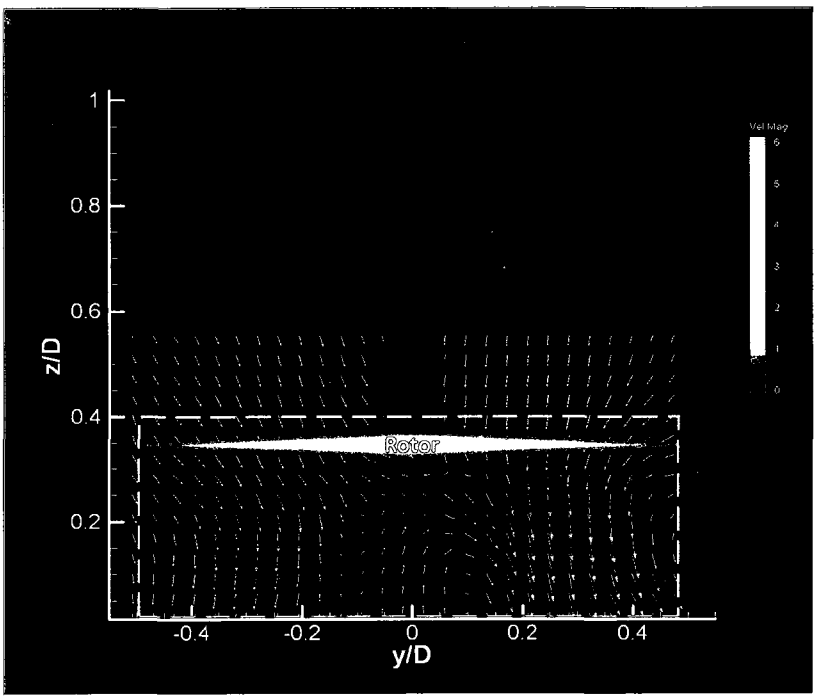

Figure 6.55 Rotor with ship airwake V_∞=5.14 m/s (x/D=1.5; z/D=0.35) (C_T=0.0174)

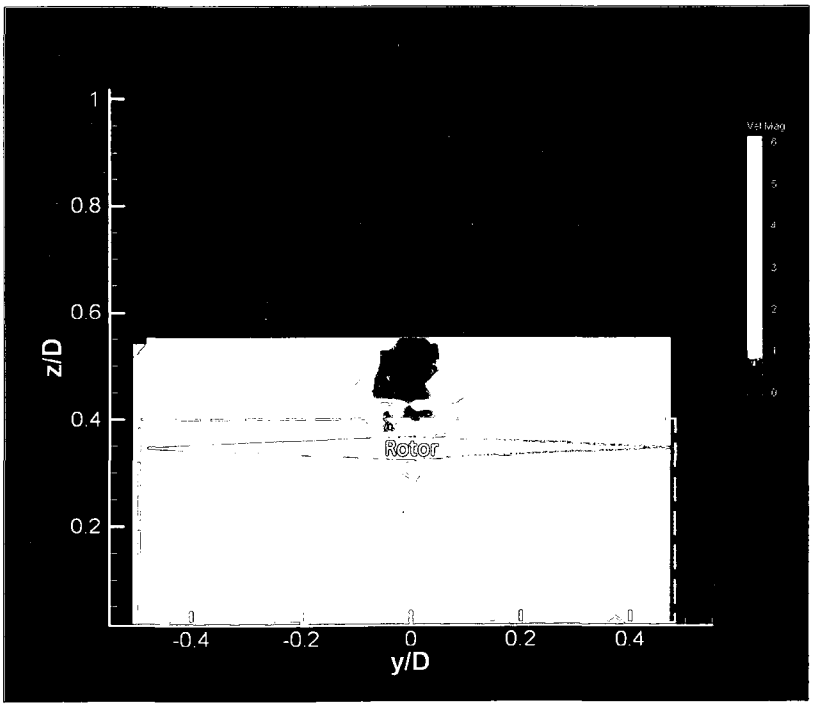

Figure 6.56 Rotor with ship airwake V_∞=5.14 m/s (x/D=1.5;z/D=0.35) (Contour Plot)

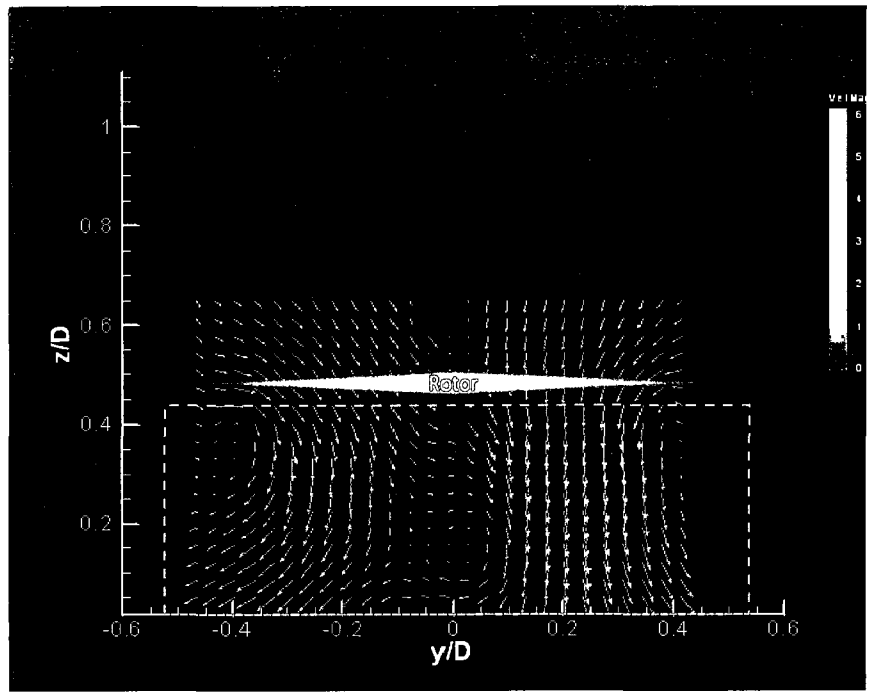

Figure 6.57 Rotor with ship airwake V_∞=5.14 m/s (x/D=1.5; z/D=0.55) (C_T=0.0176)

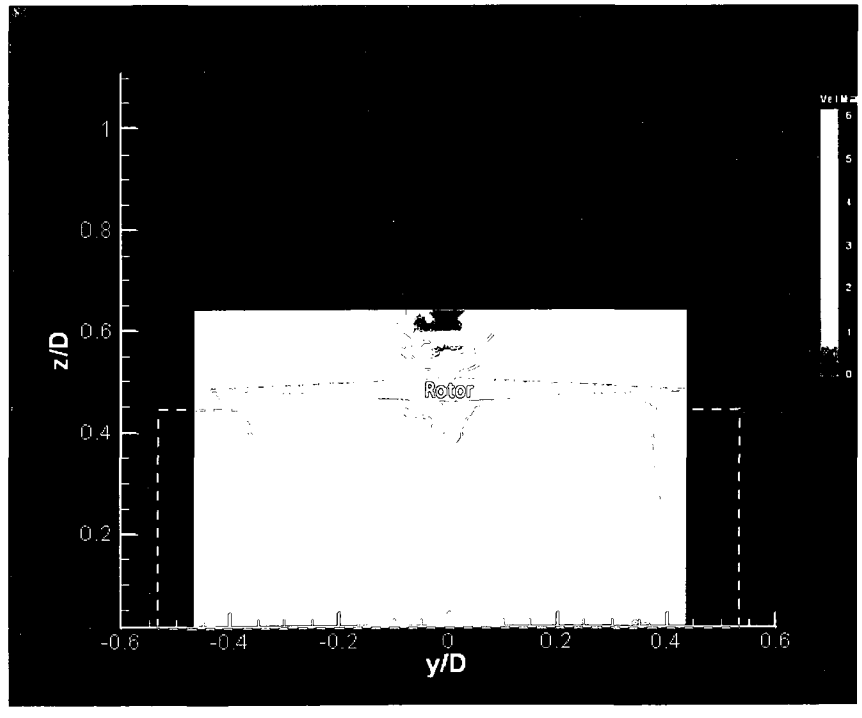

Figure 6.58 Rotor with ship airwake V_∞=5.14 m/s (x/D=1.5;z/D=0.55) (Contour Plot)

For the design point x/D=1.5; z/D=0.75, the recirculation zone vanishes because the rotor downwash effect decreases with increasing vertical distance above landing deck. The velocity vector and the contour plot for this case are presented in Figure 6.59 and Figure 6.60.

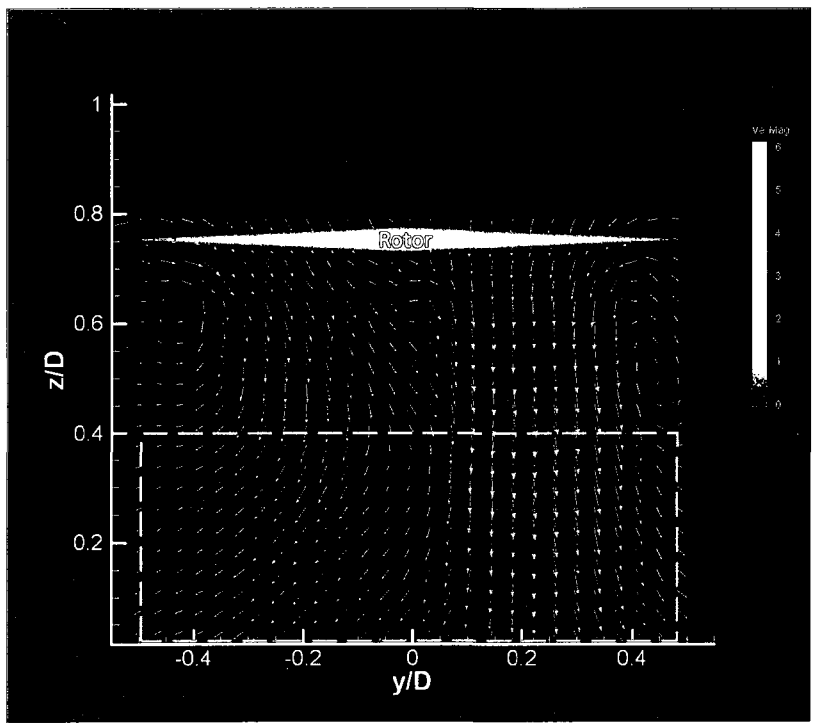

Figure 6.59 Rotor with ship airwake V_∞=5.14 m/s (x/D=1.5; z/D=0.75) (C_T=0.0175)

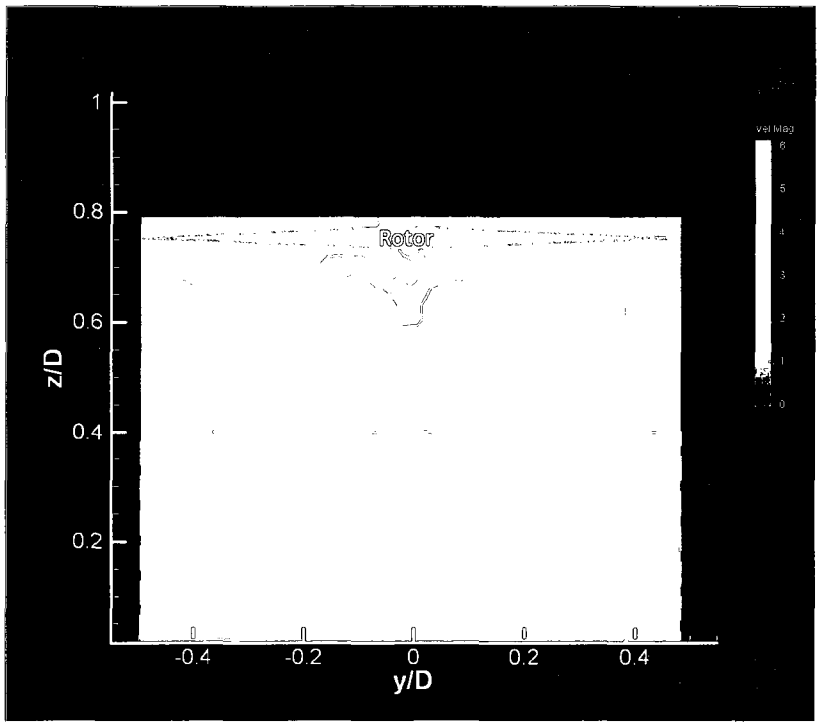

Figure 6.60 Rotor with ship airwake V_∞=5.14 m/s (x/D=1.5;z/D=0.75) (Contour Plot)

6.6 Example of Coupled Flow

In this section, the ship airwake and the rotor downwash are superposed to see the difference between the measured coupled flowfield and the computed superposed case at the same location. For the tship in isolation case and the rotor in isolation case, longitudinal and vertical velocity components of the velocity field were added and are presented in Figure 6.61. The PIV survey of the fully coupled flowfield at the same location over the deck is shown for comparison in figure 6.62. As seen in the earlier sections, this case represents an extreme example in that the rotor is located in close proximity to the deck. The differences between the resulting velocity fields are great as

expected. In comparing the velocity magnitude and angle of inclination, large differences are evident.

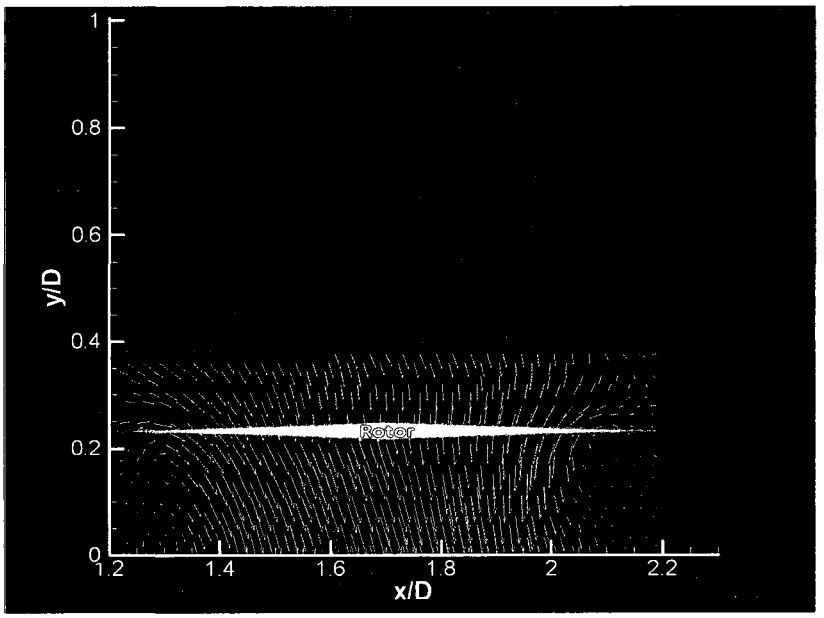

Figure 6.61 Ship Airwake + Rotor Downwash (Superposed)

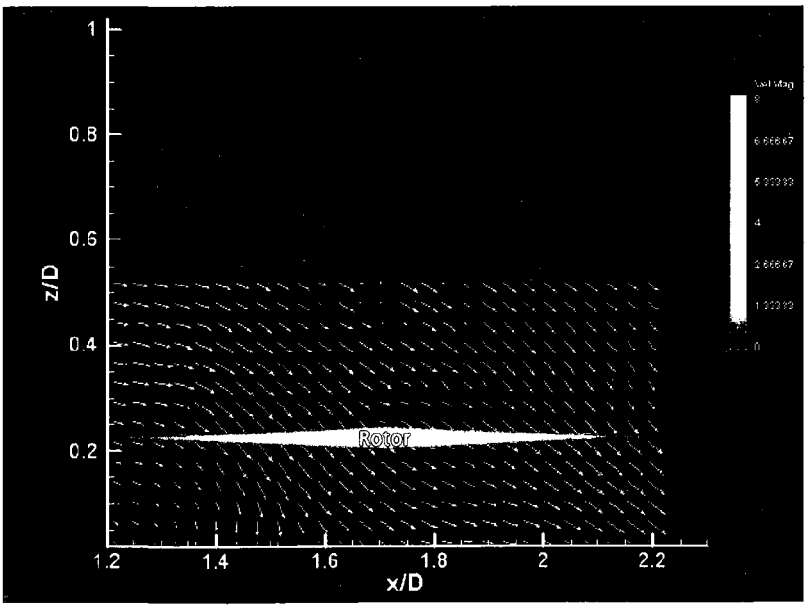

Figure 6.62 Ship Airwake/Rotor Downwash (Measured)

7. DISCUSSION, CONCLUSIONS AND FUTURE WORK

7.1 Discussion of Results

The PIV velocity survey and rotor torque measurement results of this study provided a first look at a very complex flowfield. For bow winds (WOD = 0) and the ship in isolation, the longitudinal surveys show that flow separates from the hangar top and reattaches about halfway along the flight deck. Despite the simplified geometry, this result compares qualitatively with the work of others including higher fidelity frigate models.[2,30,31,41-43] Lateral surveys were conducted only with the rotor present so the exact 3-D nature of the recirculation region was not measured for the ship in isolation. To understand the 3-D nature, one also needs to consider the side inflow over the landing deck just downstream of the hangar door. A composite sketch based on the longitudinal measurements of this study and the work of Zan shows the fundamental features of the 3-D flowfield in figure 7.1[41]. The recirculation zone is an unsteady aerodynamic structure, so the instantaneous attachment location varies with time. The higher speed outer flow (green) is redirected by the recirculation zone from the top and sides of the hangar to the mid-deck attachment line. The lower pressure serves to redirect flow over the deck sides inward towards the longitudinal center plane. Flow above the recirculation zone is in general directed downward for the time-averaged flowfield. Flow inside the recirculation zone is of lower velocity magnitude than the external flow and highly unsteady. Wakefield, found that the lowest pressure on the landing deck is found at the base of the

hangar face, inside the recirculation zone[43]. The highest pressure was found at the reattachment point which was again approximately in the center of the landing deck[43].

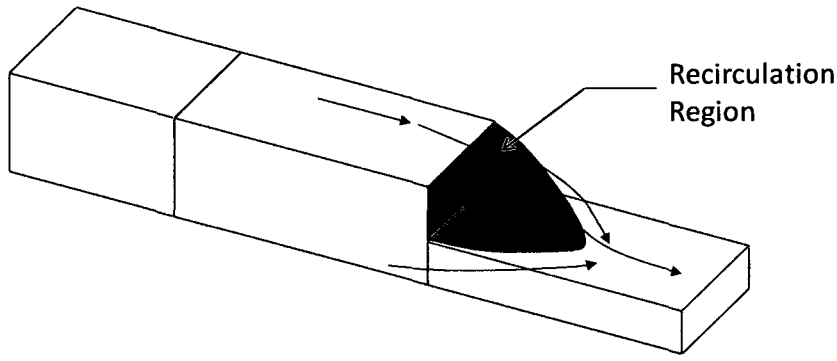

Figure 7.1 Flowfield over the Frigate Landing Deck

Aft of the attachment locations, the flow quickly returns to the streamwise direction; Zan found the measured surface pressures at the aft end of the landing deck were very close to freestream values again (Cp near zero).[31]

In general the dividing line between the outer flow and the recirculation region of the frigate in isolation is not steady and the reattachment line oscillates primarily in a longitudinal sense. When the rotor moves into the recirculation region very near the deck x/D~0.5, z/D~0.25, the interaction is powerful. A sketch with the probable dominant flow features is shown in figure 7.2. The recirculation region is trapped upwind of the rotor axis and the downwash from the rotor drives the outer flow from the top (yellow) through the rotor disk (blue) onto the deck and downstream to the stern. When compared to the ship in isolation, the outer flow streamlines from the sides (green) are displaced laterally outward by the rotor downwash outflow and the strong recirculation (red) on the hangar

door. The rotor thrust in this region is reduced by the re-ingestion of flow on the rotor upwind side, but this loss is balanced by the rotors close proximity to the deck which affords an increase in thrust due to ground effect. As the vertical distance (.25<z<.55) is increased the strength of the recirculation region decreases while the overall size (expanding aft) increases. The overall flow features remain the same as the rotor height above deck is increased to the hangar height. The thrust will increase as the height is increased beyond the hangar height due to the rotor encountering the higher velocity outer flow from the top of the ship superstructure.

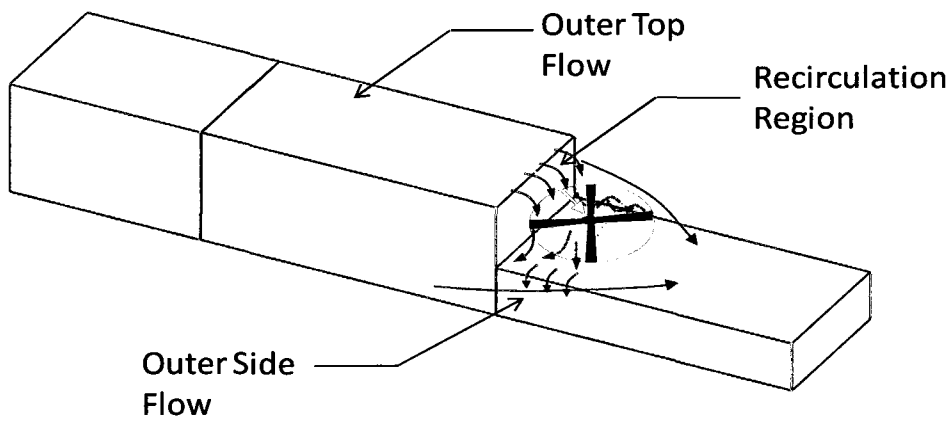

Figure 7.2 Flowfield with Rotor near Hangar Door and Deck (x/D~0.5; z/D~0.25)

As the rotor is moved longitudinally aft of the landing deck centerline, starting from the point x/D=1.4, the rotor appears to be free of re-ingestion of the recirculation flow for the heights surveyed in this study. It is assumed that the recirculation region behind the hangar door is now self contained and the outer top flow is simply redirected by the rotor. Further measurements will be required to fully define this flowfield, but a conceptual

sketch is shown in Figure 7.3. The outer side flow (green) interacts with the rotor downwash with one outcome being the outflow over the landing deck side (red).

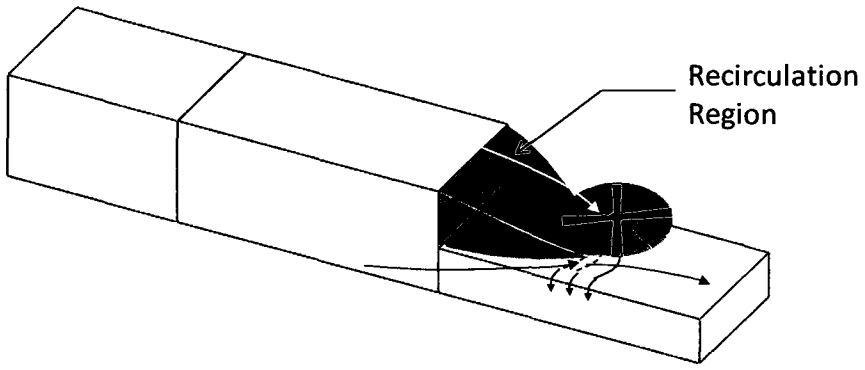

Figure 7.3 Flowfield with Rotor Position aft of Mid Deck (x/D~1.4; z/D~0.45)

The thrust coefficient increases with increasing height due in part to the reduced downwash of the airwake with height, but also to the increase in airwake velocity with height. Reviewing the thrust mapping of figure 5.12, it is seen that as the rotor reaches the stern of the frigate, the thrust coefficient decreases again. This drop in thrust coefficient is felt to be due in part to the downstream rotor blades overhanging the stern resulting in an increased ground clearance as shown in figure 7.4. The outer flow (shown in green and yellow) are entrained in the rotor downwash field. Flow off the top of the ship superstructure combines with the rotor downwash below the rotor. Off-surface flow displaced vertically from the ship top may be directed through the rotor disk as shown by the upper yellow streamline. The outer side flow, shown as the green streamlines, will be deflected toward the ship centerline aft of the recirculation region and become confluent with the rotor downwash.

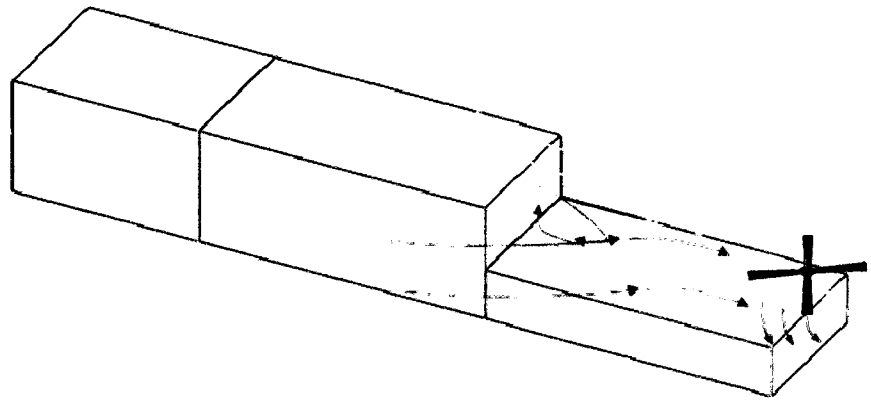

Figure 7.4 Flowfield with Rotor position at the Stern (x/D~2; z/D~0.45)

7.2 Conclusions and Future Work

The results presented for this fundamental research demonstrate the feasibility of using a statistically robust comparison experiment to analyze the changes in rotor thrust due to helicopter downwash/frigate airwake interaction. While this is not explicitly a test for coupling, it is representative of the signal to noise ratio expected when evaluating coupled versus uncoupled flow regions. Future work may build on this concept by developing a comparison test between superposed measured velocity flowfields from an isolated rotor and isolated ship airwake versus measured combined flowfields. A new response metric will need to be devised as thrust coefficients can not be superposed.

The limited PIV flowfield surveys conducted in this study served to enhance the understanding of the changes in the thrust response as a function of rotor to ship proximity. More detailed surveys including off-ship and near-ship regions are required for a full understanding. Future work will require more comprehensive PIV surveys at a

given rotor location which will include not only areas directly adjacent to the rotor, but complete flowfield evaluations from upstream of the hangar door to downstream of the stern. The use of 3-D PIV surveys, an automated rotor positioning traverse and ultimately a dual camera positioning traverse will greatly aid in this effort.

Longitudinal center plane thrust coefficient mapping over the landing deck revealed that gradients are relatively mild for the 0.075 advance ratio over the region $0.25<x/D<2$; $0.25<z/D<0.85$. The next logical step is to expand the thrust survey region over the same longitudinal space but for at least one rotor diameter lateral displacement.

Other near-term objectives include varying WOD angles and advance ratios that are of interest to Naval operations. The final suggestion is to increase the model fidelity after a comprehensive test of the simple frigate model is complete.

REFERENCES

[1]Bridges, D.O., Horn, J.F., Alpman, E. and Long, L.N., *Coupled Flight Dynamics and CFD Analysis of Pilot Workload in Ship Airwakes*, AIAA Atmospheric Flight Mechanics Conference and Exhibit, Hilton Head South Carolina, 20-23 August 2007.

[2]Zan, S.J. and Garry, E.A., *Wind Tunnel Measurements of the Airwake Behind a Model of a Generic Frigate*, NRC-IAR-LTR-AA-13, June 1994.

[3]Syms, G.F. and Zan, S.J., Analysis of Rotor Forces in a Ship Airwake, 75th AGARD FDP Meeting on *Aerodynamics and Aeroacoustics of Rotorcraft*, Berlin, Germany, AGARD-CP-552, October 1994.

[4]http://www.history.navy.mil/photos/images/u170000/u172866.jpg.

[5]Wilkinson, C.H., Zan, S.J., Gilbert, N.E. and Funk, J.D., *Modelling and Simulation of Ship Airwakes for Helicopter Operations-A Collaborative Venture*, Fluid Dynamics Problems of Vehicles Operating Near or in the Air-Sea Interface, 1999.

[6]http://mig.sms1835.no/harlan/2007/Sanne/SHOLS/system_and_future_concepts.pdf.

[7]Wadcook, A.J., Yamauchi, G.K., Heineck, J.T., Silva, M.J. and Long, K.R., *PIV Measurements of the Wake of a Tandem-Rotor Helicopter in Proximity to a Ship*, AHS 4th Decennial Specialist`s Conference on Aeromechanics, San Francisco, CA, 21-23 January 2004.

[8]Tate, S.J., A Dynamic Challenge: Helicopter/Ship Interface Simulation-Development, Integration and Application. AGARD-FDP Symposium on *Flight Simulation: Where are the Challenges?*, Braunschweig, Germany, May 1995.

[9]http://journals.pepublishing.com/content/xm443012w6083013/

[10]Geyer, W.G., Keller, J. and Smith, E.C., Validation and Application of a Transient Response Analysis for Shipboard Engage/Disengage Operations, Proceedings of the *52nd American Helicopter Society Forum*, Washington, DC, June 1996.

[11]Keller, J.and Smith, E.C., Experimental/Theoretical Correlation of Analysis for Helicopter Blade-Droop Stop Impacts, Proceedings of *38th AIA/ASME/ASCE/AHS/ASC Structure, Structural Dynamics and Materials Conference*, Orlando, April 1997.

[12]Liu, J. and Long, L.N., Higher Order Accurate Ship Airwake Predictions for the Helicopter/Ship Interface Problem, *American Helicopter Society 54th Annual Forum*, Washington, DC, 20-22 May 1998.

[13]Healey, J.V., The Prospects for Simulating the Helicopter/Ship Interface, *Naval Engineers Journal*, March 1987, pp. 45-63.

[14]Healey, J.V., Establishing a Database for Flight in the Wake of Structures, *Journal of Aircraft*, Vol.29, No.4, July-August 1992, pp. 559-564.

[15]Hurst, D.W. and Newman, S. J., Wind Tunnel Measurements of Ship Induced Turbulence and the Prediction of Helicopter Rotor Blade Response, *Vertica*, Vol.12, No.3, 1988, pp. 267-278.

[16]Rhoades, M.M. and Healey, J.V., Flight Deck Aerodynamics of a Nonaviation Ship, *Journal of Aircraft*, Vol. 29, No.4, July-August 1992, pp. 619-626.

[17]Williams, S. and Long, K.R., Dynamic Interface Testing and the Pilots Rating Scale, *The 53rd AHS Forum*, April 1997.

[18]Garnett, T.S., *Investigation to Study the Aerodynamic Ship Wake Turbulence Generated by a FF-1052 Frigate*, Boeing Vertol Report D210-11140-1, December 1976.

[19]Zan, S.J., *On Aerodynamic Modelling and Simulation of the Dynamic Interface*, Journal of Aerospace Engineering, Proc. IMechE, Vol.219 Part G, 2005.

[20]Zan, S.J. and Syms, G.F., *Numerical Modelling of Rotor Forces in an Experimentally-Determined Ship Airwake*, NRC-IAR-LTR-AA-15, September 1995.

[21]Taghizad, A., Verbecke, Ch. and Desopper, A., Aerodynamic Perturbations on the Frigate La Fayette Deck: Effects on the Helicopter Flight Dynamics. NATO/RTO/AVT Symposium on *Fluid Dynamic Problems of Vehicles Operating in or near the Air/Sea Interface*, Amsterdam, NATO-RTO-MP-15, October 1998.

[22]Fang, R., Krijns, H.W. and Finch, R.S., Dutch/British clearance process. Part 1 of NATO-RTO-AGARDograph 300, Helicopter/Ship Qualification Testing, Flight Test Testing Series, Vol.22, February 2003.

[23]Lee, R.G. and Zan, S.J., Wind Tunnel Testing of Unsteady Loads on a Helicopter Fuselage in a Ship Wake. 23rd Congress of the International Council of the Aeronautical Sciences, Toronto, Canada, September 2002.

[24]Lee, R.G. and Zan, S.J., Wind Tunnel Testing of a Helicopter Fuselage and Rotor in a Ship Airwake. 29th Europian Rotorcraft Forum, Friedrichshafen, Germany, September 2003.

[25]Maslow, L.A., Valuev, N.O. and Zharinov, A.V., The Experince of Aerodynamic Disturbances Research Behind Aircraft-Carrier Ship with Elements for Safe Operation of Ship-Based Aircraft. NATO/RTO/AVT Symposium on *Fluid Dynamic Problems of*

Vehicles Operating in or Near the Air/Sea Interface, Amsterdam, NATO-RTO-MP-15, October 1998.

[26]Polsky, S.A. and Bruner, C.W.S., *Time-accurate Computational Simulations of an LHA Ship Airwake*, AIAA-2000-4126, 2000.

[27]Polsky, S.A. and Ghee, T.A., Application and Verification of Sub-grid Scale Boundary Conditions for the Prediction of Antenna Wake Flowfields. 5th International Colloquium on *Bluff Body Aerodynamics*, Ottawa, Canada, July 2004.

[28]Landsberg, A.M., Boris, J.P., Sandberg, W. and Young, T.R., Jr, Analysis of the Non-linear Coupling Effects of a Helicopter Downwash with an Unsteady Airwake. 33rd Aerospace Sciences Meeting, Reno< NV, AIAA-95-0047, January 1995.

[29]Tattersall, B., Albone, C.M. and Soliman, M.M., Prediction of Ship Airwakes over Flight Decks using CFD. NATO/RTO/AVT Symposium on *Fluid Dynamic Problems of Vehicles Operating in or near Air/Sea Interface*, Amsterdam, NATO/RTO/MP-15, October 1998.

[30]Syms, G.F., Simulation of Ship Airwakes using a Lattice Boltzmann Method. Proceedings of the Annual CFD Society Conference of Canada, Windsor, Canada, July 2003.

[31]Zan, S.J., Surface Flow Topology for a Simple Frigate Shape. *Can.Aeronaut.Space J.*, 2001, 47(1),33-40.

[32]Koc, I., "An Experimental Study of Automotive Wakes For Drag Breakdown," Master's Thesis, Aerospace Engineering Dept., Old Dominion University, Norfolk, VA, August 2003.

[33]Koc, I., "Experimental Investigation of Active Control of Bluff Body Vortex Shedding" PhD Thesis, Aerospace Engineering Dept., Old Dominion University, Norfolk, VA, December 2008.

[34]www.apcprop.com,

[35]www.dantecdynamics.com, [cited in 2002].

[36]http://thequalityportal.com/q_know02.html,

[37]Montgomery, D.C., *Design and Analysis of Experiment* 6th ed., Wiley, New York, 2005.

[38]http://www.itl.nist.gov/div898/handbook/pri/section7/pri7.html,

[39]Box, G.E.P et al., *Statistics for Experimenters*, Wiley, New York, 1978

[40]Kuehl, R,O., *Design of Experiments: Statistical Principles of Research Design and Analysis*, 2nd ed., Duxbury Press, 2000

[41]Zan, S.J., Syms, G.F. and Cheney, B.T., Analysis of Patrol Frigate Air Wakes RTO/AVT Symposium on *Fluid Dynamic Problems of Vehicles Operating in or near Air/Sea Interface*, Amsterdam, RTO, 5-8 October 1998.

[42]Zan, S.J., Experimental Determination of Rotor Thrust in a Ship Airwake. *Journal of American Helicopter Society*, 2002, 47(2), 100-108.

[43]Wakefield, N.H., Newman, S.J. and Wilson, P.A., Helicopter Flight Around a Ship`s Superstructure, *Journal of Aerospace Engineer*, IMechE Vol.216, Part G, 2002.

[44]Leishman, J.L., *Principles of Helicopter Aerodynamics*, Cambridge University Press, 2001

VITA

DEGREES

- ***Master of Science Aerospace Engineering***
  Middle East Technical University, Ankara, June. 2003

- ***Bachelor of Science Mechanical Engineering***
  Turkish Air Force Academy, Istanbul, Aug. 1997

PROFESSIONAL CHRONOLOGY

- 2nd Main Jet Base Flight School, Izmir, Pilot Training, June 1997- July 1998

- Middle East Technical University, Ankara, MSc Student, September. 1999-September 2002

- 7th Main Jet Base, Malatya, Aircraft Maintenance Officer, September 2002-August 2006,

- Turkish Air Force Academy, Istanbul- Aerospace Engineering Department, Old Dominion University, Norfolk, VA, PhD Student, September 2006-September 2009

PROFESSIONAL MEMBERSHIPS

- American Institute of Aeronautics and Astronautics (AIAA) - *Student Member*

SCHOLARY ACTIVITIES

Alemdaroglu, N., Uysal, H., **Nacakli, Y.**, Sahin, T., Quagliotti, F., Guglieri , G., Roll Oscillatory Test in a Low Speed Wind Tunnel, paper no: AIAA 2003-0398 ,AIAA, 41 st Aerospace Sciences Meeting and Exhibition, Vol :AIAA 2003- No :2003-0398 Publisher :AIAA, American Inst. of Aeronautics and Astronautics, VA 20191-4344 Editor(s) :AIAA Month: 1 Year: 2003

APPENDIX-A

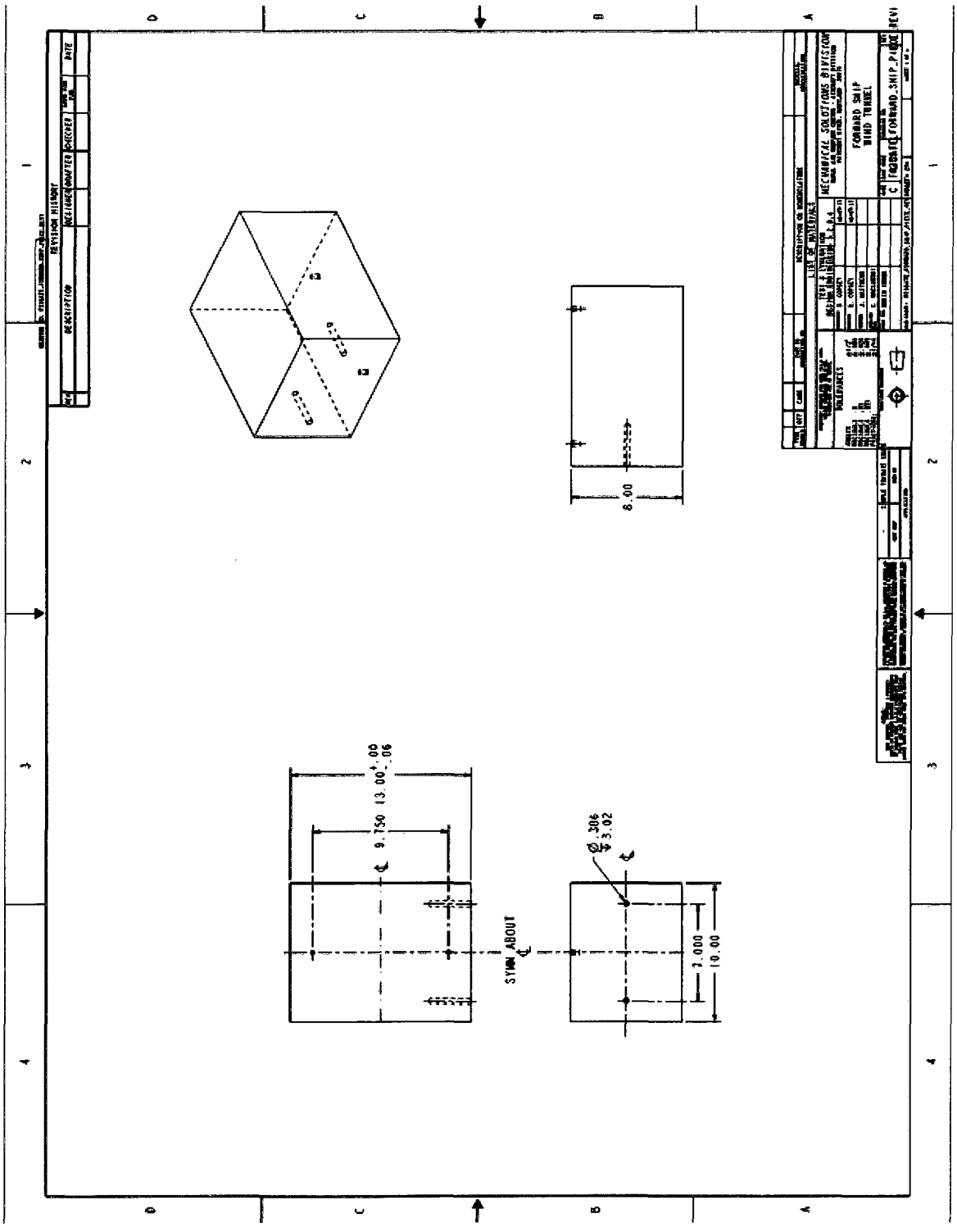

Figure A-1 Frigate Forward Ship Piece

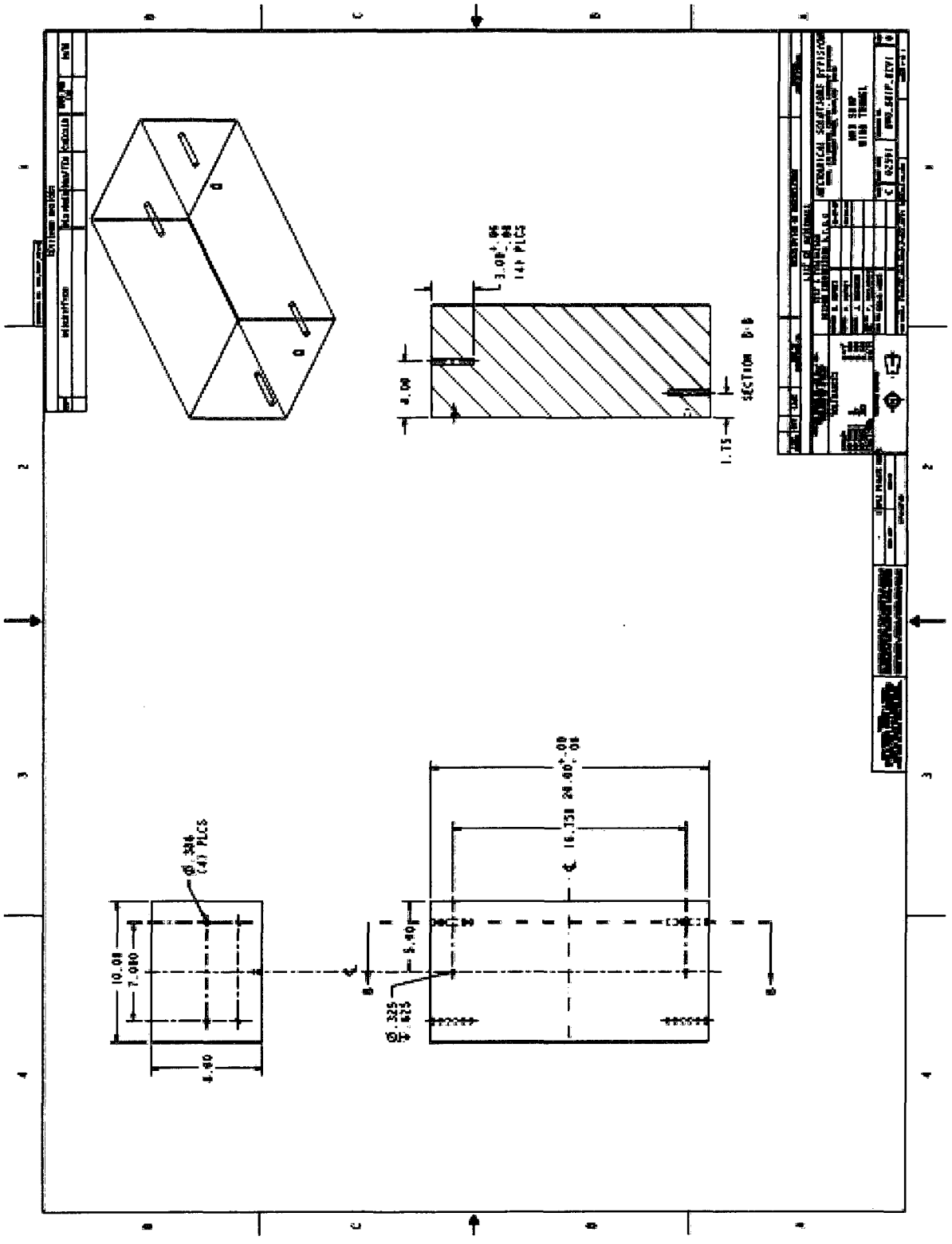

Figure A-2 Frigate Middle Ship Piece

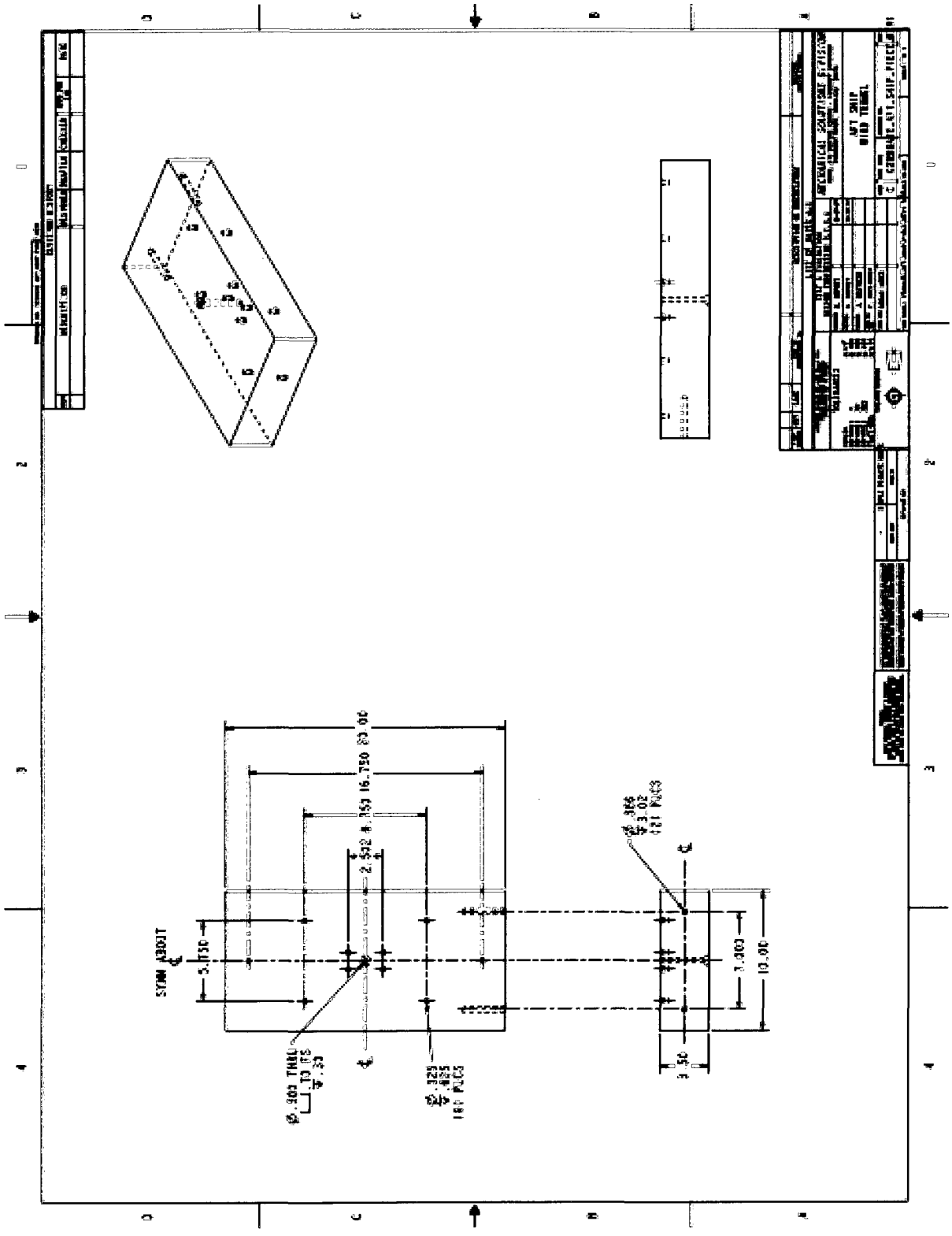

Figure A-3 Frigate Aft Ship Piece

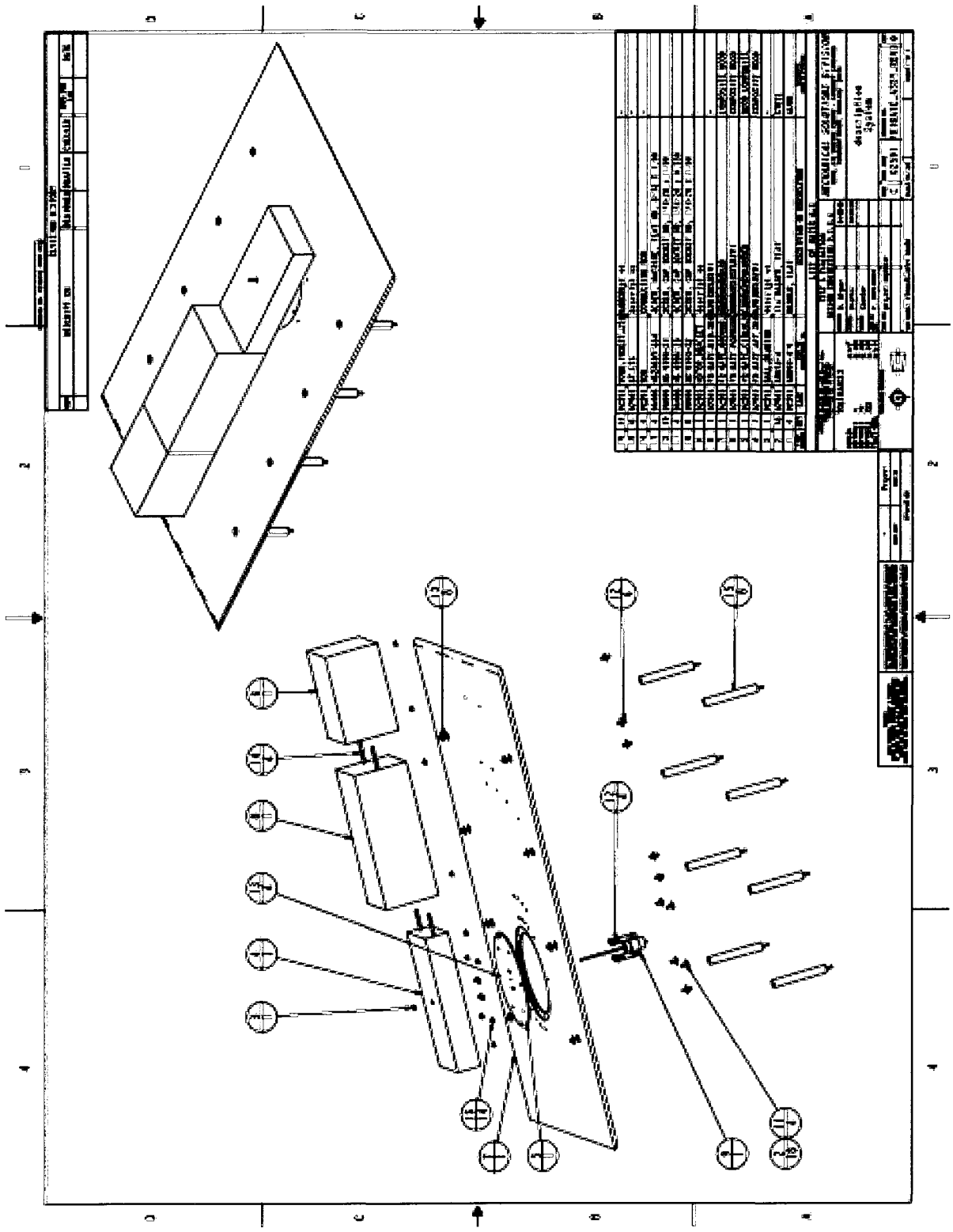

Figure A-4 Frigate Assembly

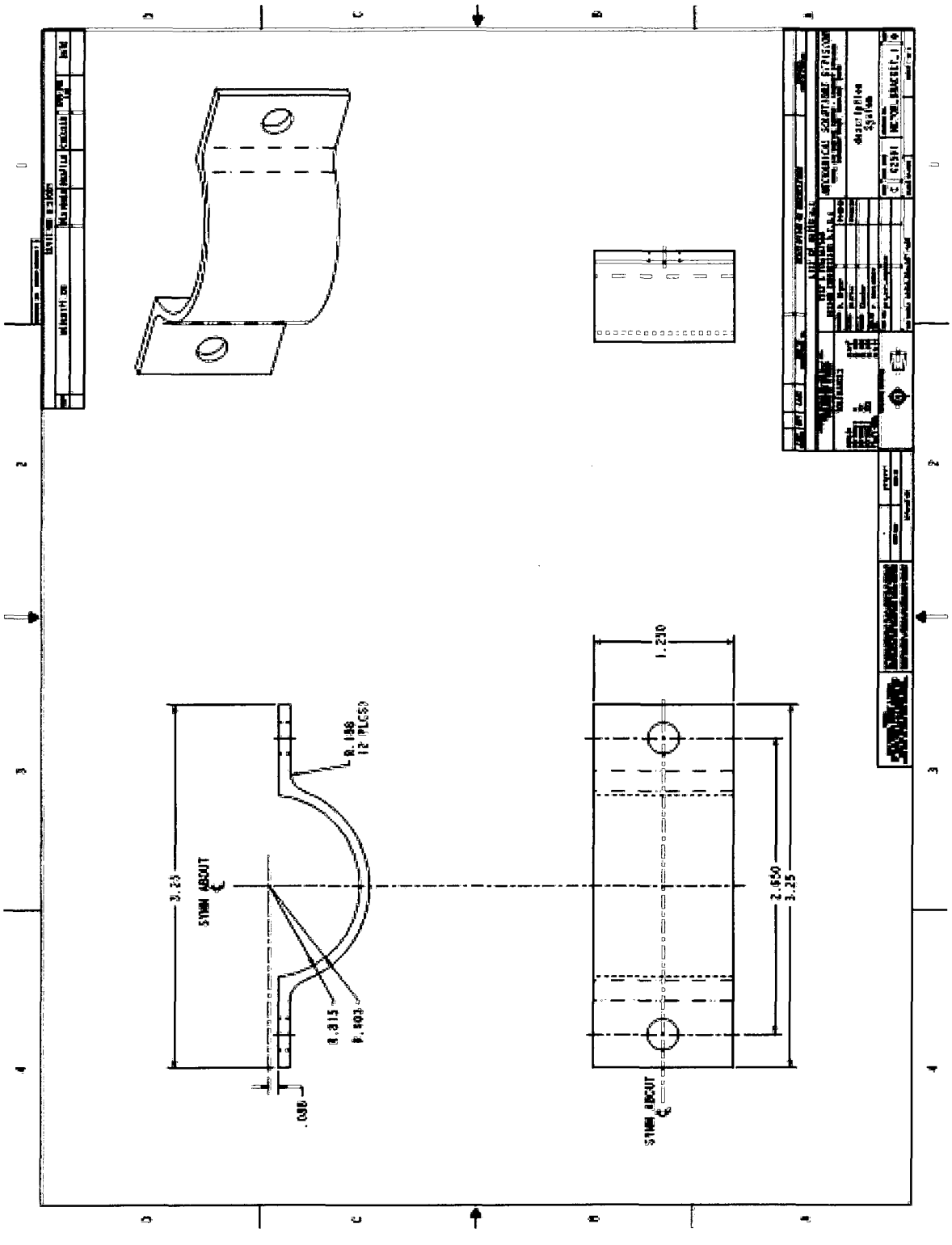

Figure A-5 Motor Bracket 1

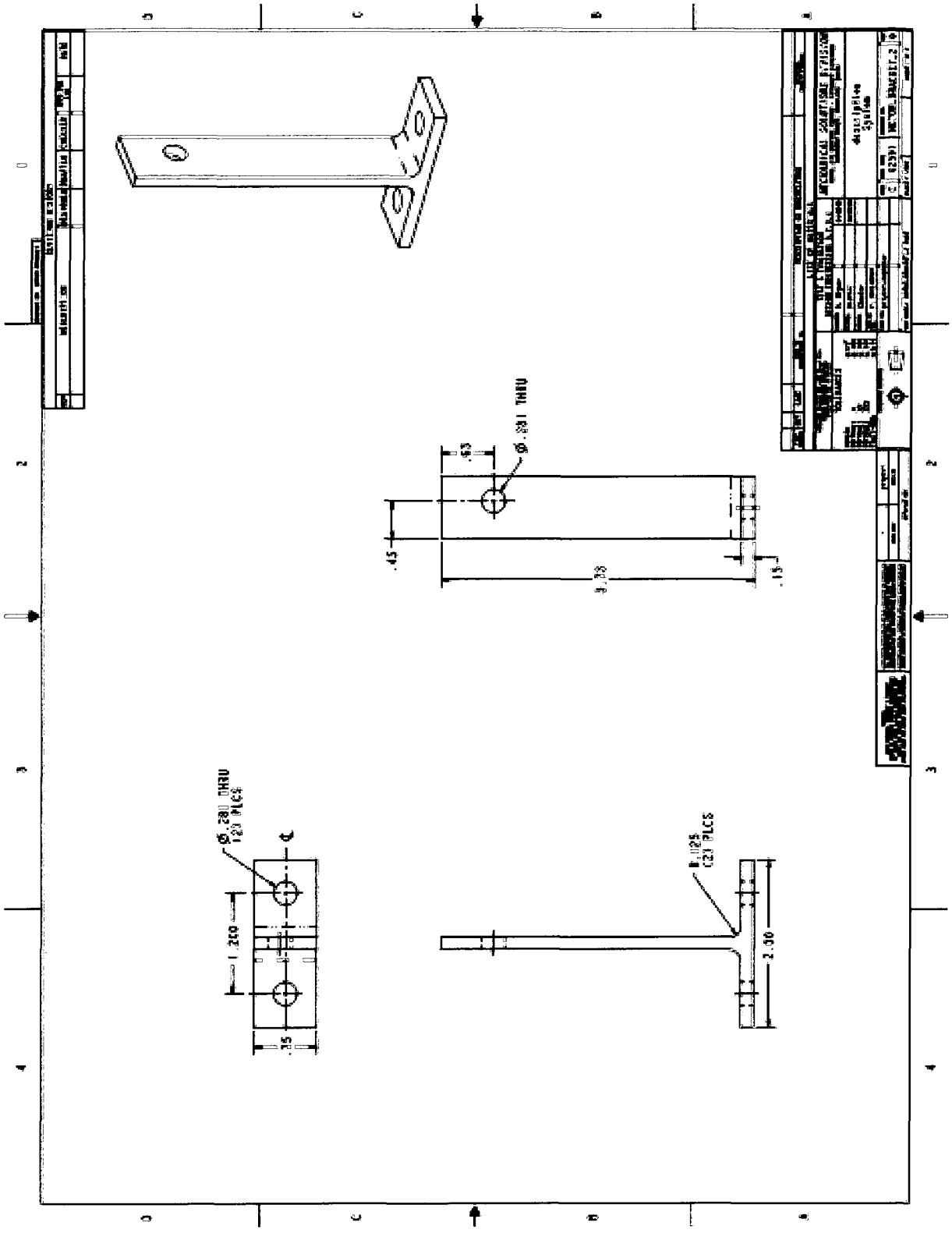

Figure A-6 Motor Bracket 2

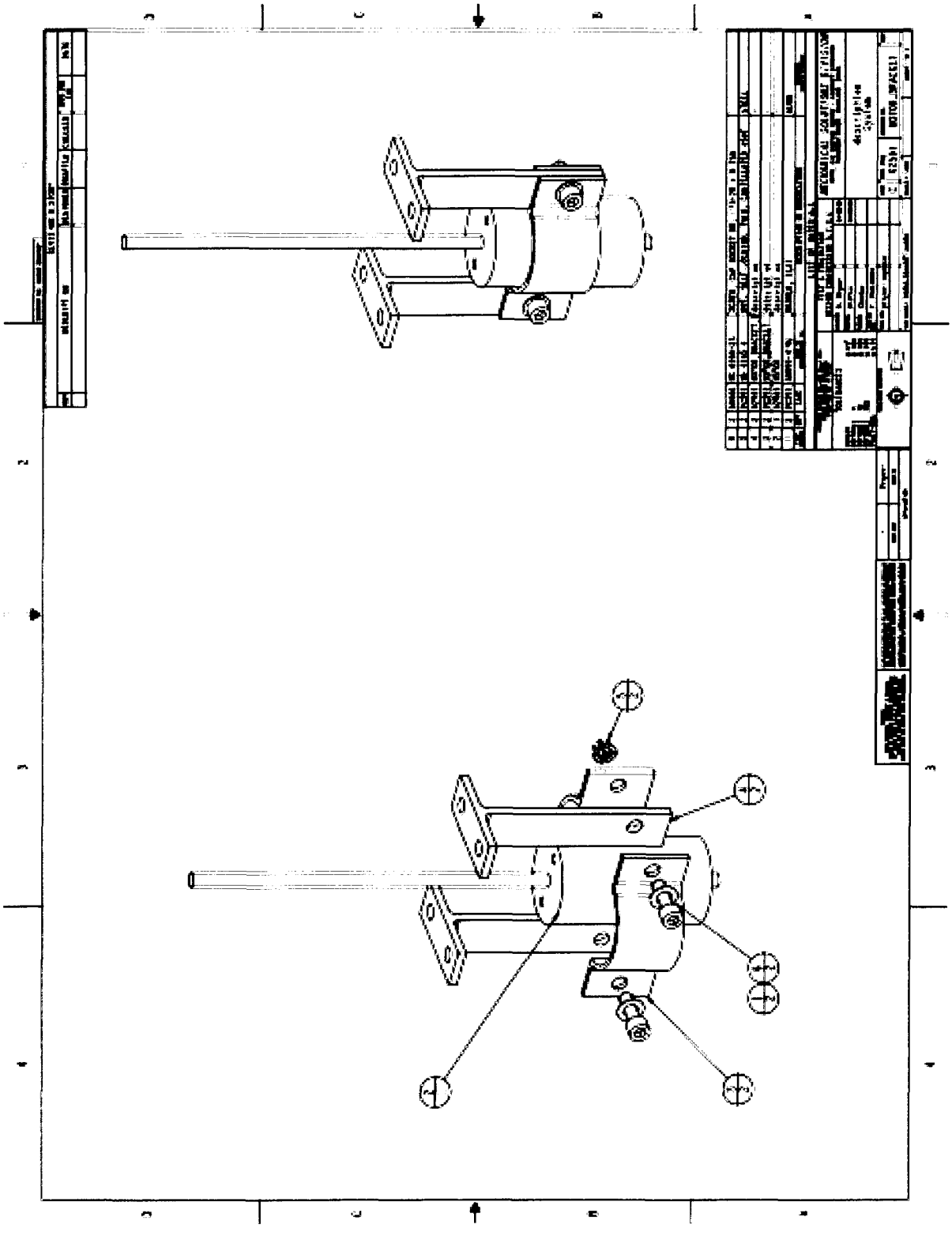

Figure A-7 Motor Bracket

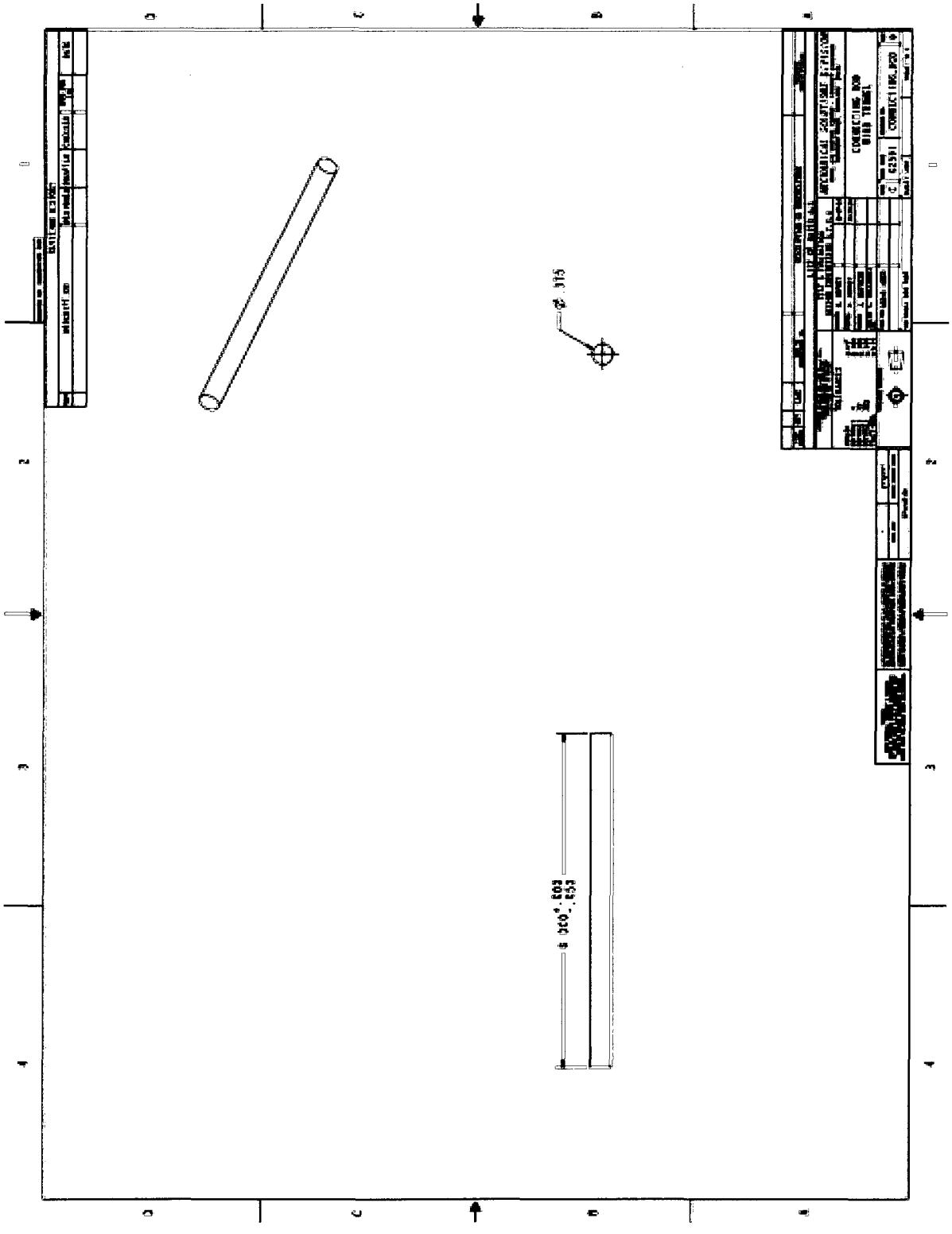

Figure A-8 Motor Shaft